1974

DC breakdown and anode corona characteristics of sphere and rod-plane gaps insulated with compressed sulphur hexafluoride.

Robert Lawrence. Hazel
University of Windsor

DC BREAKDOWN AND ANODE CORONA CHARACTERISTICS OF SPHERE AND ROD-PLANE GAPS INSULATED WITH COMPRESSED SULPHUR HEXAFLUORIDE

by

ROBERT LAWRENCE HAZEL

A DISSERTATION

Submitted to the Faculty of Graduate Studies
through the Department of Electrical Engineering.
in Partial Fulfillment of the Requirements for the
Degree of Doctor of Philosophy at the
University of Windsor

Windsor, Ontario,

Canada

1974

ABSTRACT

This dissertation describes an experimental study of the DC breakdown and anode corona discharge characteristics of SF_6 insulated non-uniform field gaps, and investigates methods of determining a theoretical prediction of the discharge performance of an SF_6 insulated system.

An analysis is made of prebreakdown currents and visual manifestations resulting from corona discharge activity in hemispherically capped rod-plane gaps insulated with SF_6 at gas pressures ranging from 1 to 5 atmospheres. Also analized is the relationship between breakdown voltage-gas pressure characteristics and anode corona. The investigations indicate that DC anode corona in SF_6 differs considerably from its counterpart in air. An interpretation of the experimental findings is made on the basis of reported experimental and theoretical analyses of anode corona in various gases and gas mixtures.

A numerical technique is presented which eliminates trial and error type implementation of streamer onset criteria to SF_6 insulated gaps of any configuration. A comparison of experimental results with calculated streamer onset voltages demonstrates that this technique yields an accurate estimate of the minimum DC voltage at which any form of anode discharge is observed.

A semi-empirical criterion is proposed which yields the minimum gas pressure at which corona free breakdown occurs

in an SF_6 insulated gap. On the basis of this criterion it is demonstrated that, to a good approximation, the minimum pressure of corona free breakdown is a function only of the radius of curvature of the anode. This result is verified experimentally for hemispherically capped rod-plane gaps.

ACKNOWLEDGEMENT

I would like to express my sincere thanks to Dr. E. Kuffel, the supervisor of this project, for his many helpful suggestions and his words of encouragement. I also wish to thank Mr. Minoru Matsuyama for his valuable assistance and my wife Marilyn for both typing the dissertation and providing moral support.

I am indebted to the National Research Council for providing funds for this project and to Prof. J. P. C. McMath of the University of Manitoba for kindly allowing the use of the HVDC generator.

LIST OF FIGURES

LIST OF TABLES

TABLE OF CONTENTS

LIST OF SYMBOLS

V - gap voltage

E - electric field intensity

α - ionization coefficient

η - attachment coefficient

A^* - metastable atom of species A

p - gas pressure

μ - photon absorption coefficient

CHAPTER I

INTRODUCTION

1.1 Historical Background

In 1937 Goldman and Wul (1) discovered that an increase in the sparking voltage of a gas insulated system did not necessarily result from an increase in the pressure of the gas insulation. Their studies on a nitrogen insulated point-plane electrode system indicated that in certain regions of gap length and pressure, a considerable drop in the impulse and AC breakdown voltage was observed to accompany a slight increase of the nitrogen pressure. Also, a considerable corona current was observed to precede breakdown at pressures below that at which the transition from high to low breakdown strength occurred. As a consequence of these observations Goldman and Wul suggested that the initial enhanced breakdown was a result of a field distortion due to a space charge accumulation around the point.

In 1939 Pollock and Cooper (2) conducted a similar study on a number of gases, including SF_6, using an electrode system consisting of a 1 inch diameter sphere and a hemispherically rounded tungsten wire point. They found that a decrease in the DC breakdown voltage accompanied an increase in the gas pressure only when at least one constituent of the gas insulation was electronegative and when the point electrode was of positive polarity. The basic pressure-sparking voltage characteristics exhibited by all of the

gas compounds with electronegative constituents tested by Pollock and Cooper are illustrated in Figure 1.1. Their results indicated a considerable variation among the gases tested in the local maximum and minimum sparking voltages (denoted respectively as V_{max} and V_{min} in Figure 1.1) as well as the pressures at which the maximum and minimum were observed (P_{vmax} and P_{vmin} respectively).

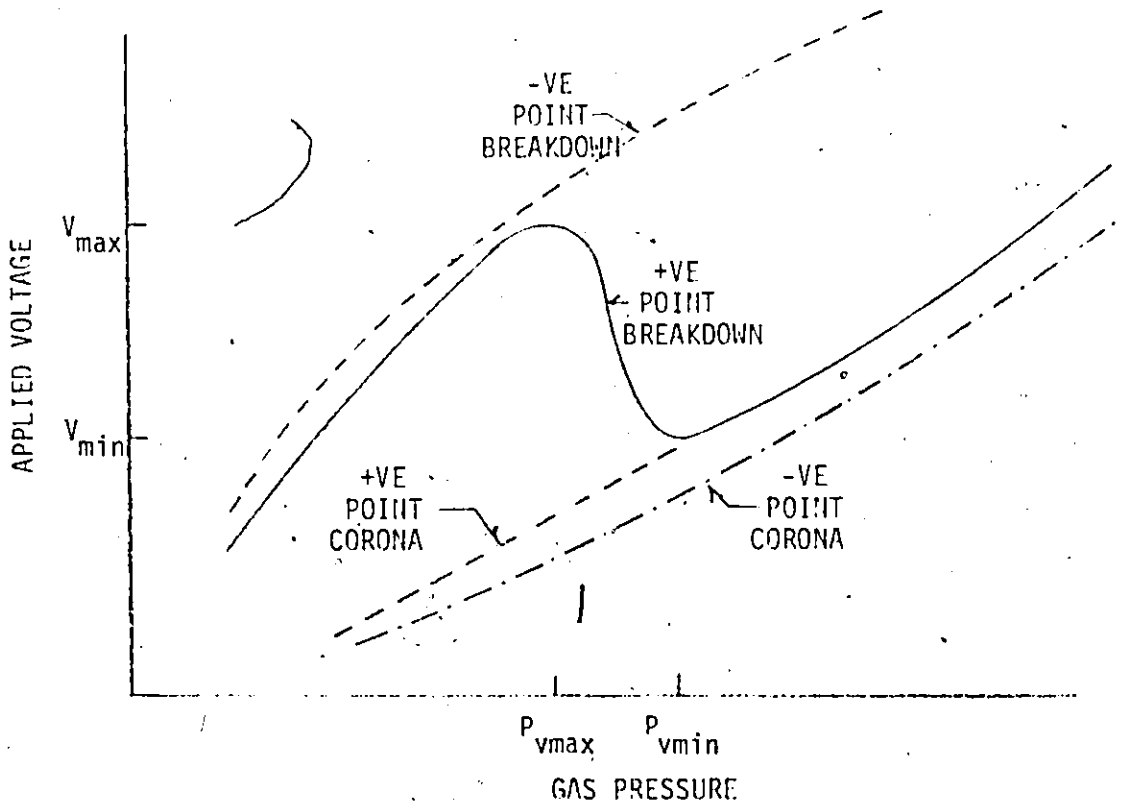

FIGURE 1.1. BREAKDOWN AND CORONA CHARACTERISTICS OF POINT-PLANE GAPS INSULATED WITH ELECTRONEGATIVE GASES.

All of the gases exhibited a negative point corona onset voltage which was consistently lower than that of the positive point at the same gas pressure. At pressures below

P_{vmax}, some of the cases exhibited a negative point breakdown voltage which was lower than the corresponding positive point breakdown strength. However, the negative point breakdown strength was observed in all cases to be superior at pressures exceeding P_{vmax}.

Pollock and Cooper also conducted oscillographic studies of corona current in the positive point-plane gap. They reported that isolated streamer pulses were observed at the threshold voltage of corona initiation in the gas. At voltages slightly greater than the threshold level, isolated burst pulses appeared, generally preceded by a single streamer. Steady burst activity resulted from a further increase of the applied voltage.

Pollock and Cooper attributed the high breakdown strength and sustained burst corona observed at low pressure to the formation of a negative ion sheath which choked off individual streamers. Breakdown occurred when the streamers became so vigorous that the sheath could no longer completely inhibit their propagation. At higher gas pressures the ability of a streamer to propagate across the gap was enhanced and consequently the first streamer formed in the gas was able to completely bridge the gap and initiate a breakdown. This would account for the sudden decrease in dielectric strength with increasing gas pressure and the lack of corona activity prior to breakdown at high gas pressures.

Foord (3) reported observing breakdown sparks of pronounced curvature in an SF_6 insulated positive point-plane gap at pressures between P_{vmax} and P_{vmin}. He suggested that the gas pressure has several effects on streamer propagation. The diffusion coefficient of electrons is in inverse proportion to the gas pressure and this causes a greater field distortion at the streamer tip and enhanced photon production at higher gas pressure. The photon absorption coefficient of the gas is also in inverse proportion to the gas pressure and this, along with the effects of reduced electron diffusion, results in an enhancement, with increasing gas pressure, of the streamer's ability to propagate.

Foord proposed that the corona observed at low gas pressures plays two roles in enhancing the sparking potential of the gas. The spread of the corona discharge over the anode surface effectively increases the radius of the point electrode and consequently decreases the non-uniformity of the field. Secondly, positive ions produced by the corona discharges form a mid-gap space charge which further reduces the electric field gradient at the anode surface. At pressures greater than P_{vmax} the enhancement of propagation properties is sufficient to allow streamers to follow low field paths, thus circumventing the space charge. The shielding effect of the positive ion space charge is reduced at higher pressures as a result of a reduced diffusion of the positive ions and consequently streamers are

capable of circumventing the space charge at lower applied potentials. Thus the negative slope region of the sparking voltage-pressure characteristics is observed. At pressures above P_{vmin}, the initial discharge phenomenon in the gas coincides with a complete breakdown. In this case the breakdown streamers do not encounter a space charge and hence the observed spark channel is straight.

Foord (4) investigated the properties of N_2-SF_6 gas mixtures insulating a positive point-plane electrode system. With the partial pressures of SF_6 constant and N_2 varying, the system displayed sparking voltage-total pressure characteristics which were basically the same as those of the 100% SF_6 system. An increase in the partial pressure of SF_6 increased the breakdown strength of the system for any total pressure. However, the total pressure at which the minimum breakdown voltage occurred was relatively unaffected by this parameter variation. The maximum corona current prior to breakdown at any gas pressure below P_{vmin} appeared to be directly proportional to the N_2 partial pressure.

Works and Dakin (5) investigated the effect of gap length on the sparking voltage of a 1/16 inch diameter hemispherical rod-plane electrode configuration insulated with compressed SF_6. The breakdown voltage-pressure characteristics of this system displayed a negative slope region under AC voltages and DC voltages with the rod of positive polarity. Of the four quantities which characterize the

negative slope region, V_{max}, V_{min}, P_{vmax}, and P_{vmin}, only P_{vmax} was significantly different in the AC and DC tests. The DC breakdown characteristics exhibited a P_{vmax} which decreased with increasing gap length while the AC characteristics exhibited a P_{vmax} which remained virtually the same at all gap lengths. This resulted in a difference in the pressures for maximum AC and DC breakdown strength which increased with increasing gap length. A detailed comparison of positive and negative point DC and AC breakdown and corona inception voltages was obtained for one electrode configuration and is reproduced in Figure 1.2.

The authors (5) reported encountering difficulties in determining breakdown voltages at pressures between P_{vmin} and P_{vmax} under positive point DC voltages. The system appeared to possess two distinct breakdown levels and sparking voltages were recorded at each, but breakdown never occurred at a voltage between these two levels.

In a subsequent paper, Berg and Works (6) reported on the behavior of an SF_6 insulated 1/16 inch diameter hemispherical rod-plane system subjected to a DC voltage plus a superimposed (1.5×40 μsec) impulse voltage, both of positive polarity. At gas pressures below P_{vmin} they observed that the peak value of combined voltage at which sparking occurred was independent of the relative magnitudes of the DC and impulse voltage components, provided that the DC level was below the corona onset voltage. At DC levels above corona onset

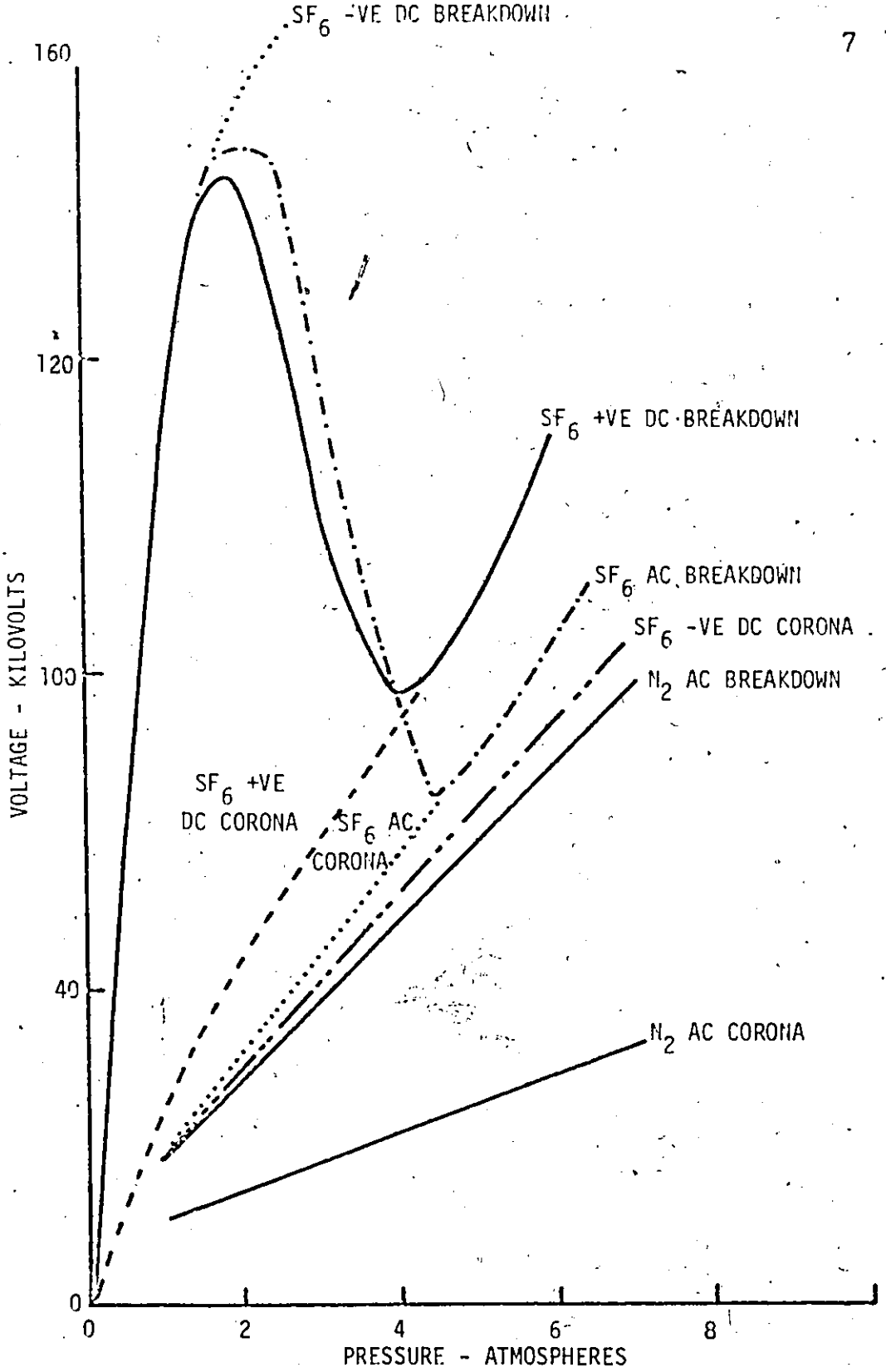

FIGURE 1.2. BREAKDOWN AND CORONA ONSET VOLTAGES OF A 1/16 INCH DIAMETER ROD-PLANE GAP OF 1.0 INCH LENGTH (FROM REFERENCE 5).

(the impulse was applied while a corona discharge was present in the gas), the peak value of the combined voltage at which breakdown occurred increased with an increase of the DC component. This behavior was observed at DC levels up to the DC breakdown voltage of the system. At gas pressures higher than P_{vmin}, sparking occurred at a constant peak value of combined voltage, independent of the DC level. Berg and Works believed that the results experimentally confirmed that corona stabilized breakdown[1] was a result of space charge distortion created by corona discharges in the gas. They explained the results as follows:

> When the system was subjected to an impulse voltage plus a DC voltage below the corona onset level, the space charge free breakdown level was reached before a stabilized space charge was established. Consequently, sparking occurred at a voltage lower than the DC breakdown voltage of the system. Under a combined voltage with a DC component above the corona onset level, the space charge was established before the total voltage reached the space charge free breakdown level and as a result, breakdown occurred at an enhanced voltage. An increase in the DC component resulted in an increase of the magnitude of the space charge and hence an increase of the breakdown voltage of the system.

---

[1] "Corona stabilized breakdown" is a term introduced by Camilli et al (7) in reference to the SF_6 pressure range at which breakdown is at an appreciably higher voltage than the corona onset voltage.

Similar tests conducted on the same system, insulated with air, indicated that an increase in the DC voltage effected a decrease in the peak value of the combined voltage at which breakdown occurred. The presence of a corona discharge did not appear to be of importance in this case and the breakdown behavior was explained as follows:

Breakdown of the system occurred when the applied voltage exceeded the breakdown voltage for a period exceeding the statistical and formative time lag of the breakdown process. As Figure 1.3 illustrates, for a given peak value of applied voltage and a given breakdown level, the duration of the overvoltage increased with increasing DC component. Therefore, if the duration of the overvoltage is important in determining whether or not a breakdown occurs, an increase in the DC level should have reduced the peak value of applied voltage at which breakdown occurred. The fact that this behavior was not observed in SF_6 at DC levels below the corona stabilized level suggests that the time lags associated with breakdown in SF_6 are of much shorter duration than those in air.

Howard (8) has published a considerable amount of data obtained from AC, DC, and impulse breakdown and corona studies of a number of gases, including SF_6. The performance of each gas was examined over a wide range of pressures and electrode configurations. The positive DC sparking voltage-gas pressure curves obtained for an SF_6 insulated hemispherical rod-sphere

gap (0.198 and 5 cm diameters respectively) exhibited a decrease of P_{vmax} with increasing gap length similar to that reported by Works and Dakin.

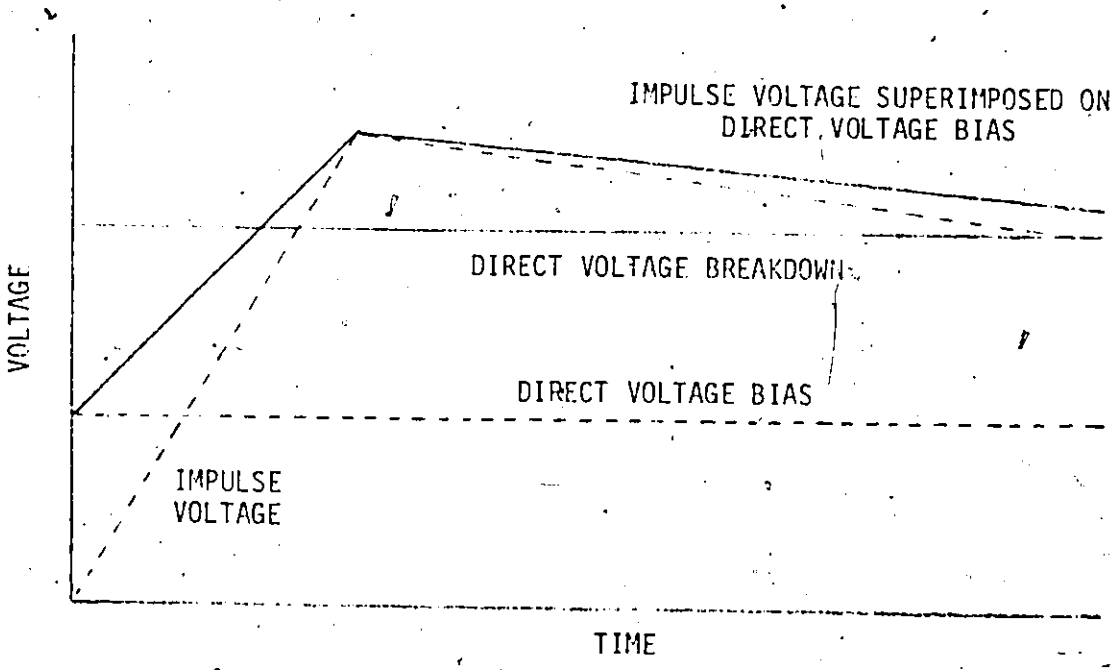

FIGURE 1.3. EFFECT OF DC BIAS ON IMPULSE OVERVOLTAGE TIME DURATION.

In a subsequent paper, Howard (9) discussed the processes contributing to breakdown in electronegative gases. He proposed that breakdown or corona onset occurs when

$$(E/p) = (E/p)_{crit} \qquad (1.1)$$

where $(E/p)_{crit}$ = ratio of electric field to pressure at which the ionization and attachment coefficients of the gas are equal

E = field at the high stress electrode

p = gas pressure.

This discharge onset criteria for non-uniform fields is essentially an extension of the condition for uniform field breakdown in electronegative gases proposed by Geballe and Reeves (10).

Measurements of ionization and attachment coefficients by Bhalla and Craggs (11) yield an $(E/p)_{crit}$ value of 86.1 kv cm/kg for SF_6.

Howard tested his hypothesis by determining the theoretical discharge onset voltage of the point-plane system used in his experimental work when insulated with SF_6, difluorodichloromethane, and carbon tetrachloride at various pressures. The calculation of the electric field at the rod tip was based on the assumption that the electric field distribution along the symmetry axis and in the vicinity of the hemispherical rod was that of a hyperboloid point-plane geometry; that is, at a distance x from the point

$$E = \frac{2V}{R \log_e 2x/R} \qquad (1.2)$$

where R = radius of the rod.

The theoretical discharge inception values corresponded quite closely to the experimental corona onset voltages at gas pressures below P_{vmin}, and to the experimental breakdown voltages at higher pressures. Howard also calculated theoretical discharge inception levels for the test systems used by Foord, Works and Dakin, and Pollock and Cooper,

however, the theoretical and experimental results were not always in good agreement.

In a discussion of the negative slope region of the sparking voltage-pressure characteristics of electronegative gases, Howard suggested that the increase of photoabsorption with increasing gas pressure is the most important factor enabling streamers to propagate through low field regions at the higher gas pressures. He proposed that a positive ion accumulation in the gas causes avalanche activity at the cathode, and also effects an increase in the breakdown voltage by establishing a low field barrier to streamers advancing from the anode.

Breakdown occurs when avalanche activity at the cathode produces negative ions at a rate sufficient to neutralize the positive ion barrier, at least locally, and allow streamers to penetrate and initiate a spark. The neutralization would occur in a random fashion allowing streamers to penetrate any part of the positive ion space charge. Those streamers penetrating the outer regions would initiate sparks displaying a considerable degree of curvature. Sparks of high curvature have been observed experimentally in the negative slope region.

Pedersen (12) proposed a streamer breakdown criterion for electronegative gases which he considered applicable to SF_6 insulated electrode systems subjected to steep fronted impulses, and as such precluded the development of a Townsend

breakdown. The basis for his proposed criterion is the assumption that an avalanche-streamer transition occurs when photon production within the avalanche head reaches a critical value It was originally proposed by Hopwood (13) that the most probable source of photons is electron-positive ion recombination reactions within the avalanche head. On this basis the rate of photon production can be determined from the equation

$$\frac{dn_p}{dt} = \beta N_e N_+ \tag{1.3}$$

with

$$N_+ = \frac{\alpha_x N_e dx}{\pi r^2 dx} = \frac{\alpha_x N_e}{\pi r^2}$$

where n_p = number of photons

β = radiative recombination coefficient

N_e = total number of electrons in avalanche head

N_+ = volume density of positive ions

r = radius of the avalanche head

α = ionization coefficient

Assuming a critical rate of photon production of value k, an avalanche-streamer transition occurs when

$$\alpha_x N_e^2 = \frac{\pi r^2 k}{\beta} \tag{1.4}$$

Substituting $N_e = \exp\left[\int_0^x (\alpha-\eta)dx\right]$, where η is the attachment coefficient, and rewriting the equation in logarithmic form, the streamer inception criterion simplifies to

$$\frac{1}{2}\ln(\alpha_x) + \int_0^x (\alpha-\eta)dx = f(x,p) \tag{1.5}$$

Assuming that α_x and $f(x,p)$ are relatively insensitive to variations in x and p, the streamer inception criterion further simplifies to

$$\int_0^x (\alpha - \eta)dx = K \qquad (1.6)$$

where K is a constant. Pedersen estimated the value of K to be 18. The streamer inception voltage corresponds to the breakdown or corona inception voltage depending on degree of field non-uniformity.

Pedersen compared theoretical and experimental breakdown values of a 5 cm sphere-sphere electrode configuration of 0.5 and 1.0 gap lengths, insulated with SF_6 at various pressures. A favourable comparison was obtained.

The performance of compressed SF_6 insulation in long non-uniform field gaps subjected to AC, impulse, and switching surge voltages has been the subject of a number of studies conducted recently in Japan. Kawaguchi et al (14) determined the theoretical breakdown strength of SF_6 for a number of field configurations of slight non-uniformity. They based their calculations on the assumption that breakdown occurs when the maximum electric field gradient in the gas reaches a critical value given by

$$E_{crit} = 86.1p \text{ kv/cm}$$

where p is the gas pressure in kgm/cm^2. A numerical

technique was adopted for the calculation of the electric field distribution in the gas. A comparison with experimental results indicates that this method yielded a reasonably accurate prediction of the dielectric strength of the system when the highly stressed electrode was of positive polarity, or when the gas was at atmospheric pressure. It otherwise appeared that field emission lowered the breakdown voltage to well below the theoretical value.

Nitta and Shibuya (15) developed the following theoretical formulation for predicting the breakdown or corona onset voltage V_s for gaps in SF_6,

$$V_s = \left(\frac{E}{p}\right)_{crit} \cdot u \cdot p \cdot L \left(1 + \frac{k}{\sqrt{pR}}\right) \qquad (1.7)$$

where $k = 0.175$ atm$^{\frac{1}{2}}$ cm$^{\frac{1}{2}}$

R = radius of curvature of highly stressed electrode in cm.

u = ratio of average to maximum electric stress in the gap.

L = gap length in cm.

p = gas pressure in atm.

The development of this equation was based on the following assumptions:

1. an avalanche-streamer transition occurs when the number of electrons in an avalanche reaches a critical number, namely 10^8,

2. avalanches only occur in the vicinity of the highly

stressed electrode in a volume in which the ionization coefficient of the gas exceeds the attachment coefficient,

3. the electric field distribution near the surface of the highly stressed elctrode is the same as the field distribution between concentric spheres with a) the inner sphere possessing the same radius of curvature as the highly stressed electrode at the point of maximum electrical stress and b) a gradient at the surface of the inner sphere equal to the maximum surface gradient of the highly stressed electrode.

Breakdown and corona onset calculations based on the above formulation were in close conformity with experimental results for sphere-sphere and rod-rod gaps subjected to AC voltages, at gas pressures below 4 atm. At higher pressures breakdown occurred at voltages considerably lower than the theoretically predicted values. This discrepancy was also observed at lower pressures when roughened electrodes were used. In the more non-uniform fields, the theoretical values corresponded to the corona onset voltages.

A similar theoretical analysis was performed by Takuma and Watanabe (16). A favourable correlation was achieved between the theoretical and experimental breakdown voltages of sphere-plane gaps subjected to positive switching surges of 400 μsec wavefront duration. Negative surge breakdown voltages were however considerably lower that the theoretical values.

Takuma and Watanabe (17) also investigated the switching surge flashover characteristics of very long (50 cm), highly non-uniform gaps in compressed SF_6. They obtained unexpectantly low breakdown voltages, in some cases lower than that of a comparable air insulated system. They attributed this to a modification of the electric field distribution by a migrating space charge resulting from corona activity. This field modification was more significant in SF_6 than in air, accounting for the reduced dielectric strength of SF_6 relative to that of air.

1.2 SF_6 and High Voltage Engineering

Since 1940, when SF_6 first became of technological interest as a high voltage gas insulation, the type and number of high voltage apparatus employing SF_6 as a component of their insulation system has increased significantly. At present, total substations insulated with compressed SF_6 are being constructed. The widespread application of SF_6 is reason alone to conduct studies which further the understanding of its insulation properties, not only with respect to AC and impulse voltage stressing, but under DC stress conditions as well. SF_6 should play an increasingly significant role in the insulation of high voltage DC apparatus and distribution systems. Also, current trends indicate the construction of progressively larger SF_6 insulated AC substations in the future. It is probable that field testing of such installations will be conducted under DC

voltages in order to circumvent the difficulties incurred by the increased charging current demands of the larger substations.

The dielectric strength of SF_6 relative to air at the same pressure varies widely, with values ranging approximately from 0.7 to 4.0; it is a function of many parameters, with the time and spatial variation of the electric field stressing the gas being the most important. Therefore, it is not generally feasible to assess the performance of SF_6 by consulting the host of data available on the high voltage insulation properties of air.

Intelligent design of high voltage equipment employing SF_6 insulation requires a thorough understanding of the properties of the gas subjected to a wide variety of conditions. A study of the literature indicates that deficiencies of information exist in many areas of SF_6 insulation behavior.

Several authors have reported considerable success in calculating the performance of SF_6 insulation subjected to AC and impulse voltages under a variety of stress configurations. The calculations are based on relatively simple discharge onset criteria and, depending on the gas pressure and field non-uniformity, yield either the minimum breakdown or corona onset voltage of an SF_6 insulated electrode system. It is of importance to determine whether these calculation techniques can yield an accurate prediction of SF_6 performance under DC stress.

There is relatively little information in the literature on the nature of corona discharges in SF_6. An important aspect of design of the high voltage equipment insulated with SF_6 is the prevention or minimization of corona discharge activity. Consequently, a thorough understanding of the corona related properties of SF_6 is required. Also, the aforementioned calculations of the performance of SF_6 insulated systems yield minimum corona onset voltages for a range of pressure-field non-uniformity conditions. Exactly how these calculated voltages relate to the corona discharge characteristics of the system is unclear.

1.3 Scope of Work

The principal objective of this work is to contribute information which will further the understanding of the performance of SF_6 as a high voltage insulation. To this end the following studies were conducted:

1. An experimental study was made of breakdown and corona discharge phenomena in sphere-plane and hemispherically capped rod-plane gaps of different radii and gap lengths, insulated with SF_6.

2. Theoretical breakdown and corona onset voltages of the experimental systems were determined using various streamer onset and breakdown criteria proposed in the literature. This necessitated the development of several special techniques to perform calculations based on these criteria. An assessment was made of the applicability of

these criteria on the basis of a comparison between experimental and theoretically predicted results of the same system.

3. A corona free breakdown[1] criterion was developed and assessed by comparing the theoretically calculated and experimentally determined pressure at which the initial discharge activity coincided with a breakdown for each system tested.

Throughout the experimental investigations DC voltages were used, with the non-uniform electrode of positive polarity. Gas pressures ranged from a minimum of one atmosphere to a maximum of five atmospheres. This is the pressure range of greatest technical importance. Sphere-plane and hemispherical rod-plane electrode systems were used in the investigations because they allow visual observation of the highly stressed region of the gap. Also, such systems do not present the alignment and fabrication difficulties inherent to concentric cylinders and confocal paraboloid gaps.

1.4 Organization of Dissertation

Chapter I summarizes past studies which are relevant to the investigation treated in the dissertation.

Chapter II describes the various components of the system used to perform the experimental investigations.

---

[1] A corona free breakdown is a breakdown occurring in the absence of prebreakdown current pulses exceeding 0.5 microamperes peak, and in the absence of an average current exceeding 10^{-10} amperes.

Chapters III and IV summarize the results of experimental studies of prebreakdown and breakdown phenomena.

Chapter V discusses discharge phenomena in SF_6. The discussions are based on the experimental findings of the present investigation and the experimental results of other studies and theoretical discussion of SF_6 insulation found in the literature.

Chapter VI describes the calculations of the theoretical performance of the experimental systems based on streamer onset and breakdown criteria found in the literature. The theoretical prediction of the minimum gas pressure coinciding with the corona free breakdown is also discussed.

Chapter VII presents an overall summary of the findings of the present study.

CHAPTER II

EXPERIMENTAL SYSTEM

The experimental facilities can be considered as grouped into four main parts; the pressure vessel, pressure-vacuum system, current measurement circuitry, and high voltage circuitry.

2.1 Pressure Vessel

A sectional view of the pressure vessel used in the experimental work is illustrated in Figure 2.1. The cylindrical wall was in two sections with the lower section #9 of 0.25 inch thick stainless steel and the upper section #1 of 0.375 inch thick carbon steel. The upper cylinder functioned as an extension to accomodate the high voltage bushing. The base plate of the vessel was also of stainless steel material. The high voltage bushing was a General Electric 115 KVAC air blast breaker bushing. It was comprised primarily of two porcelain cylinders #7, #8, two end plates, a mounting flange, and a hollow conductor #6. The space enclosed by the porcelain cylinders and end plates was sealed from the atmosphere and from the pressure vessel. The bushing contained SF_6 gas at a pressure of 75 psig. The vessel was tested hydraulically at a pressure of 250 psig for a five hour duration.

Three of the four viewing ports #10 were utilized for visual observation of the discharge phenomena while the fourth served as a gas inlet port. The windows were

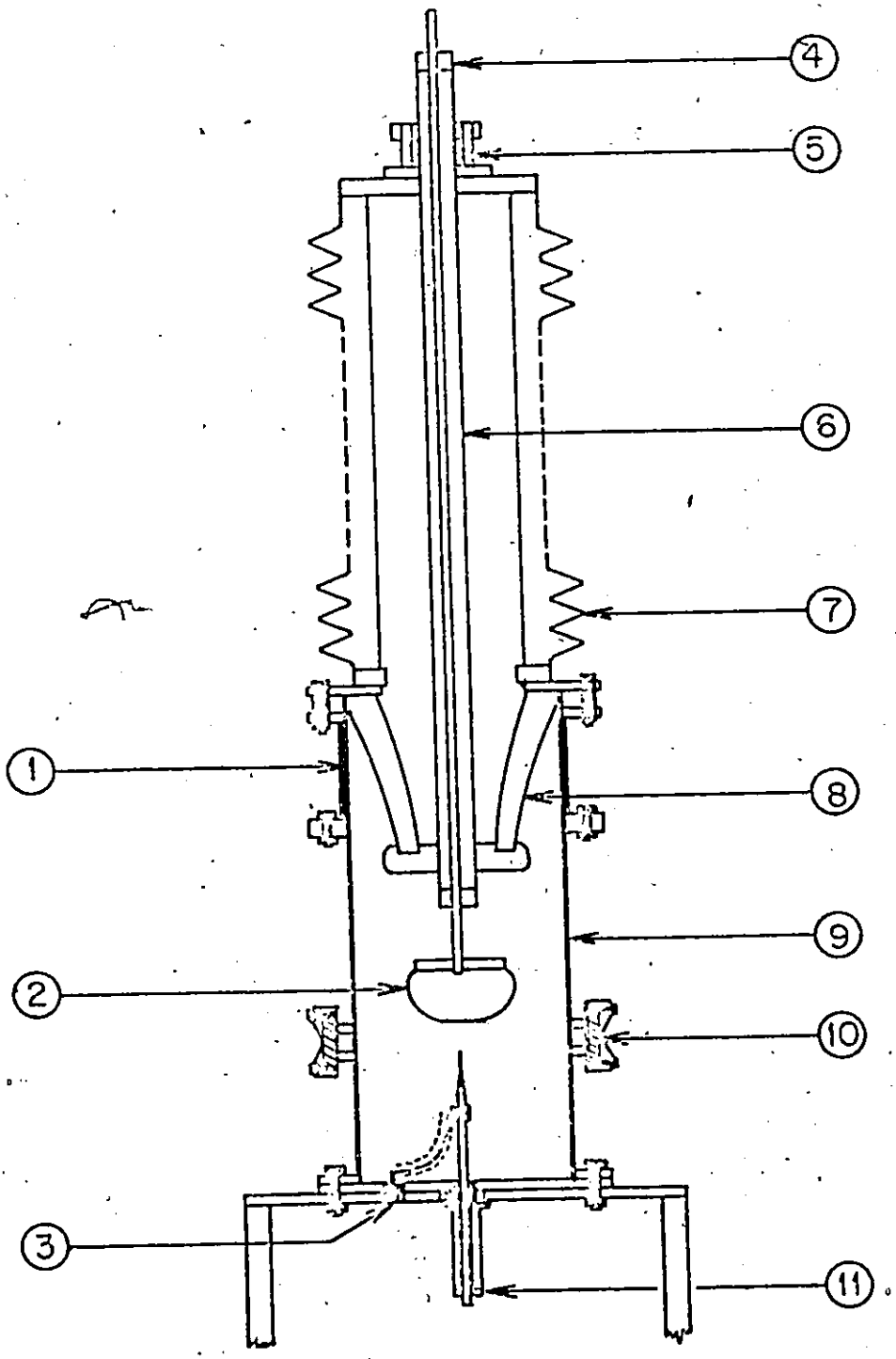

FIGURE 2.1. PRESSURE VESSEL AND ELECTRODE ASSEMBLY.

quartz disks, 2 inches in diameter and 1/2 inch thick. A gas discharge-vacuum port was located in the base plate; it is not shown in Figure 2.1.

The electrodes were attached to two 0.5 inch diameter connecting rods. The upper rod passed through the bushing conductor and both the upper end of the rod and the plug at the top of the conductor #4 were threaded with a 1/2 x 40 inch thread. With this arrangement, the rod was displaced vertically when rotated. A guage at the top of the bushing indicated the vertical displacement with a precision of .001 inch. The bottom rod passed through the base plate and possessed a similar threading arrangement #11 which was not utilized in the experiments.

The details of the electrode system are illustrated in Figure 2.2. The 5.28 inch diameter 90° Rogowski profile electrode served as the plane electrode in all of the experimental work. The different non-uniform field electrodes used in the investigations were attached to the connecting rod with an insulating plexiglass coupler. All of the non-uniform field electrodes and the Rogowski profile electrode were of brass material.

Before each test series, the electrodes were polished, first with a compound (Brasso) containing abrasive chalk of a maximum particle size of 20 microns, then with a 1 micron red rouge lapping compound, and finally with a 0.1 micron alumina particle distilled water compound. The electrode

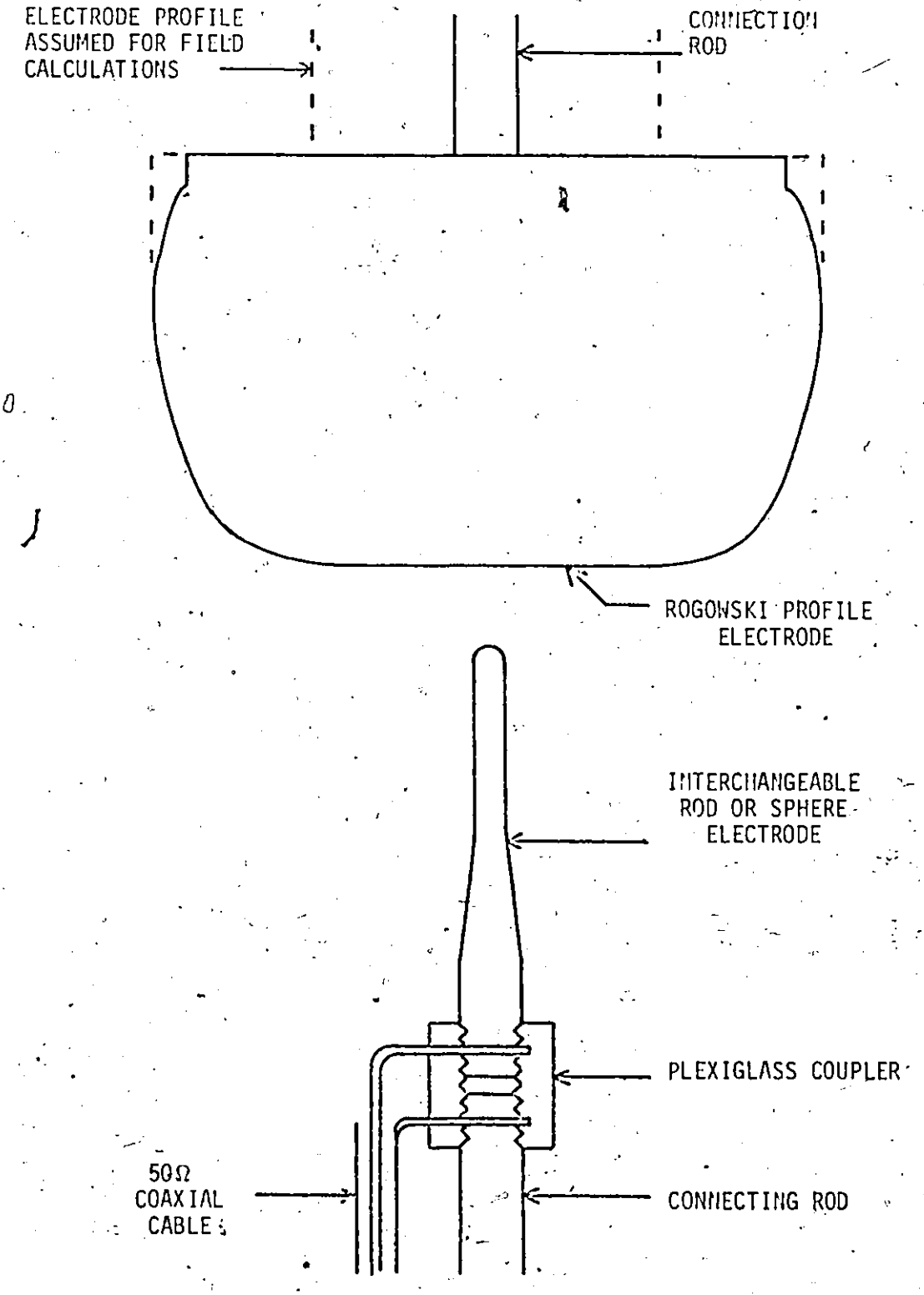

FIGURE 2.2. ELECTRODE ASSEMBLY.

surfaces were then degreased with acetone and freon solvents.

The low voltage electrode was electrically connected to a length of 50 ohm coaxial cable attached to a feed-thru in the base plate of the vessel (#3, Figure 2.1).

The gap length was adjusted by first carefully lowering the plane electrode until contact between the two electrodes was attained, as indicated by an ohmmeter. The gap length was then set by rotating the upper connecting rod the required number of revolutions, raising the plane electrode. Errors in the gap setting introduced by the tolerance limitations of the thread and the backlash were negligable. However, elongation of the vessel walls and warping of the base plate resulting from pressurization of the vessel had a considerable effect on the gap length. The variation of the gap length with pressure was measured and the results are shown in Figure 2.3. A correction factor was determined from the data and applied to the various calculations whenever it was considered significant.

2.2 Pressure Vacuum System

The pressure-vacuum system is schematically illustrated in Figure 2.4.

The pressure guages employed in the measurement of the gas pressure within the vessel were checked against test guages possessing an accuracy of 0.25%. When measuring the gas pressure of the same line, the discrepancy between the indications of the test guage and the system guage (the guage

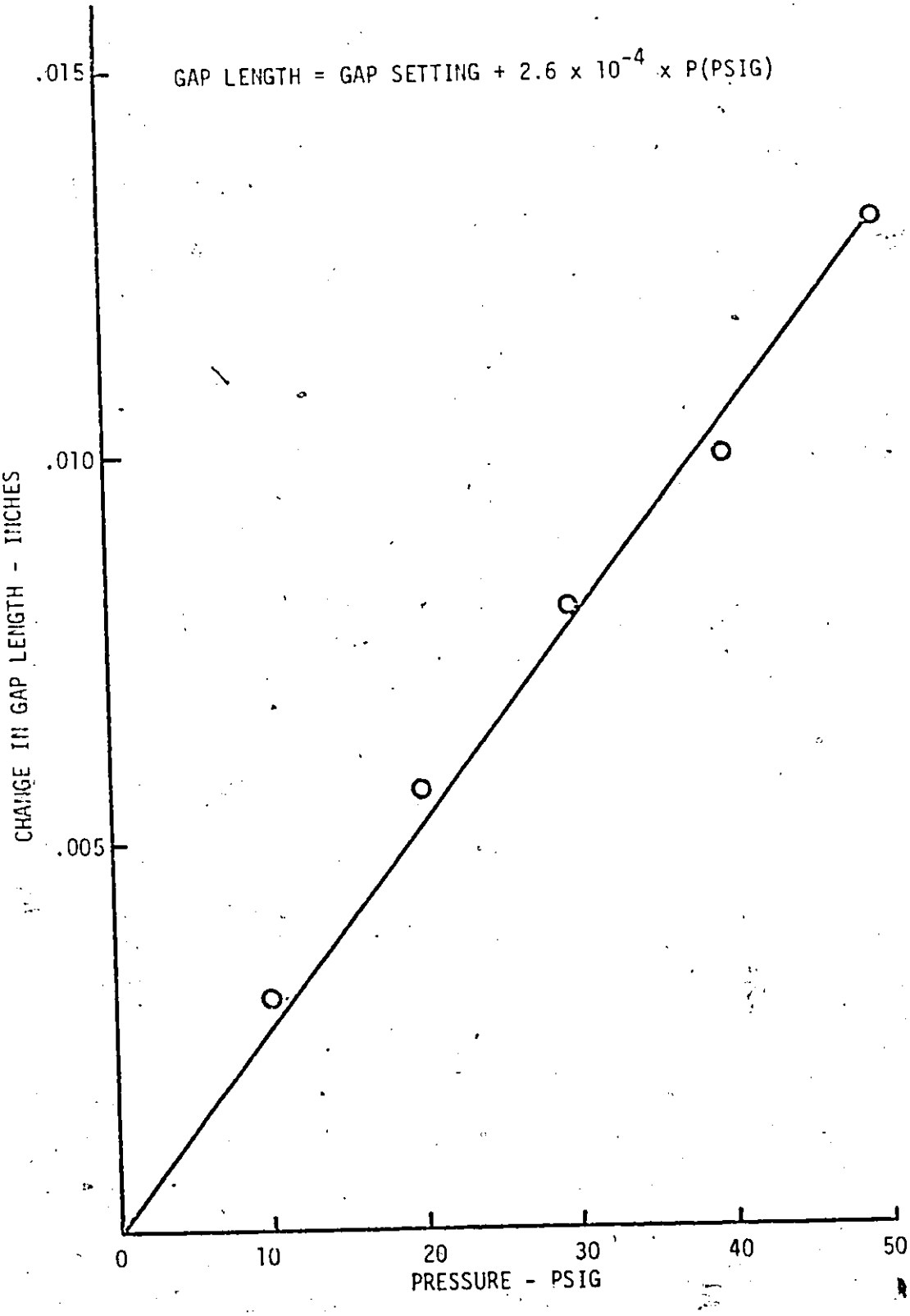

FIGURE 2.3. EFFECT OF GAS PRESSURE ON GAP LENGTH.

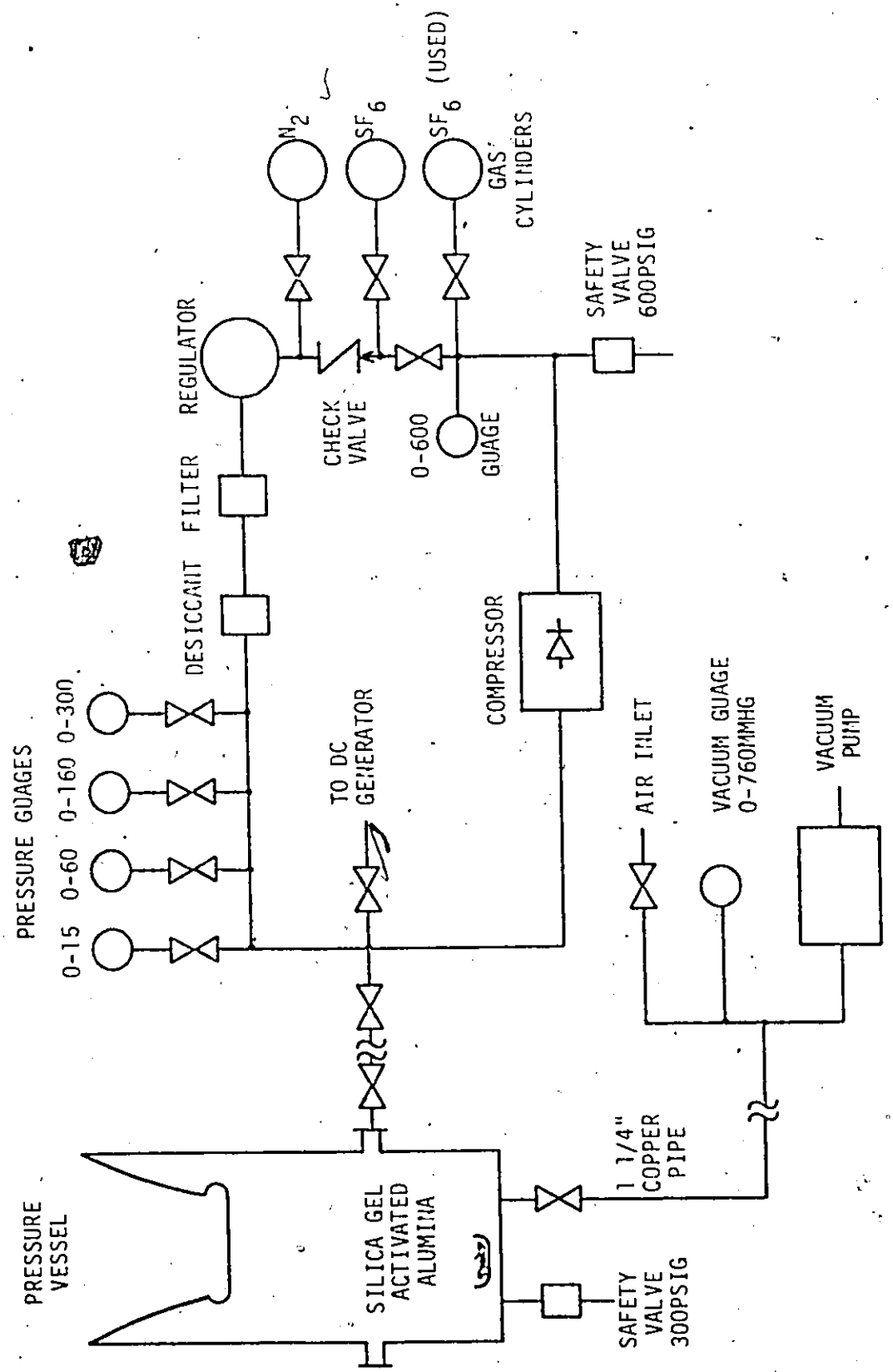

FIGURE 2.4. PRESSURE - VACUUM SYSTEM.

which gave an indication closest to full-scale) was at all gas pressures within 1% of the pressure indicated by the test guage. The guages indicated the gas pressure in pounds per square inch guage. The absolute pressure of the gas within the vessel was determined by adding the pressure indicated by the guage system to the atmospheric pressure of the laboratory which was measured by a mercury barometer.

The procedure adopted for the filling of the vessel with the test gas was as follows:

1. All surfaces within the vessel were subjected to a blast of N_2 from a commercial grade cylinder, just prior to final vessel assembly.

2. After assembly was complete, the vessel was evacuated and subsequently filled with commercial grade N_2.

3. The vessel was then evacuated to a pressure of approximately 0.01 torr, as measured by a McLeod guage attached to the gas inlet port, and remained in this evacuated state for several hours.

4. The vessel was filled with the test gas to the desired pressure.

5. The vessel was always pressurized with the test gas at a pressure greater than atmospheric when not in use.

The SF_6 used in the tests was of commercial purity (99.8% minimum) and was manufactured by The Matheson Company Inc. Gas admitted to the pressure vessel was first passed through a 0.03 micron filter and subsequently through a gas

purifier containing a desiccant which ensured that the dew point of the gas was no greater than -100°F. A porcelain dish containing silica gel and activated alumina was placed in the pressure vessel just prior to the final assembly of the vessel after each change of electrode. The silica gel served as a desiccant and the activated alumina removed corrosive gas compounds which resulted from electrical discharges in the gas.

Because of the relatively high cost of the commercial grade SF_6, a gas reclaiming system was utilized. The compressor used to transfer the test gas from the pressure vessel to a storage cylinder was a gas pressure booster and operated on the laboratory's compressed air supply. It was theoretically capable of pumping gas up to pressures of 1000 psig. The booster required no lubricant and this essentially eliminated any possibility of test gas contamination in the reclaiming process.

2.3 Current Measurement Circuitry

Current flow in the test circuit resulting from discharges in the gas was measured with a microammeter inserted in series with the test gap or with an oscilloscope displaying the voltage drop across a resistor or cable impedance in series with the gap. The microammeter was capable of measuring DC currents of magnitudes ranging from 1 microampere to 1 milliampere and was utilized when information on the DC level of the corona current was required.

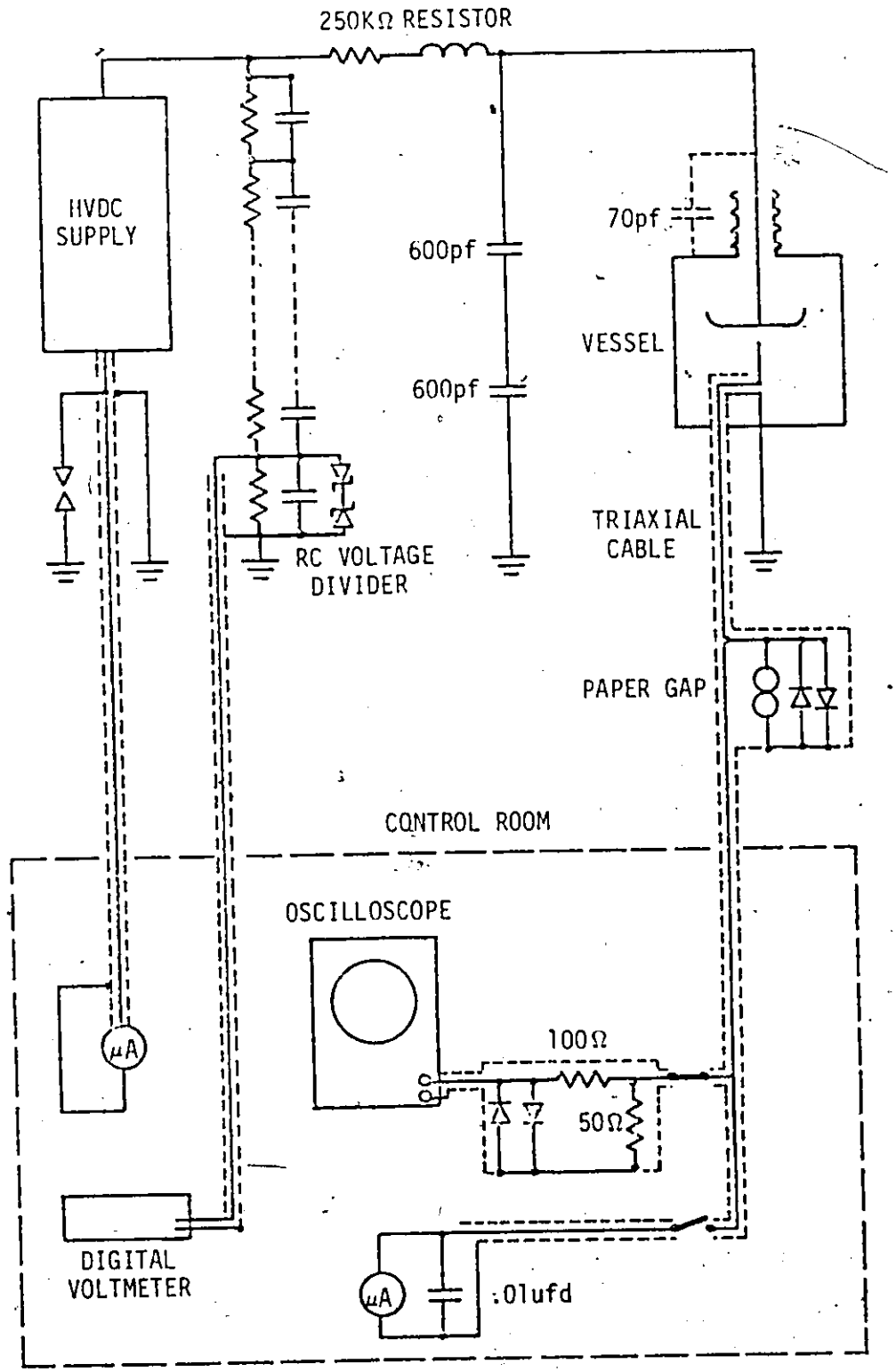

FIGURE 2.5 SCHEMATIC OF HIGH VOLTAGE AND MEASUREMENT CIRCUITRY.

The oscillographic studies were conducted utilizing a Textronix 549 storage oscilloscope with a 1A1 or 1A7A plug-in unit, a Hewlitt Packard 183A oscilloscope, and a Hewlitt Packard 462A amplificr. The 1A7A unit is a high gain, low noise amplifier with adjustable bandwidth and a maximum rise-time of 350 nanoseconds. The use of this unit permitted the measurement of currents as low as 2×10^{-10} amperes at a bandwidth of 10 hz. The risetimes of the 549 oscilloscope with the 1A1 plug-in, the 183A oscilloscope, and the 462A amplifier are 13 nsec, 1.4 nsec, and 4 nsec respectively. Figure 2.5 gives the schematic representation of the high voltage and discharge current measurement circuitry.

The triaxial cable which connected the low voltage electrode in the pressure vessel to the oscilloscope or microammeter was approximately 8 meters in length. It was therefore necessary to terminate the cable with its characteristic impedance when examining the high frequency components of the discharge current. This eliminated distortion of the waveform which reflections at the cable terminations would otherwise introduce and limited the maximum value of the resistance in series with the gap to the characteristic impedance of the cable (50 ohm).

The electromagnetic field in the laboratory due to external sources induced a substantial RF noise voltage in the high voltage circuitry. This voltage generated a displacement current in the test gap which, in addition to the

corona current, was detected by the measurement apparatus. The magnitude of the detected noise current was a function of the bandwidth of the measurement apparatus and the capacitance of the test gap. Table 1.1 gives noise current values for a 1/16 inch diameter rod-plane gap of 1.5 inch gap spacing as a function of the oscilloscope bandwidth.

TABLE 2.1. THE EFFECT OF THE SYSTEM BANDWIDTH ON THE MAGNITUDE OF THE DETECTED NOISE CURRENT

System Bandwidth	Noise Current (μamp peak to peak)
1 KHZ	0.02
10 KHZ	0.06
100 KHZ	0.12
300 KHZ	0.2
1 MHZ	0.4
30 MHZ	2.
90 MHZ	12.
250 MHZ	20.

A paper gap and back to back diodes were included in the circuit for the purpose of protecting the oscilloscope from overvoltages resulting from a breakdown of the test gap.

2.4 High Voltage Circuitry

Figure 2.6 is a photograph of the experimental circuit. The high voltage bushing of the pressure vessel (foreground) was connected to the HVDC generator with a 4 inch diameter copper pipe and a 250 kilohm wirewound resistor which sat atop the bushing.

The output voltage of the HVDC generator is continuously variable from 0 - 1000 kv. The variations in this voltage due to ripple and regulation are within 0.01% of the output voltage for output currents from 0 - 2 milliamperes, the maximum available DC output current. A 300 picofarad, 1000 kv capacitor was included in the circuit and this appears in the left hand side of the figure. This capacitor was essentially in parallel with the test gap and its primary function was to increase the electrode capacitance ensuring that the discharges in the gap were not inhibited by lack of stored charge.

The output voltage of the generator (the gap voltage) was measured with a RC voltage divider coupled to a digital voltmeter. The divider ratio was calibrated with an electrostatic voltmeter accurate to ±0.5% of the applied voltage, at voltages below 50 kv, and with a 25 cm sphere gap in the voltage range 50 kv to 300 kv. The calibration assured an accuracy in the measurement of the applied voltage of within ±2% (18) for the range of voltages applied in the experimental work.

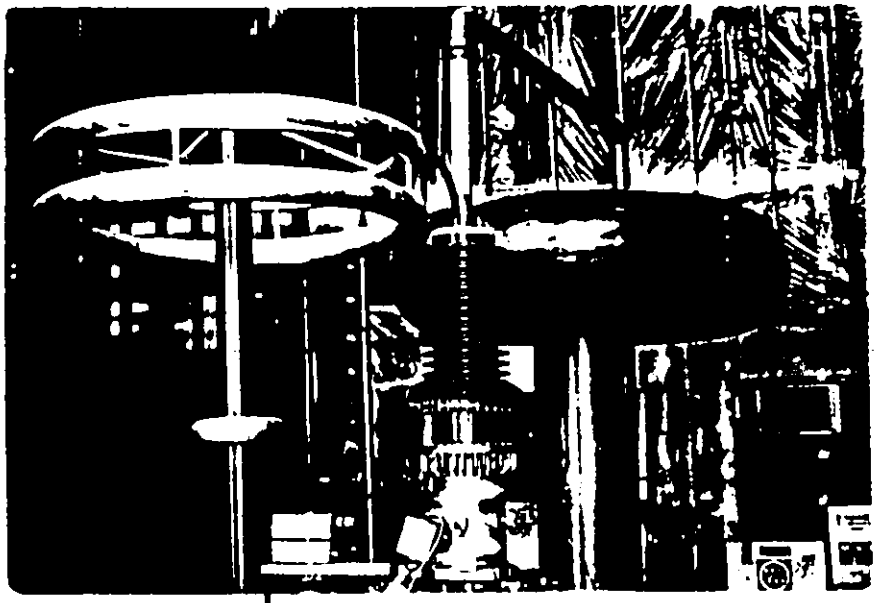

FIGURE 2.6. PHOTOGRAPH OF EXPERIMENTAL SET-UP..

CHAPTER III

PREBREAKDOWN DISCHARGE STUDIES

3.1 Nature of the Investigation

This chapter describes the results of an experimental investigation of prebreakdown discharge phenomena in hemispherical rod-plane gaps insulated with SF_6. The study encompassed gap lengths ranging from 0.25 to 1.5 inches and rod diameters of 1/16, 1/8, and 1/4 inch. The applied voltage was in all cases DC with the rod of positive polarity.

Discharge phenomena were examined primarily by measuring the total current flow in the gap, either with a microammeter in series with the gap or with an oscilloscope displaying the voltage across an impedance in series with the gap. A study was also conducted of the visual appearance of the discharge.

Prebreakdown current studies of a 2 inch diameter sphere-plane gap at voltages and gas pressures to 300 kv and 4.5 atmospheres respectively failed to detect any form of prebreakdown discharge current. These test results rule out the possibility that the discharges detected in other electrode configurations were at locations other than the test gap.

Unless otherwise stated, all oscillograms referred to in the discussion were obtained with the Tektronix 549 oscilloscope and 1A7A plug-in set at a pass band of 0-1 Mhz. The response of this system to a square voltage pulse of 50 nsec

risetime, applied between the low voltage electrode and ground, is illustrated in Figure 3.2, oscillogram #1. This oscillogram also indicates the writing capabilities of the system. Oscillogram #2 indicates the magnitude of the background noise detected by the system when the HVDC generator output was at zero volts.

Figure 3.1 illustrates the inception levels of the various types of prebreakdown discharge current activity observed in an SF_6 insulated 1/16 inch diameter rod-plane gap at a gap length of 1.5 inches. The corresponding data for other electrode configurations can be found in Figures 4.1 through 4.11. The discharge characteristics were observed to be of basically the same nature in all of the rod-plane configurations tested. However, the inception levels, the intensity, and the pressure range of these phenomena varied widely with changes in electrode radius of curvature or gap length.

3.2 Single Pulse Phenomenon

As the voltage applied to the gap was increased from zero volts, the first indication of discharge activity was a small current pulse detected by the oscilloscope. A typical pulse is illustrated in Figure 3.2, oscillogram #3. The pulse amplitudes varied randomly, however the maximum amplitude observed generally increased with increasing gap voltage.

A comparison of oscillograms #3 and #4 illustrates the degree of amplitude variations observed. Attempts to

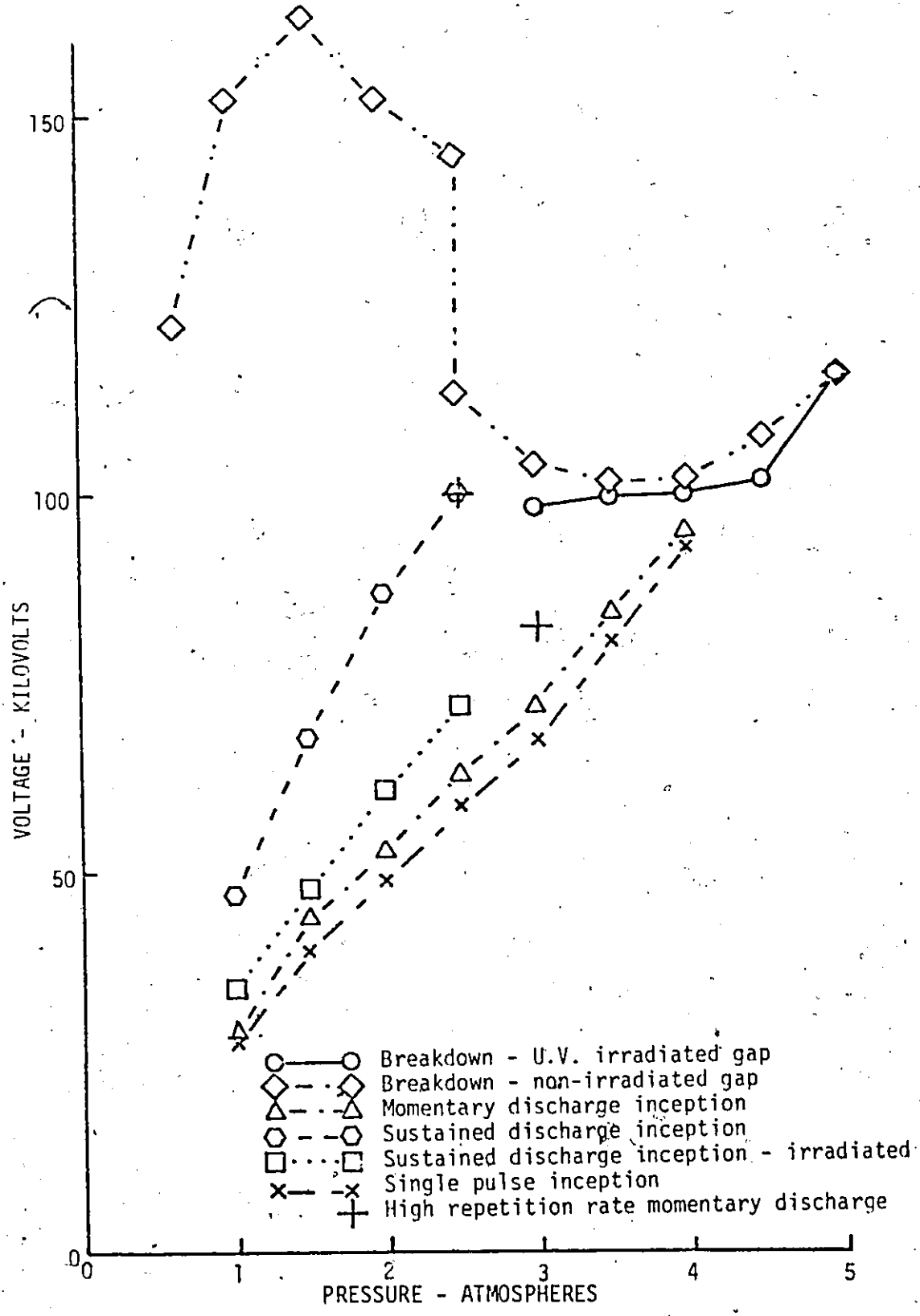

FIGURE 3.1. BREAKDOWN AND CORONA DISCHARGE INCEPTION VOLTAGES OF A 1/16 INCH DIAMETER ROD-PLANE GAP OF 1.5 INCHES LENGTH.

FIGURE 3.2 CORONA CURRENT OSCILLOGRAMS
(electrode dimensions specified as rod radius-gap length, both in inches)

1. SQUARE WAVE, 50 NSEC RISETIME
   1 μSEC/DIV HORIZONTAL

2. NOISE 1 MHZ BANDWIDTH
   1 μAMP/DIV, 2 μSEC/DIV
   ELECTRODE 1/16 - 1 1/2

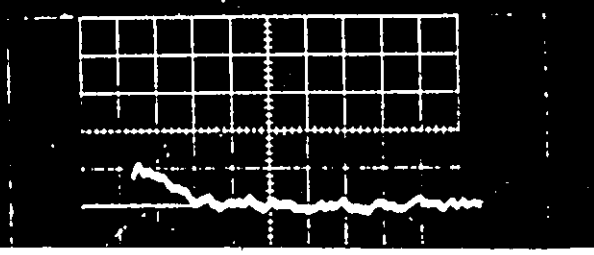

3. 1 μAMP/DIV, 1 μSEC/DIV
   P - 1 ATM, ELECTRODE 1/8 - 1/2
   V = 27 KV

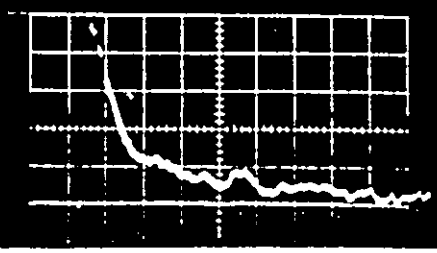

4. 1 μAMP/DIV, 1 μSEC/DIV
   P - 1 ATM, ELECTRODE 1/8 - 1/2
   V = 27 KV

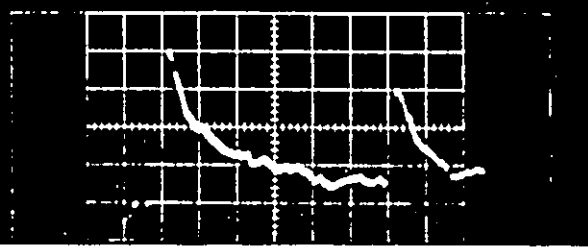

5. 1 μAMP/DIV, 1 μSEC/DIV
   P - 1 ATM, ELECTRODE 1/8 - 1/2
   V = 27 KV IRRADIATED WITH U.V.

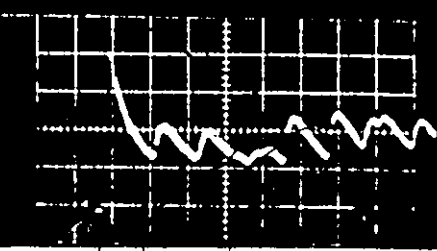

6. 4 μAMP/DIV, 1 μSEC/DIV
   P - 1 ATM, ELECTRODE 1/8 - 1/2
   V = 29 KV

7. 4 μAMP/DIV, 10 μSEC/DIV
   P - 1 ATM, ELECTRODE 1/8 - 1/2
   V = 29 KV

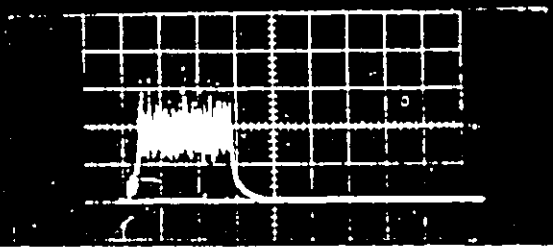

8. 10 μAMP/DIV, 200 μSEC/DIV
   P - 1 ATM, ELECTRODE 1/8 - 1/2
   V = 29 KV

9. 10 μAMP/DIV, 10 μSEC/DIV
   P - 1 ATM, ELECTRODE 1/4 - 1 1/2
   V = 70 KV

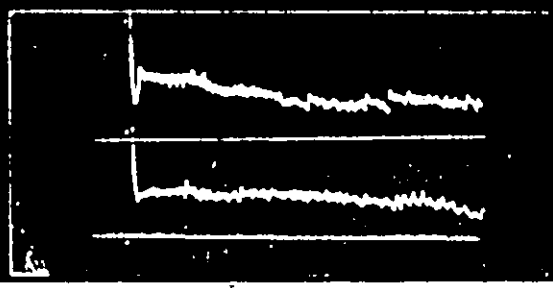

10. 20 μAMP/DIV, 5 μSEC/DIV
    P - 1.5 ATM, ELECTRODE 1/16 - 1/2
    V = 33 KV

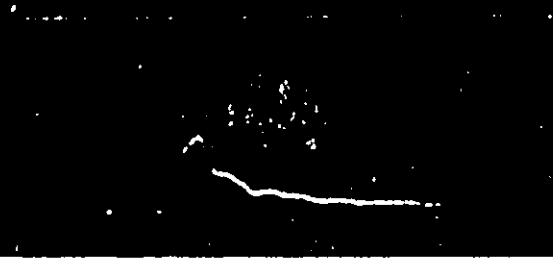

11. 1 MILLIAMP/DIV, 10 NSEC/DIV
    p - 1.5 ATM, ELECTRODE 1/16-1 1/2

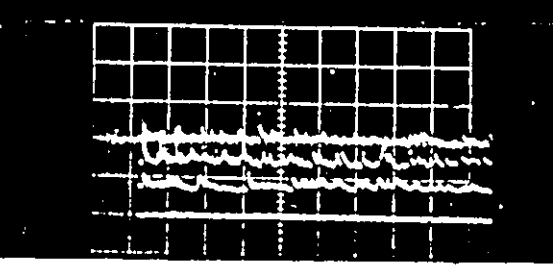

12. 20 μAMP/DIV, 10 μSEC/DIV
    p - 1.5 ATM, ELECTRODE 1/16 - 1/2

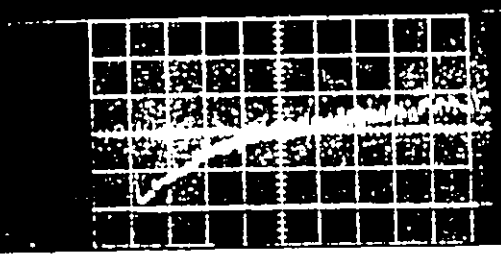

13. 20 μAMP/DIV, 10 μSEC/DIV
P - 1 ATM, ELECTRODE 1/4 - 1 1/2
V = 70 KV

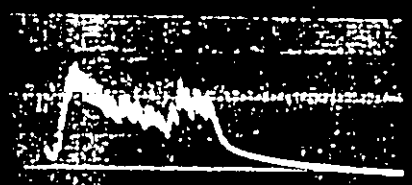

14. 10 μAMP/DIV, 100 μSEC/DIV
P - 1 ATM, ELECTRODE 1/4 - 1 1/2
V = 70 KV

15. 10 μAMP/DIV, 10 μSEC/DIV
P - 1 ATM, ELECTRODE 1/4 - 1 1/2
V = 70 KV

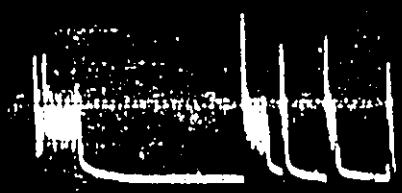

16. 4 UAMP/DIV, 1 mSEC/DIV
P - 3 ATM, ELECTRODE 1/16 - 1/2
V = 83 KV

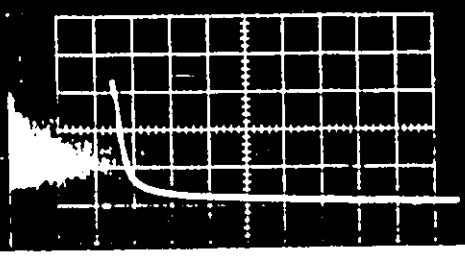

17. 100 μAMP/DIV, 1 μSEC/DIV
P - 1 ATM, ELECTRODE 1/16 - 1 1/2
NITROGEN GAS

record the pulse shapes at higher bandwidths were hampered by the accompanying increase in background noise level.

The pulses occurred at random intervals (in the order of minutes) with interval times apparently independent of voltage level. The average time duration between pulses generally increased with increasing gas pressures. Irradiation of the gap with 2537 Å ultraviolet light increased the repetition rate of pulses considerably at high gap lengths (1.0 - 1.5 inch) at gas pressures near atmospheric. The radiation had a negligible effect in shorter gaps or at pressures higher than two atmospheres. Also, the radiation affected neither the inception voltage of the pulse activity nor the pulse magnitudes.

At voltages slightly higher than the single pulse inception level, a discharge consisting of several pulses in rapid succession was occasionally observed. A discharge consisting of two pulses is illustrated in oscillogram #5.

3.3 Momentary Discharge Phenomenon

The next stage of corona development accompanying an increase in gap voltage was the appearance of what may best be termed a momentary discharge. Oscillograms #6, #7, and #8 of Figure 3.2 illustrate three such discharges recorded under identical test conditions with different oscilloscope sweep rates and vertical amplifier gains. At the inception voltage of this type of discharge the pulses appeared at random intervals, as in the case of the single pulses.

Several changes in the characteristics of the discharge were observed to accompany an increase in the applied voltage. Figure 3.3 illustrates a typical variation of pulse duration, pulse magnitude, and pulse repetition rate exhibited by one set of measurements in a gap subjected to an increasing voltage. The discharge amplitudes were determined with the 1A7A vertical amplifier filter set at a 30 Mhz bandwidth.

At a voltage level at or slightly above the inception level of momentary discharge activity, the initial pulse of a discharge invariably possessed a peak amplitude which was considerably smaller than the maximum amplitude displayed by the total discharge. The amplitude of the initial pulse increase, however, with an increase in applied voltage, to a value far greater than that of any of the subsequent pulses of the discharge. Oscillogram #9 of Figure 3.2 illustrates a pulse observed at a voltage near the onset level, while oscillogram #10 illustrates a pulse observed at a higher voltage. In the latter case the pulse peaks were of sufficient magnitude to be recorded at higher bandwidths. Oscillogram #11 records a discharge initiating pulse displayed on the Hewlett-Packard 183A oscilloscope. The Hewlett-Packard 462A amplifier was also included in the measurement circuit and the total system possessed a combined risetime of 4 nsec. Oscillogram #11 illustrates that the pulse magnitudes are much greater than indicated in the oscillograms obtained from the 1 Mhz bandwidth system.

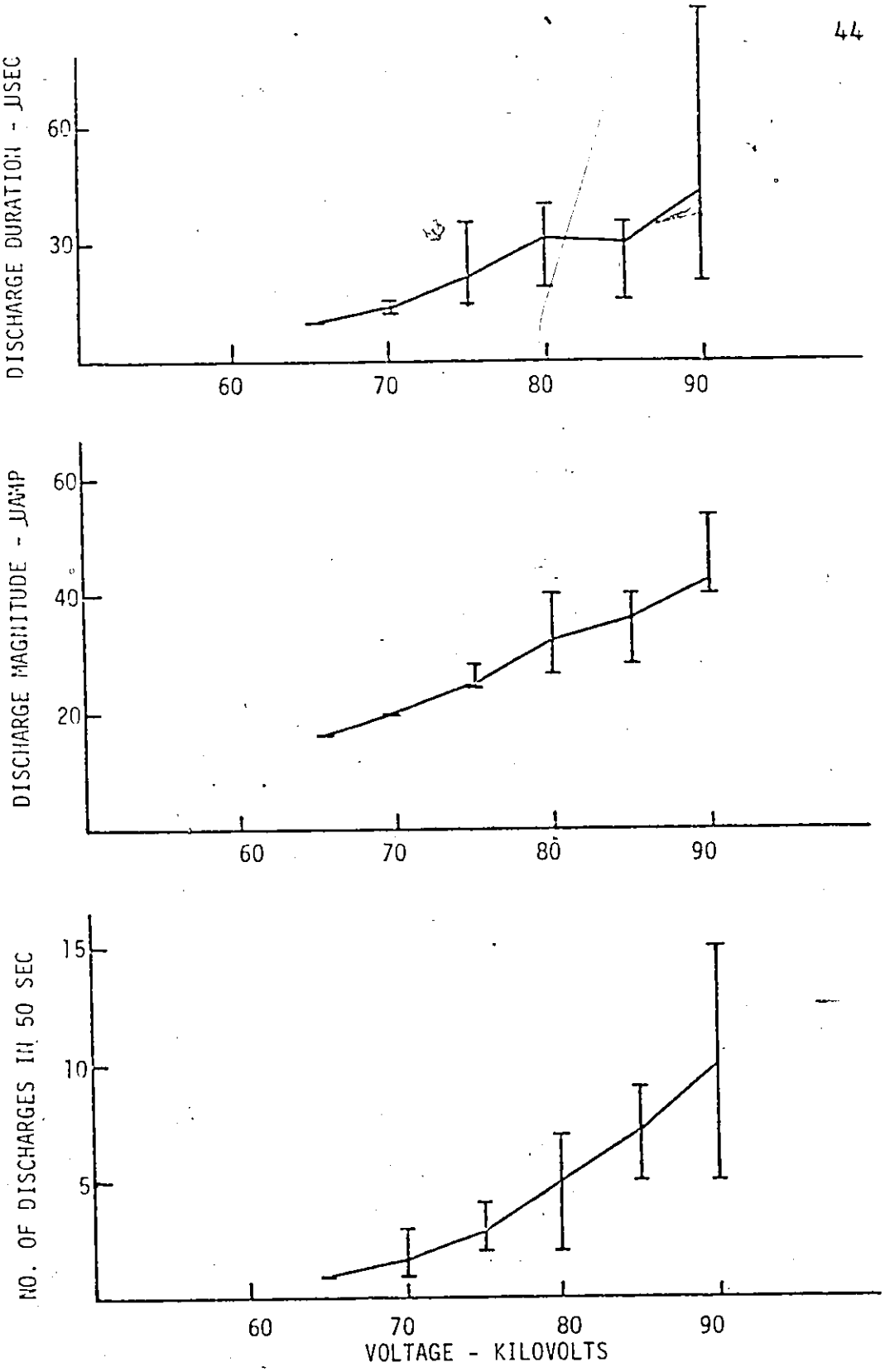

FIGURE 3.3. THE RELATIONSHIP BETWEEN APPLIED VOLTAGE AND THE MAGNITUDE, THE DURATION, AND THE REPETITION RATE OF MOMENTARY DISCHARGES IN A 1/16 INCH DIAMETER ROD-PLANE GAP OF 1.5 INCHES LENGTH, AT A GAS PRESSURE OF 2.7 ATMOSPHERES. BREAKDOWN OCCURRED AT 100 KV.

As illustrated in Figure 3.3, the repetition rate of the momentary discharges generally increased with an accompanying increase in gap voltage; the use of ultraviolet radiation tended to enhance this effect. Also, the pulse duration generally increased with increasing voltage. The relative effects of these two phenomena on the average value of corona current flowing in the external circuit were dependent upon the intensity of the radiation, the electrode geometry, and the gas pressure.

3.4 Continuous Discharge Phenomenon

An increase in the gap voltage beyond the inception level of momentary discharge activity resulted in either a spark or a transformation of discharge phenomenon to that of a continuous discharge. In a non-irradiated gap, the average corona current resulting from momentary discharge activity in the gap was generally well below 1 microampere throughout the voltage range of this activity. The transition to a steady discharge caused the microammeter to deflect suddenly and indicate a continuous DC current flow in the circuit. A further voltage increase caused an increase in the DC level of the corona current. A transition from a continous discharge to a momentary discharge occurred only when the voltage was reduced to a level significantly lower than that at which the reverse transition occurred. Figure 3.4 illustrates the relationship between

corona current and the gap voltage for one particular set of parameters.

Corona studies on the 1/16 inch diameter rod-plane gap indicated that the inception voltage of continuous discharge activity was significantly higher than the extinction voltage except when a prior continuous discharge had been present in the gap for at least a five minute duration. Under this circumstance, and only for a period of time extending several minutes past the time of extinction of the prior discharge, the inception voltage was observed to be at a reduced level coinciding with the extinction voltage. Such a reduction of inception level was not observed in studies involving the larger radii rods.

At gas pressures at which breakdown was not preceded by a steady discharge, the repetition rate of momentary discharges was in some cases sufficiently high to cause a deflection of the microammeter corresponding to an average current level of 1-10 microamperes. All observations of this phenomenon are indicated in Figures 4.5, 4.6 and 4.8. Oscillogram #16 illustrates a train of momentary pulses with an average current level of sufficient magnitude to cause a microammeter deflection. In all other cases the microammeter gave a non-zero current indiction only when a steady discharge was present in the gap.

The onset voltage of a steady discharge was observed to be lower at all electrode radii and gap lengths in the

presence of ultra-violet radiation. This reduction of onset voltage was often considerable as illustrated in Figure 3.4. Upon establishment of a steady discharge in the gap, removal of the radiation source had an insignificant effect on the average discharge current as indicated by the microammeter. and the ability of the discharge to sustain itself. As an example, with reference to Figure 3.4, a steady discharge can be established and maintained at 80 kv in a non-irradiated gap by first increasing the gap voltage to 84 kv and then reducing it to 80 kv. The same discharge conditions can be established at 80 kv by applying a voltage of 75 kv to the gap while irradiating it. Under these conditions a steady discharge will commence. The radiation source can then be removed and the applied voltage increased to 80 kv. The steady discharge condition will continue to exist.

Oscillogram #12 of Figure 3.2 shows three superimposed continuous discharge waveforms corresponding to different voltage levels. The peak magnitudes of the individual pulses are not indicated in the photograph but they were observed to be many times higher than the DC level. The oscillographic studies suggest that a continuous discharge and a momentary discharge are substantially the same with the exception that the latter is self-extinguishing.

Figure 3.5 shows a typical variation of DC corona current as a function of applied voltage and gas pressure and Figure 3.6 illustrates the effect of gap length on the

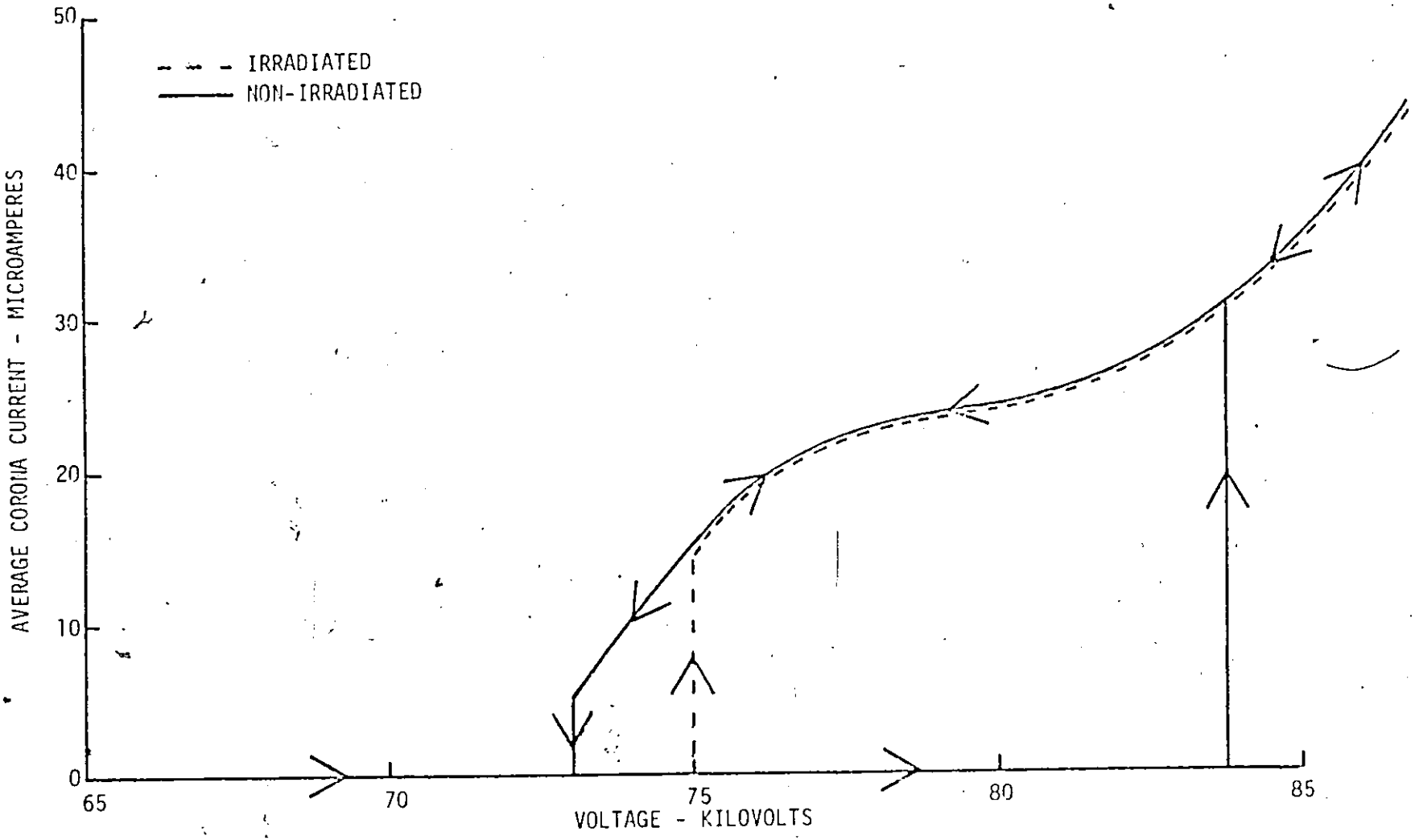

FIGURE 3.4. EFFECT OF GAP VOLTAGE VARIATIONS ON AVERAGE CORONA CURRENT IN A 1/4 INCH DIAMETER ROD-PLANE GAP OF 1.5 INCHES LENGTH.

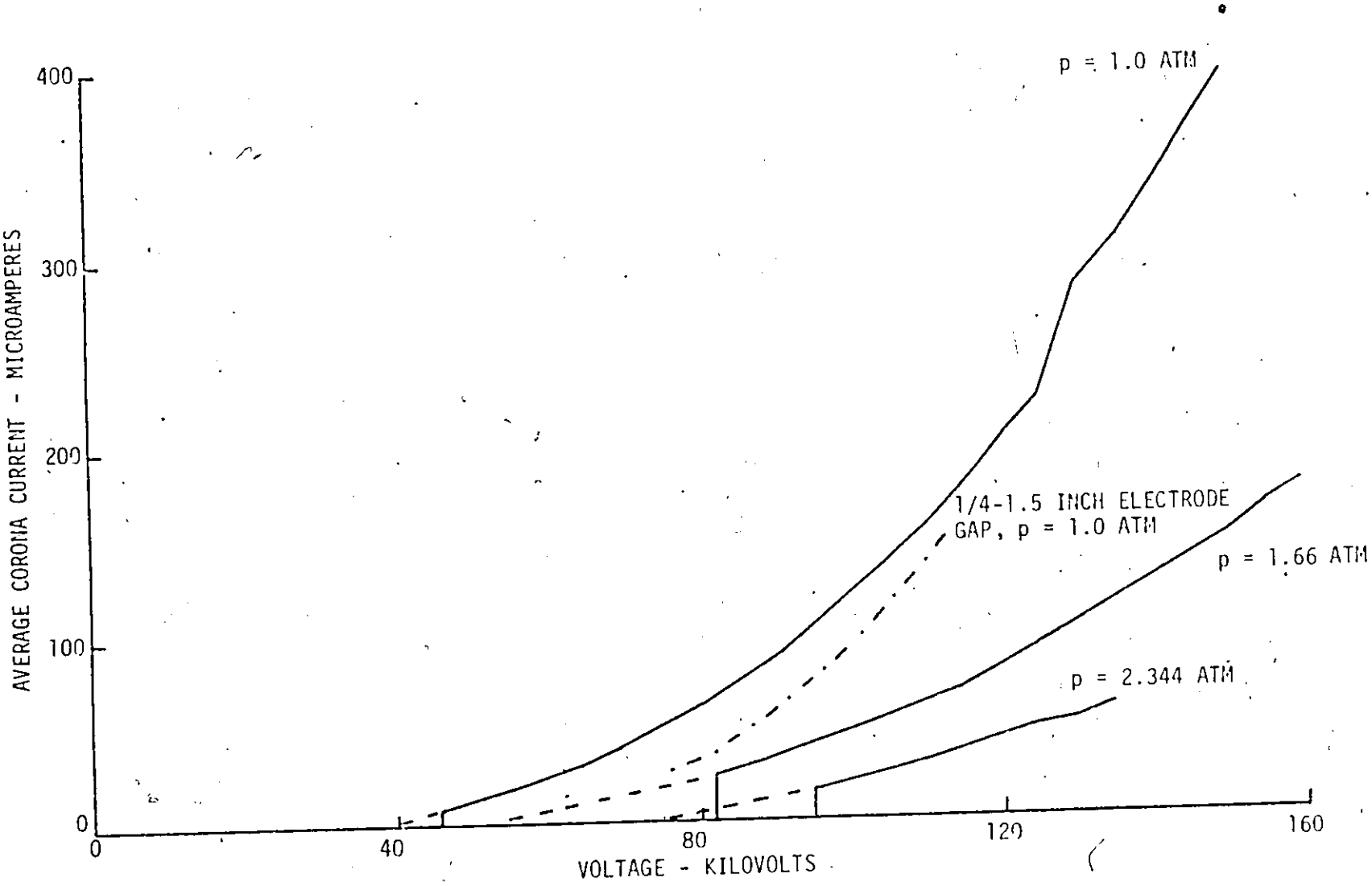

FIGURE 3.5. EFFECT OF GAP VOLTAGE AND PRESSURE ON THE MAGNITUDE OF CORONA CURRENT IN A 1/16 INCH DIAMETER ROD-PLANE GAP OF 1.5 INCHES LENGTH.

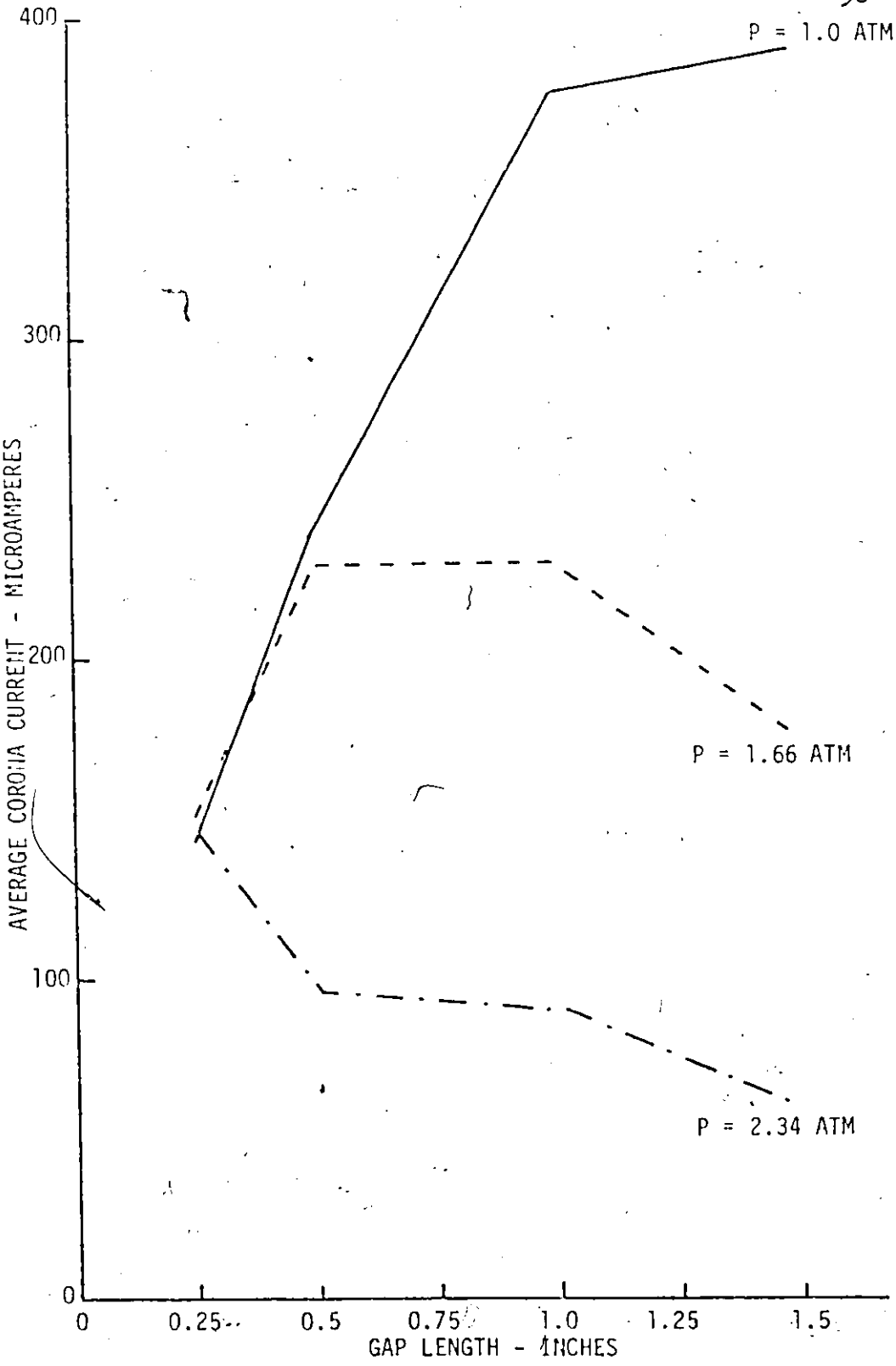

FIGURE 3.6. EFFECT OF GAP LENGTH AND PRESSURE ON THE MAGNITUDE OF THE CORONA CURRENT NEAR BREAKDOWN IN A 1/16 INCH DIAMETER ROD-PLANE GAP.

magnitude of the corona current at a voltage level just below the breakdown voltage.

A study of discharge currents at a bandwidth of 10 hz and an oscilloscope vertical amplifier gain corresponding to 10^{-10} amperes per division indicated that no discharge activity was present other than that described above and at the same voltage levels as above.

3.5 Visual Observations

Corona discharges in the test gaps were viewed with the aid of a telescope focused on the tip of the non-uniform field electrode. Activity was visible only when a continuous discharge was present in the gap, and the visual appearance of the same was observed to undergo a number of changes as the applied voltage was increased. The following is a description of the appearance of discharges at the tip of a 1/16 inch diameter rod with the gas pressure at 1 atmosphere and the gap length set at 1.5 inches.

The initial appearance of visible discharge activity coincided with the onset of a continuous discharge and was observed as a single bluish filament emanating from the rod tip as shown in Figure 3.7(a). The root of the filament emitted a more intense light than the stem and the filament jumped discontinuously over the surface of the electrode. As the voltage was raised, both the length of the filament and the rate at which the filament jumped from point to point on the anode surface increased. The area of the surface over

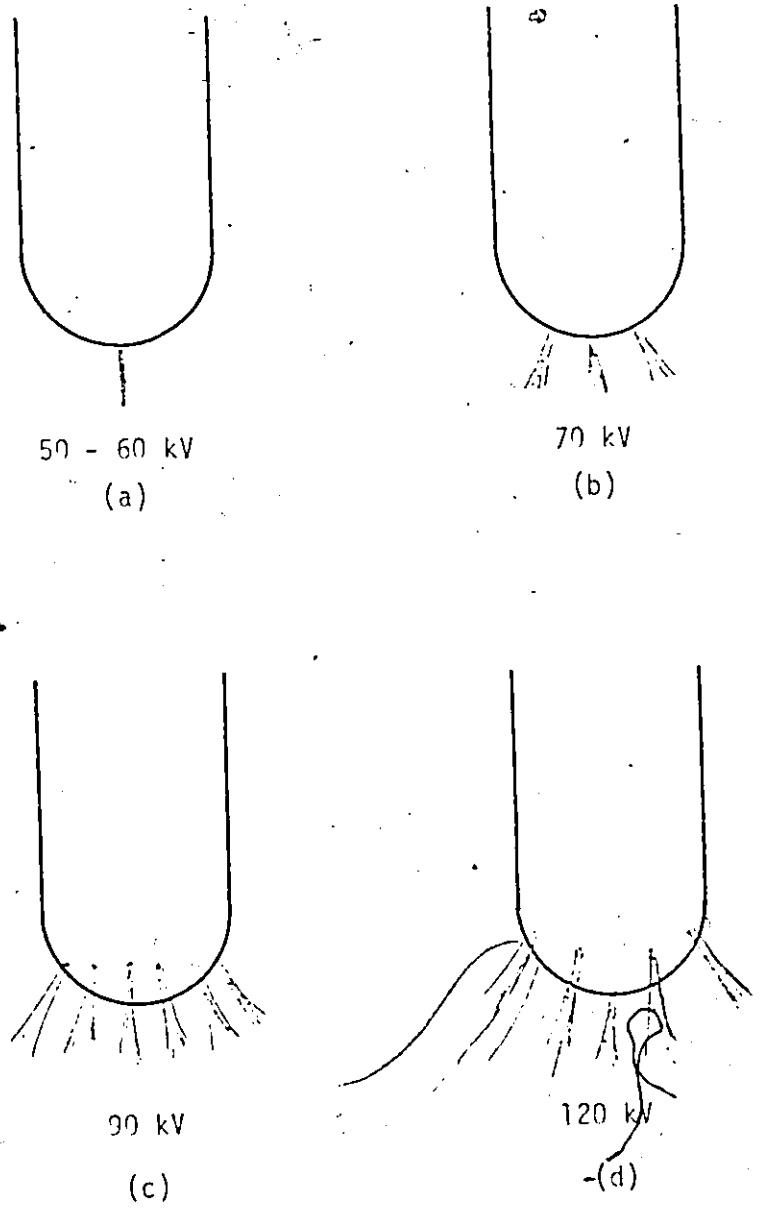

FIGURE 3.7. VISUAL APPEARANCE OF CORONA DISCHARGES IN SF_6 AT THE TIP OF A 1/16 INCH DIAMETER ROD, AT A GAS PRESSURE OF 1 ATMOSPHERE.

which the root of the filament ranged also increased.

At 60 kv, the discharge periodically changed from a single filament to multiple filaments and vice versa. The multiple filaments were more diffused in appearance than the single filament, as illustrated in Figure 3.7(b), and they moved more rapidly and ranged further from the tip of the rod.

A further increase in voltage resulted in the establishment of a continuous multiple filament discharge. The number of filaments, their length, and their displacement from the rod tip all increased with increasing voltage. The spread of the discharge across the surface appeared much more prevalent than the growth of the discharge into the gap. The filaments also appeared more diffused at the higher voltage levels. Filaments with a much brighter root and sharper definition were occasionally observed.

At an applied voltage of approximately 100 kv, the filaments became so numerous and diffused that the discharge at the electrode surface appeared as a continuous glow except at the outer edges of the discharge where the individual filaments were still distinguishable. This is illustrated in Figure 3.7(c). With increasing voltage, the glow extended into the gap as well as laterally. The length of the outer filamentary discharges also increased and intense filaments appeared periodically, emanating from all parts of the rod tip with those emanating from the edge of the discharge

remaining more prevalent. An occasional long reddish filament was observed. The general appearance of the rod tip at 120 kv, the voltage at which these phenomena were observed, is illustrated in Figure 3.7(d). This type of discharge pattern remained at voltages up to the breakdown voltage.

The same general discharge behavior was observed at the tip of the 1/8 inch and 1/4 inch diameter rods although the discharge extended further into the gap at the larger rod radii.

At gas pressures corresponding to the negative slope region of the breakdown voltage-pressure curve, the bluish glow discharge at the rod tip, bounded by filamentary discharge activity, was established in much the same sequence of events as at atmospheric pressure. Unlike the discharge growth at atmospheric pressure however, the discharge did not extend into the gap with increasing voltage but contracted and spread laterally over the surface. The occasional long reddish filament was also observed, emanating primarily from the edge of the discharge region. This general appearance continued up to breakdown.

CHAPTER IV

BREAKDOWN STUDIES

4.1 Test Procedure and Breakdown Test Results

When choosing a test procedure to determine the dielectric strength of an insulation system, several factors must be considered.

1. Do previous breakdown tests on the system affect the present dielectric strength? This includes the possible increase of the dielectric strength due to conditioning or dielectric strength reduction due to deterioration of the insulation or the electrodes.

2. In the case of DC testing, does the rate of rise of applied voltage have a significant effect on the breakdown test results? If so, what test procedure will yield results most relevant to engineering applications?

3. How many breakdown tests are necessary to yield a sufficiently accurate statistical picture of the dielectric strength of the system?

The output voltage of the HVDC generator was controlled by rotating a ten turn potentiometer. The rate of rise of output voltage was therefore proportional to the angular velocity of the potentiometer rotation. The voltage control was performed manually and this posed a limitation on the change in output voltage to a rate which should eliminate the possibility of a significant formative time lag influence

on the test results.[1] In view of this, a rather arbitrary rate of rise of 1 kv per 15 seconds was adopted for the early breakdown tests. This rate of rise was achieved by increasing the output voltage by 1 kv every 15 seconds as timed by a stop watch.

It was observed later however that the rate of rise could affect the test results significantly especially when corona discharges did not precede breakdown. The test results in Table 4.1 indicate that a slow rate of rise yielded consistently lower breakdown results but at the same time reduced the scatter. A decrease in the rate of rise below 1 kv per 60 seconds had no noticable effect. Under ultra-violet radiation the breakdown results were somewhat more consistent.

Table 4.2 indicates that the rate of rise of applied voltage had little effect on the breakdown results at lower pressures when corona discharges occurred in the gap prior to breakdown. It was also observed that the presence of radiation had an insignificant effect on the breakdown test results under these conditions.

Early test results and indeed the results of Tables 4.1 and 4.2 indicate that conditioning or deterioration introduced insignificant changes in breakdown test results.

---

[1] This statement is based on the results of time lag studies conducted in SF_6 by Kuffel and Radwan (19) and others. These studies indicate statistical and formative time lags in the order of 10's of microseconds at the longest in irradiated and non-irradiated SF_6 insulated gaps.

TABLE 4.1. EFFECT OF THE RATE OF RISE OF VOLTAGE ON DC BREAKDOWN RESULTS FOR A NON-IRRADIATED 1/16 INCH DIAMETER ROD-PLANE GAP OF 1.5 INCH LENGTH, INSULATED WITH SF_6 AT 5 ATMOSPHERES.

TEST	BREAKDOWN VOLTAGE			
NUMBER	1 kv/5 sec	1 kv/15 sec	1 kv/30 sec	1 kv/60 sec
1-4	84	77	72	71
5-8	83	78	75	71
9-12	86	76	73	73
13-16	74	75	75	72

TABLE 4.2. EFFECT OF THE RATE OF RISE OF VOLTAGE ON DC BREAKDOWN RESULTS FOR A NON-IRRADIATED 1/16 INCH DIAMETER ROD-PLANE GAP OF 1.5 INCH LENGTH, INSULATED WITH SF_6 AT 1.5 ATMOSPHERES. BREAKDOWN OCCURRED IN THE PRESENCE OF A SUSTAINED CORONA DISCHARGE.

TEST	BREAKDOWN VOLTAGE			
NUMBER	1 kv/5 sec	1 kv/15 sec	1 kv/30 sec	1 kv/60 sec
1-4	73	71	71	70
5-8	72	71	72	70

In view of these findings, two different test methods were used in the later dielectric strength studies. When corona discharges did not precede breakdown, the sparking voltage of the system was determined with a single non-irradiated breakdown test at a voltage rate of rise of 1 kv every 1.5 minutes and a single irradiated breakdown test conducted at a rate of rise of 1 kv every 15 seconds. When breakdown occurred in the presence of a continuous discharge, one irradiated and one non-irradiated breakdown test was conducted at a rate of voltage rise of 1 kv every 15 seconds. It was considered that two breakdown tests were sufficient to give a satisfactory indication of the breakdown strength, since a low scatter of results was observed for the slower rates of voltage rise, and neither conditioning nor deterioration were significant.

Breakdown tests and prebreakdown discharge studies were conducted with the 300 picofarad high voltage capacitor removed from the test circuit. This, in effect, decreased substantially the capacitance of the test gap. Under no circustances however was any difference detected between test results obtained with and without the capacitor.

Figures 4.1 through 4.11 illustrate the results of breakdown tests conducted on sphere and hemispherical rod-plane systems insulated with SF_6 at various pressures and subjected to DC voltages with the sphere or rod of positive polarity.

Breakdown values obtained with a 2 inch diameter sphere-plane gap and gap lengths of 0.25 inch and 0.5 inch are illustrated in Figure 4.1. Five breakdown tests were conducted in the absence of UV radiation at each pressure-gap length combination and the maximum, minimum, and average breakdown voltages of the five tests are plotted. The voltage was raised by 1 kv every 15 seconds.

Figure 4.2 indicates the results of tests conducted on a 1/4 inch diameter hemispherical rod-plane gap using the same test procedure as indicated above. In this case onset voltages of steady corona current are indicated as well as breakdown voltages.

Figure 4.3 shows breakdown test results of a 1/16 inch diameter hemispherical rod-plane gap. The average value of two breakdown tests conducted at each pressure-gap length combination is plotted. If the two test results differed by more than 3 percent, which was seldom the case, several more breakdown tests were conducted and the average of all of the tests is plotted. The voltage was raised by 1 kv every 15 seconds. Figure 4.3 includes test results obtained by Works and Dakin (5) for an SF_6 insulated rod-plane system. The rod was of 1/16 inch diameter and the plane electrode was a 6 inch diameter plate (this differed considerably from the plane electrode of the present study). The gap was exposed to an undisclosed amount of UV radiation.

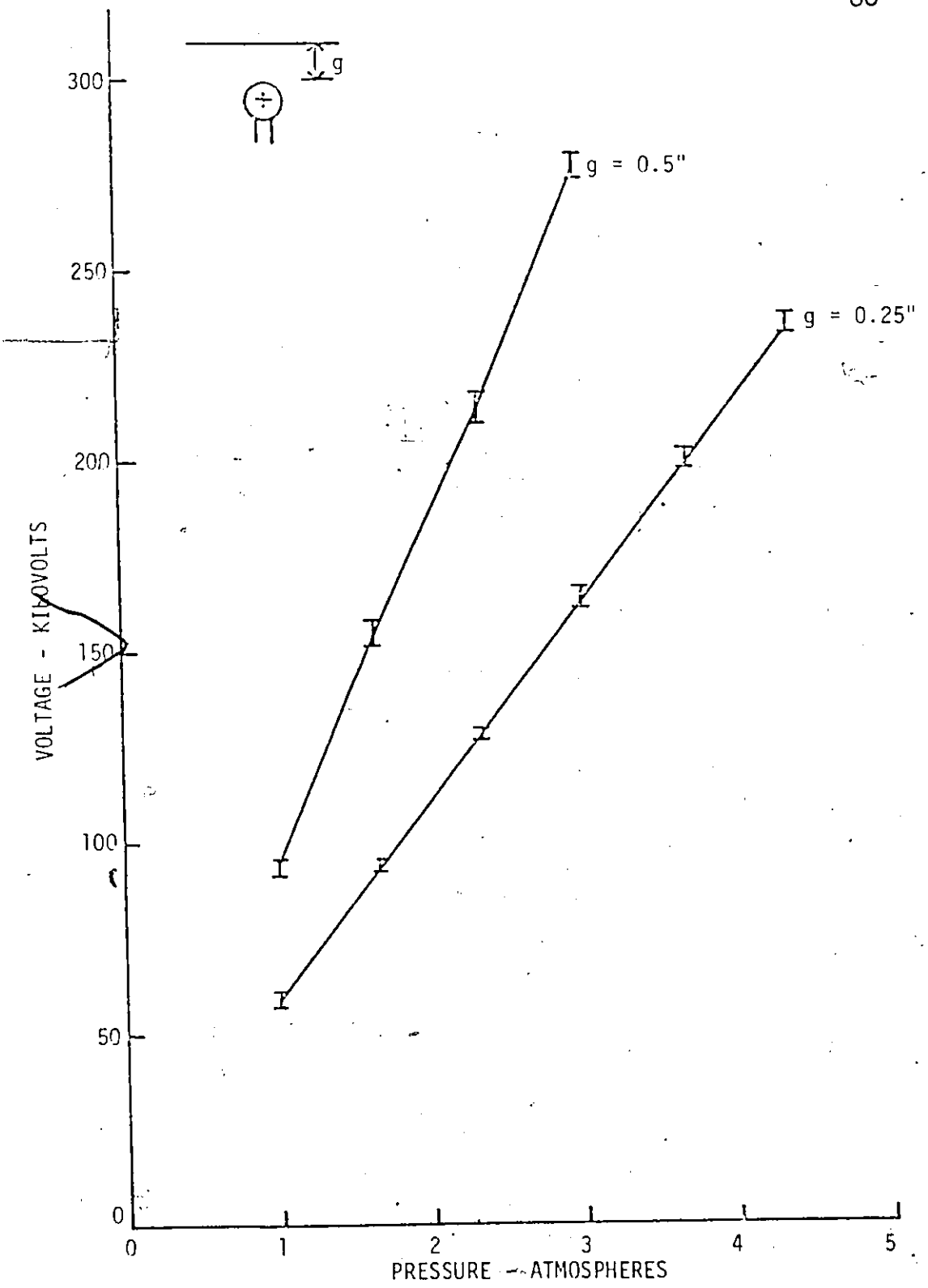

FIGURE 4.1. BREAKDOWN TEST RESULTS OF A 2 INCH DIAMETER SPHERE-PLANE GAP.

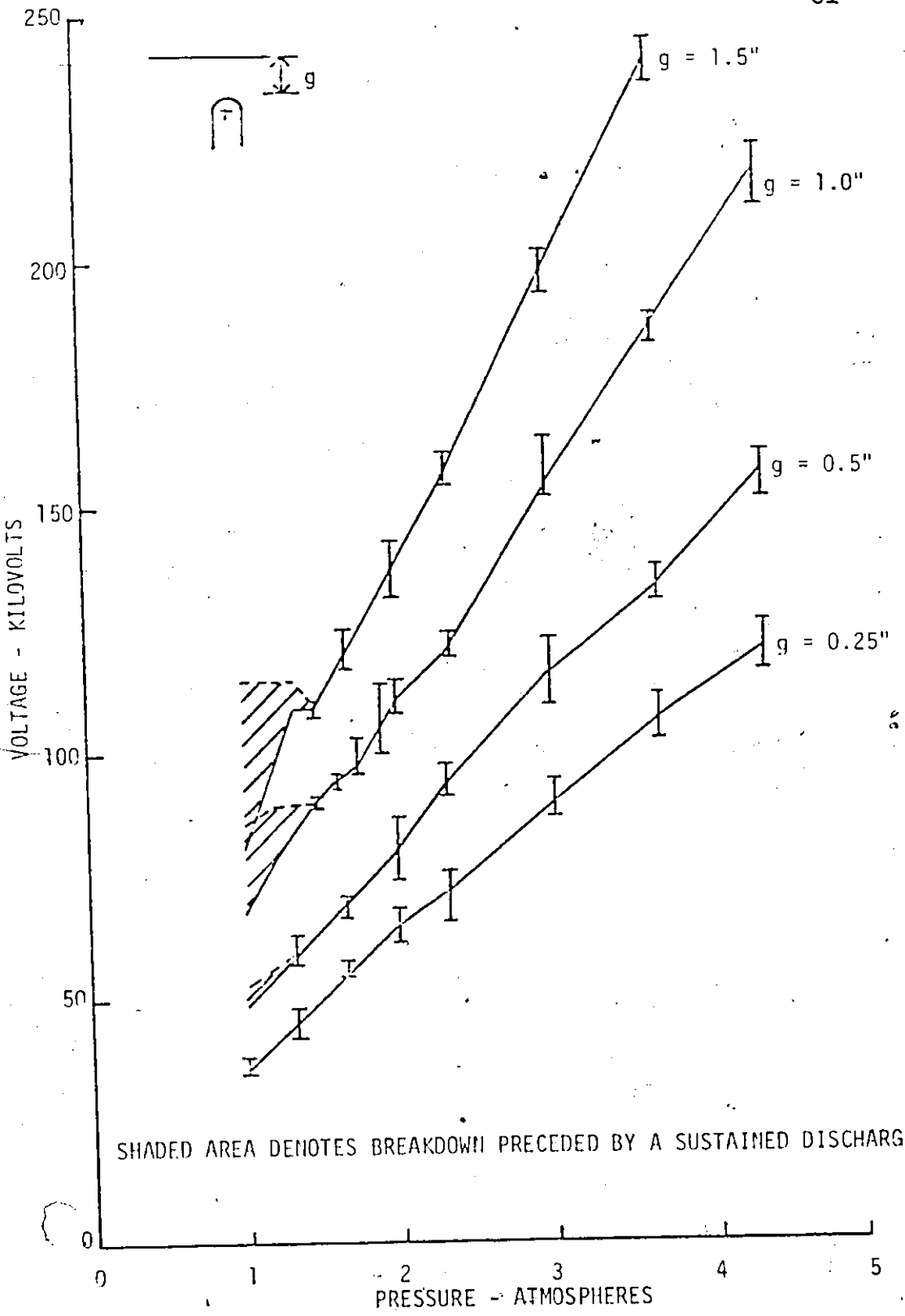

FIGURE 4.2. BREAKDOWN AND CORONA ONSET VOLTAGES OF A 1/4 INCH DIAMETER ROD-PLANE GAP.

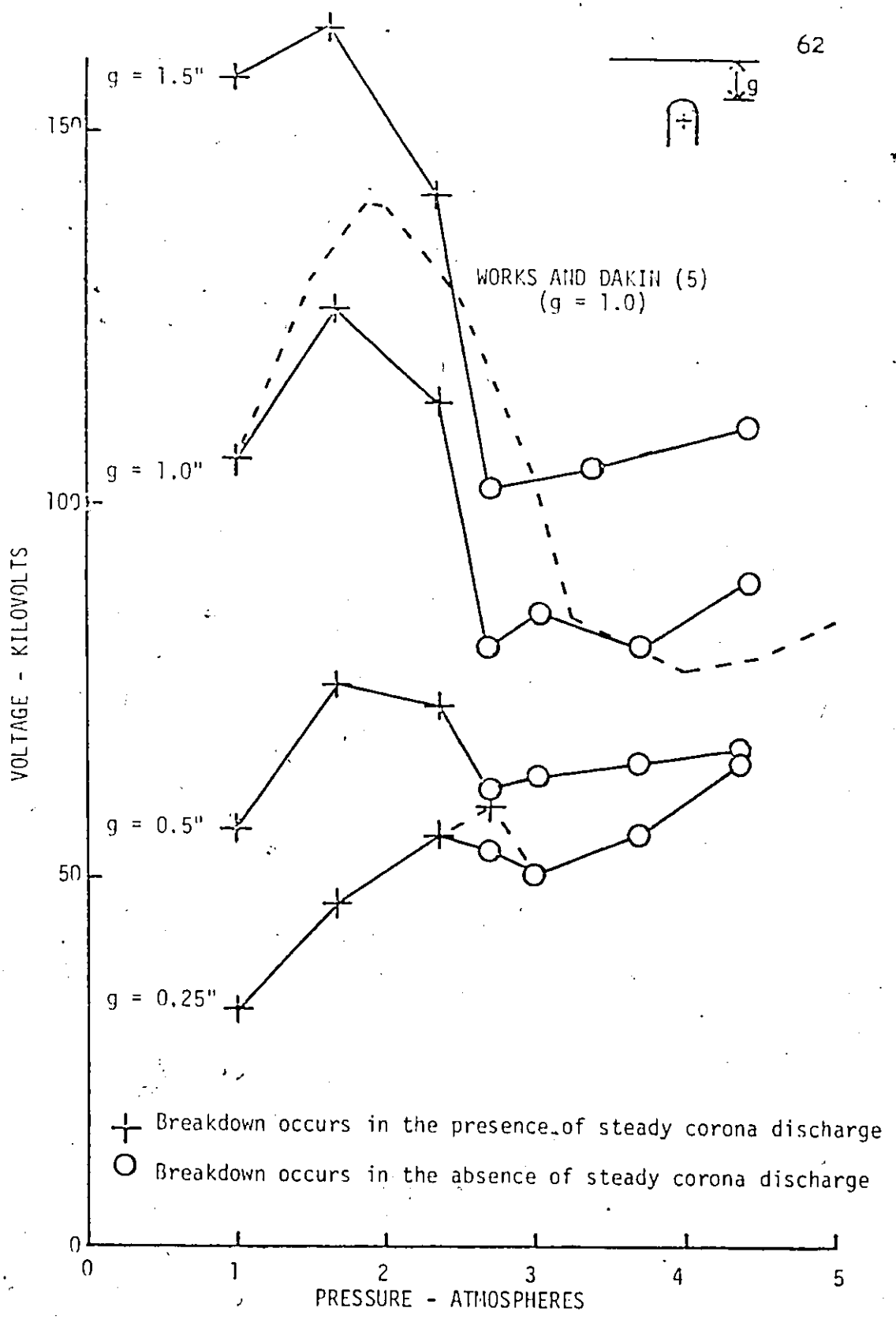

FIGURE 4.3. BREAKDOWN VOLTAGES OF A 1/16 INCH DIAMETER ROD-PLANE GAP.

Figures 4.4 through 4.6 show breakdown and corona discharge onset levels of rod-plane gaps with rod diameters of 1/4, 1/8, and 1/16 inch respectively and a gap length of 1.5 inches. Figures 4.7 through 4.9 give similar results for the same respective rod diameters and a gap length of 0.5 inches. The irradiated breakdown values were obtained by raising the applied voltage by 1 kv every 15 seconds, whereas values for the non-irradiated gaps were obtained by raising the voltage by 1 kv every 1.5 minutes. Each point which denotes breakdown in these figures is the result of a single breakdown test.

Figures 4.10 and 4.11 compare the results of two breakdown studies conducted on rod-plane gaps with essentially identical parameter values. The electrodes were refinished prior to conducting each of the two studies and the SF_6 gas used in each study was from a different cylinder. A different rate of rise of voltage was used for the breakdown tests in each case.

4.2 Spark Trajectory Studies

In addition to determining the breakdown voltage levels, the breakdown tests included a study of spark trajectories. This subject has drawn some interest in the past as is indicated in Chapter I.

The trajectories were determined using the system schematically illustrated in Figure 4.12. The mirror arrangement provided two orthogonal lines of sight, and

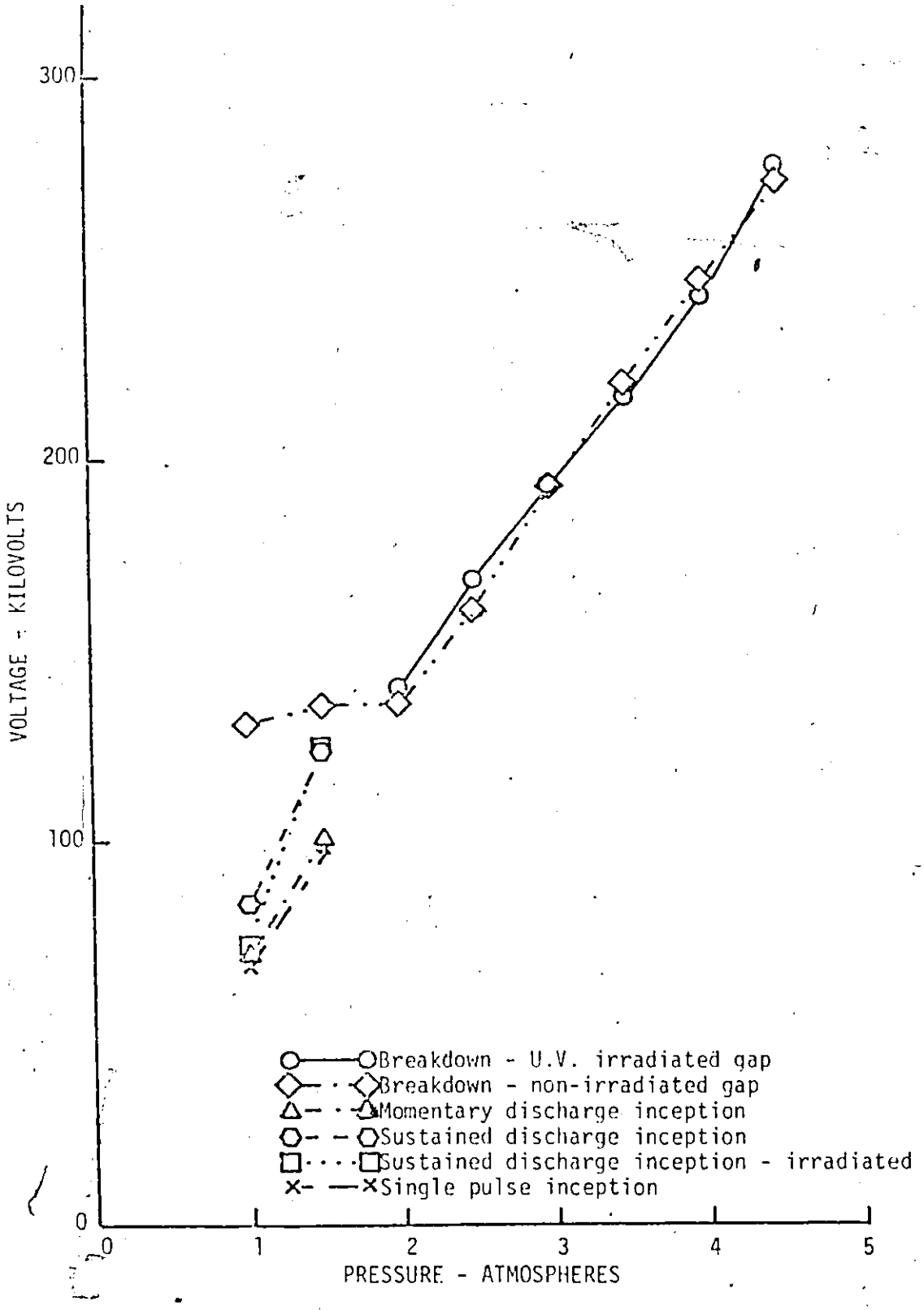

FIGURE 4.4. BREAKDOWN AND CORONA DISCHARGE ONSET VOLTAGES OF A 1/4 INCH DIAMETER ROD-PLANE GAP OF 1.5 INCHES LENGTH.

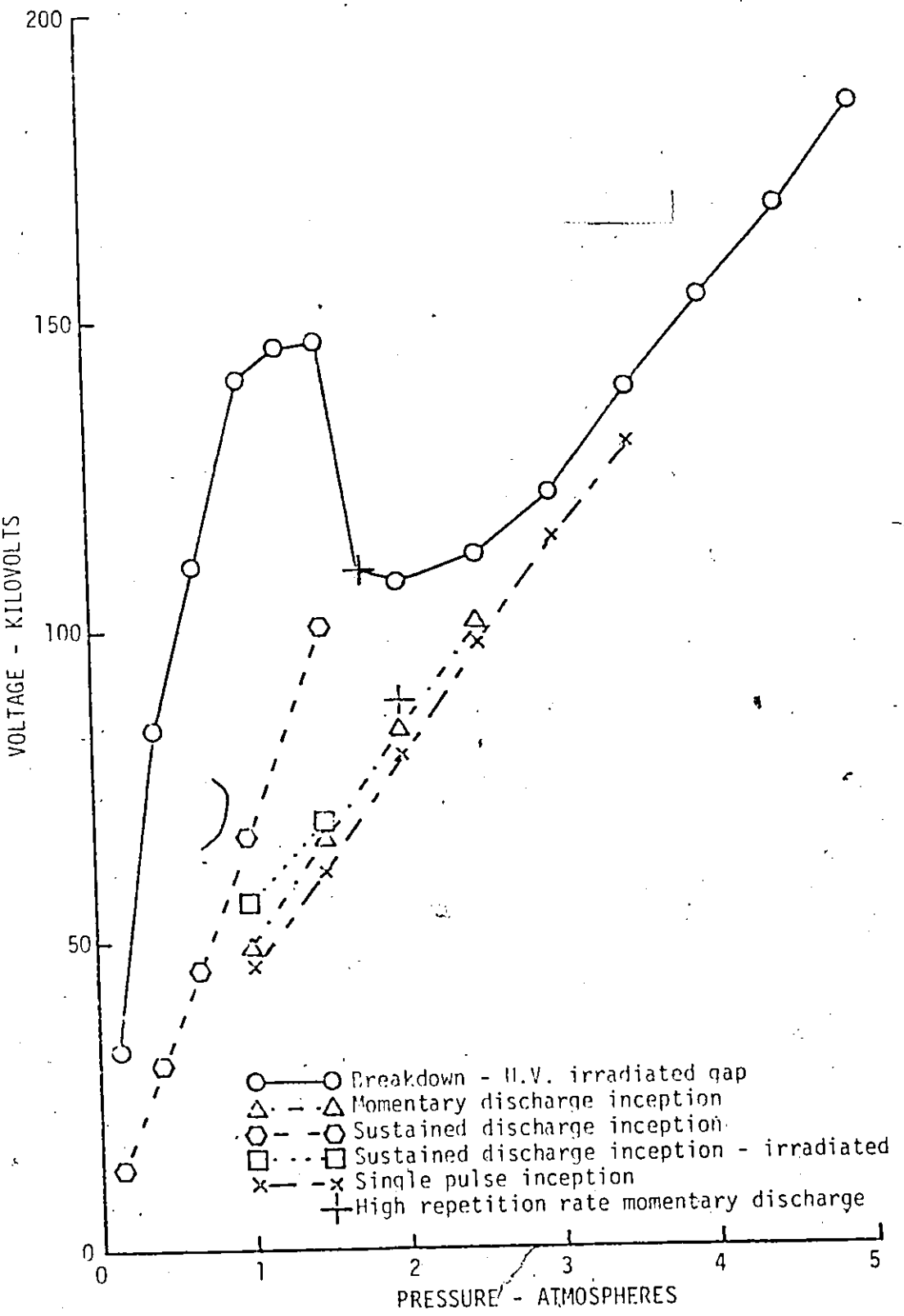

FIGURE 4.5. BREAKDOWN AND CORONA DISCHARGE INCEPTION VOLTAGES OF A 1/8 INCH DIAMETER ROD-PLANE GAP OF 1.5 INCHES LENGTH.

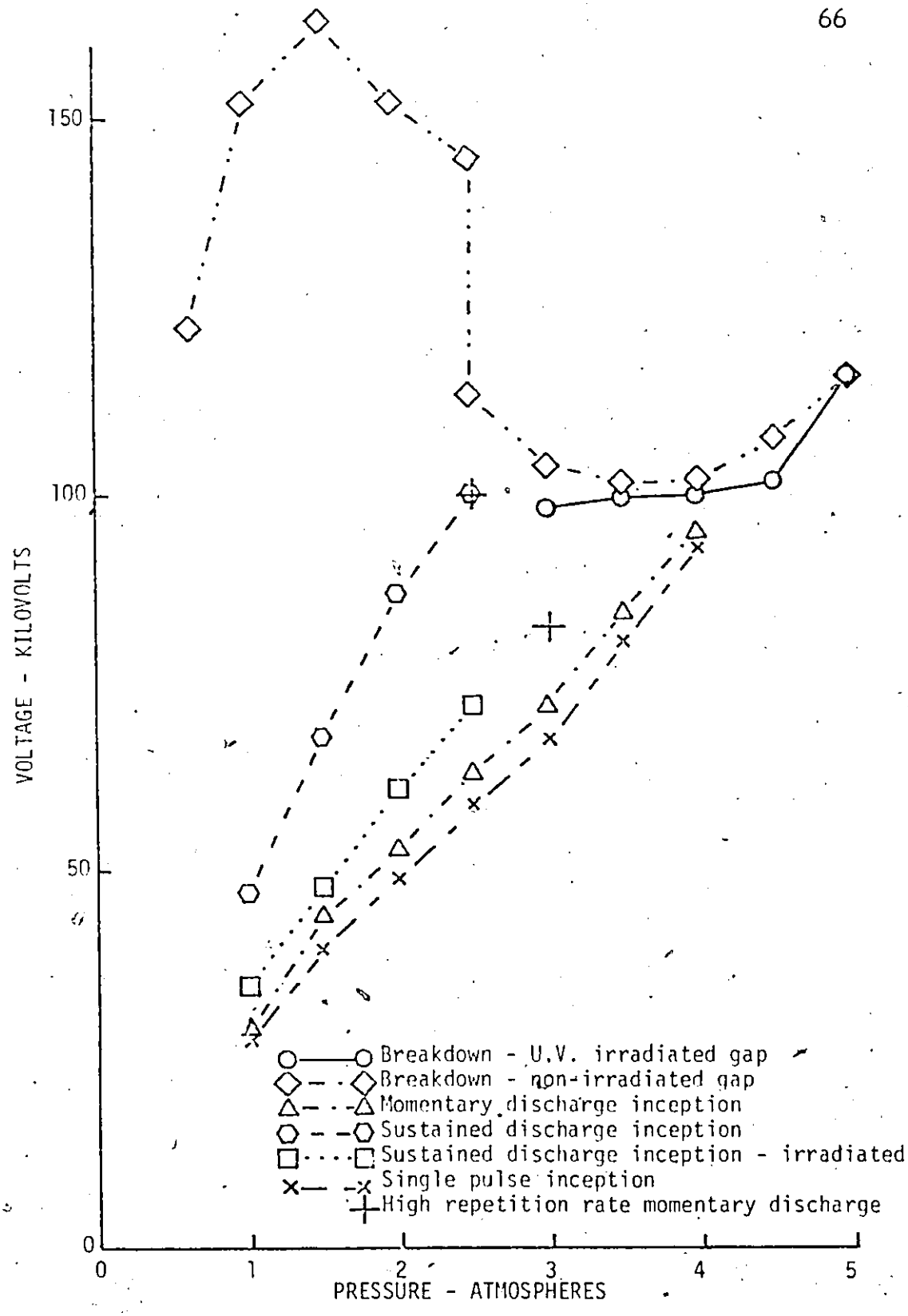

FIGURE 4.6. BREAKDOWN AND CORONA DISCHARGE INCEPTION VOLTAGES OF A 1/16 INCH DIAMETER ROD-PLANE GAP OF 1.5 INCHES LENGTH.

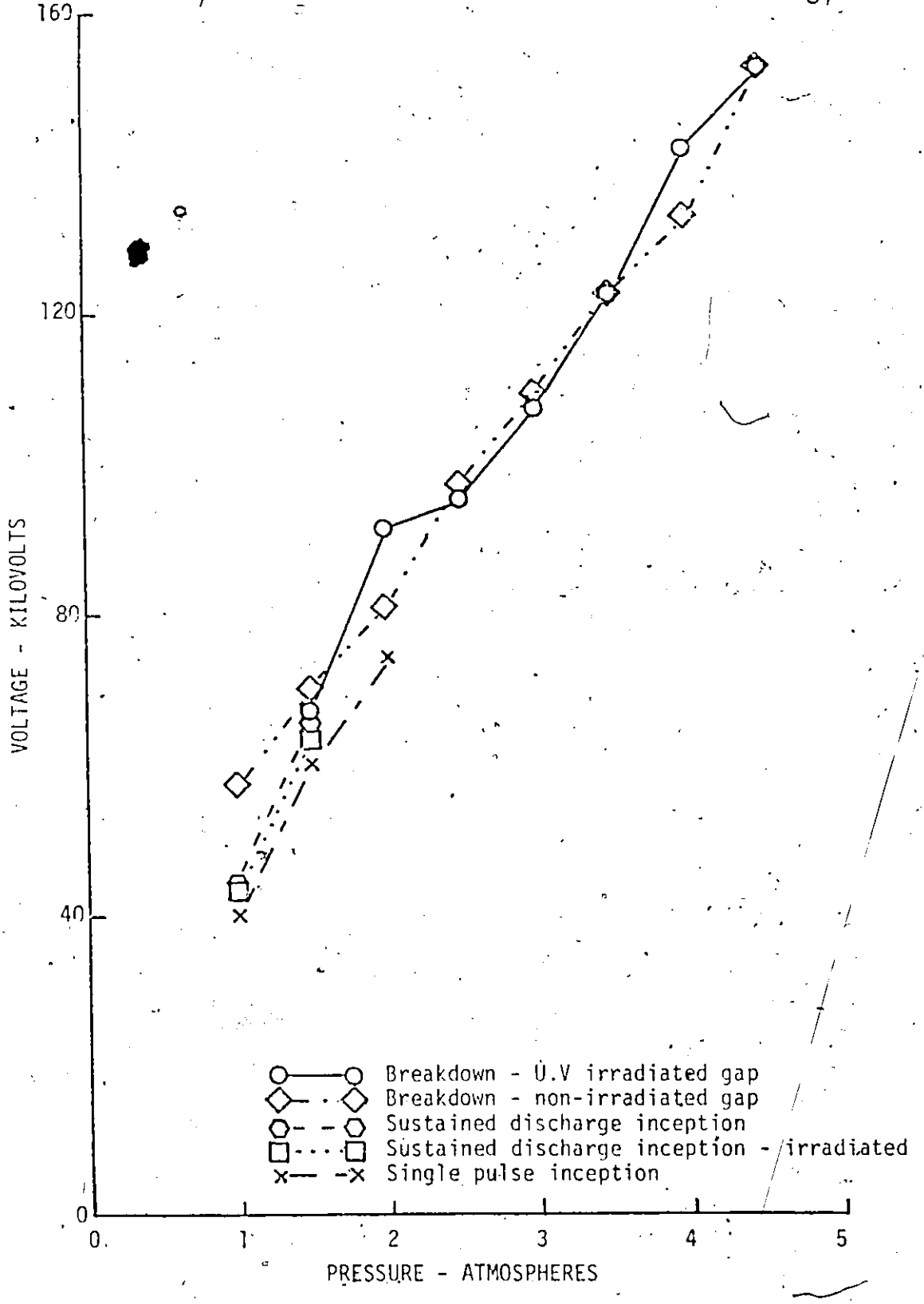

FIGURE 4.7. BREAKDOWN AND CORONA DISCHARGE INCEPTION VOLTAGES OF A 1/4 INCH DIAMETER ROD-PLANE GAP OF 0.5 INCH LENGTH.

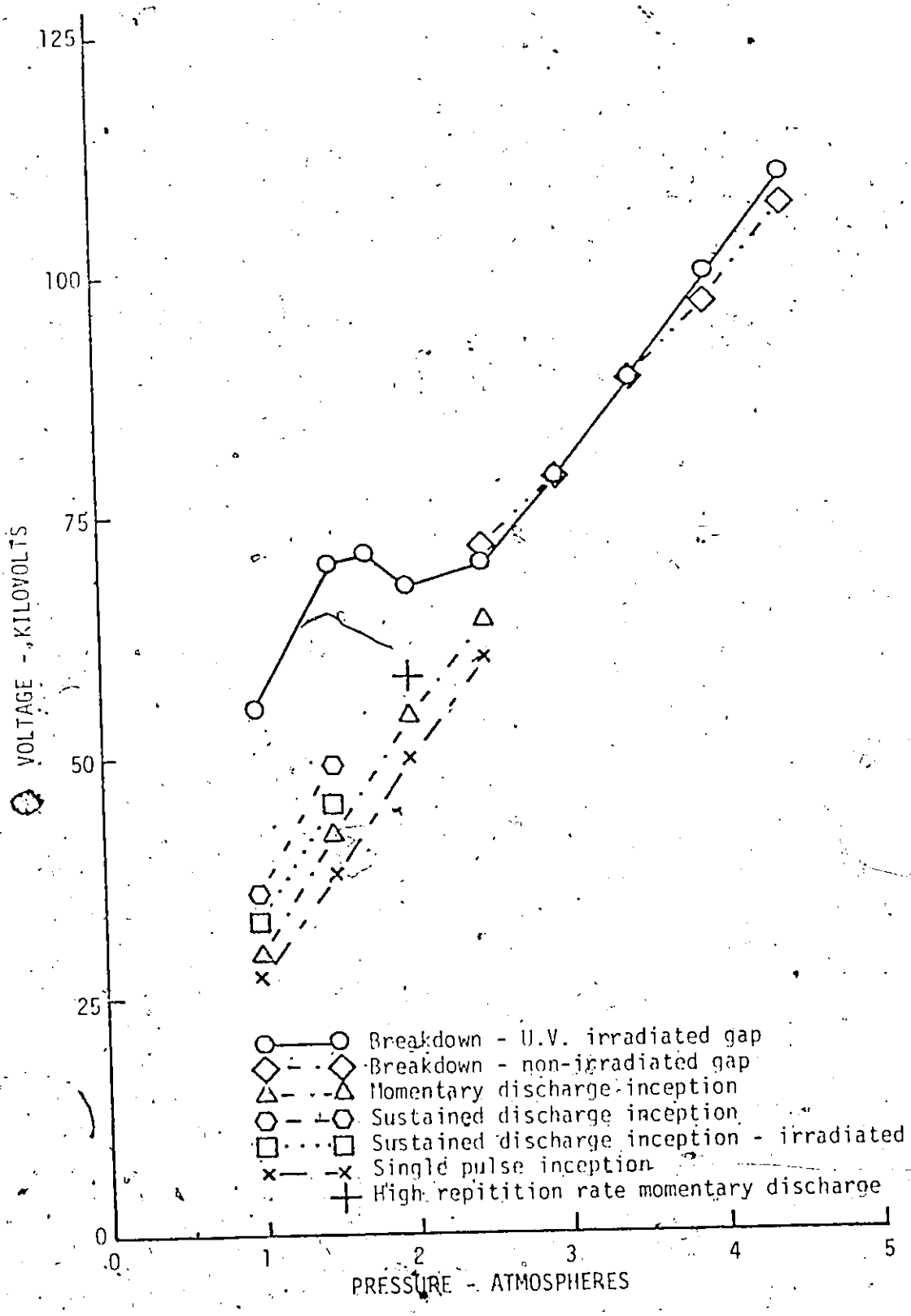

FIGURE 4.3. BREAKDOWN AND CORONA DISCHARGE INCEPTION VOLTAGES OF A 1/8 INCH DIAMETER ROD-PLANE GAP OF 0.5 INCH LENGTH.

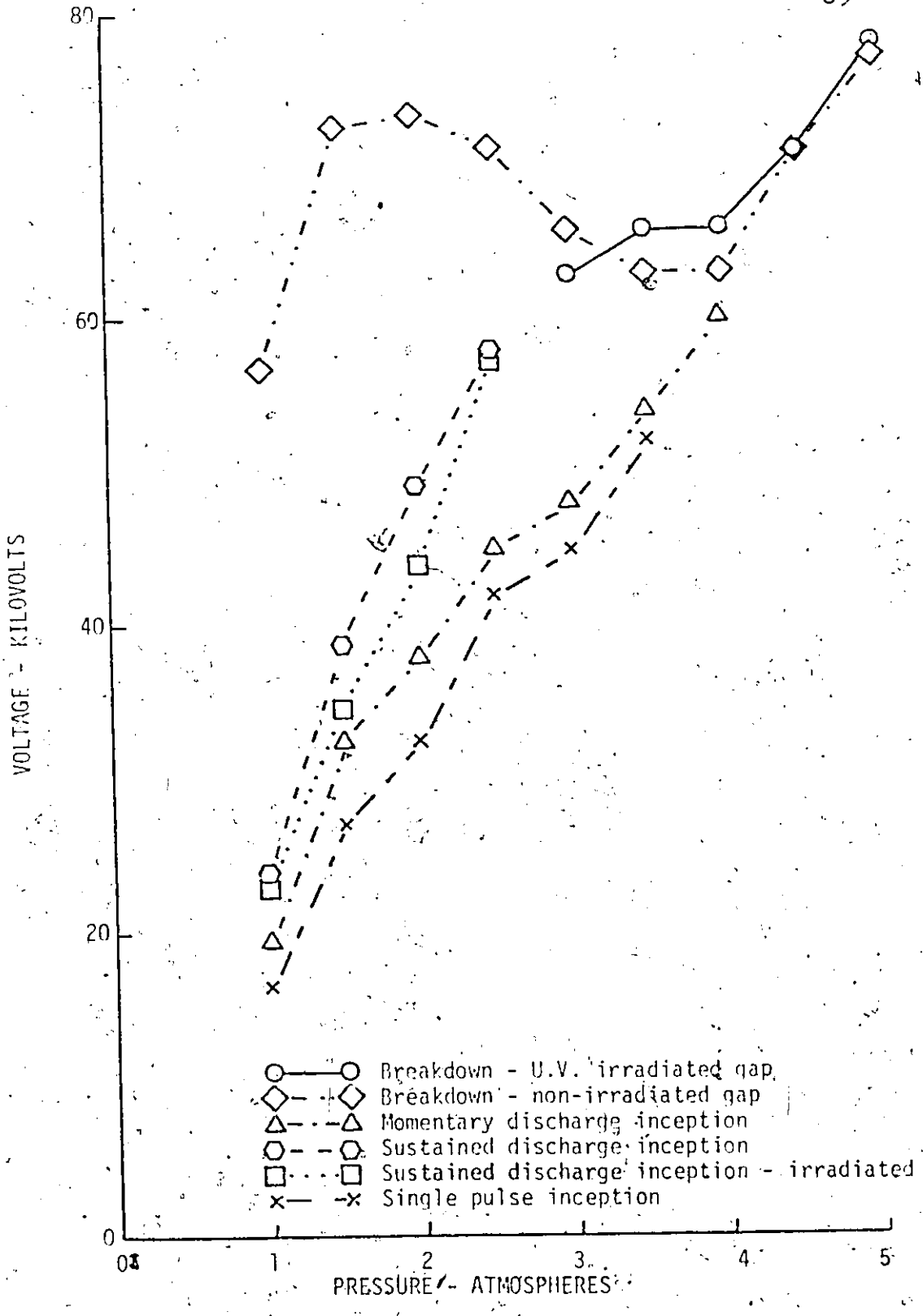

FIGURE 4.9. BREAKDOWN AND CORONA DISCHARGE INCEPTION VOLTAGES OF A 1/16 INCH DIAMETER ROD-PLANE GAP OF 0.5 INCH LENGTH.

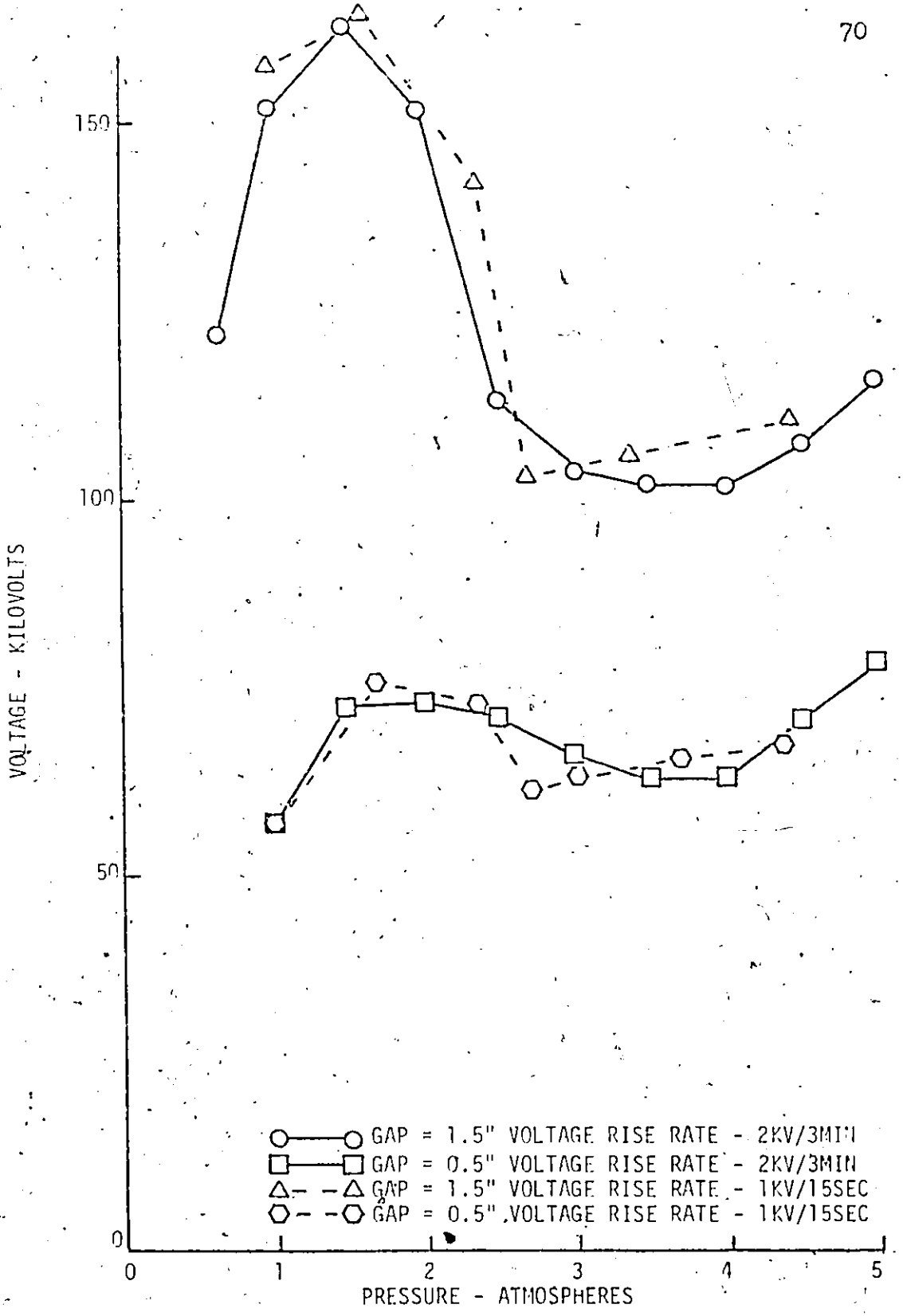

FIGURE 4.10. COMPARISON OF TEST RESULTS OBTAINED IN TWO DIFFERENT TEST SERIES OF A 1/16 INCH DIAMETER ROD-PLANE GAP.

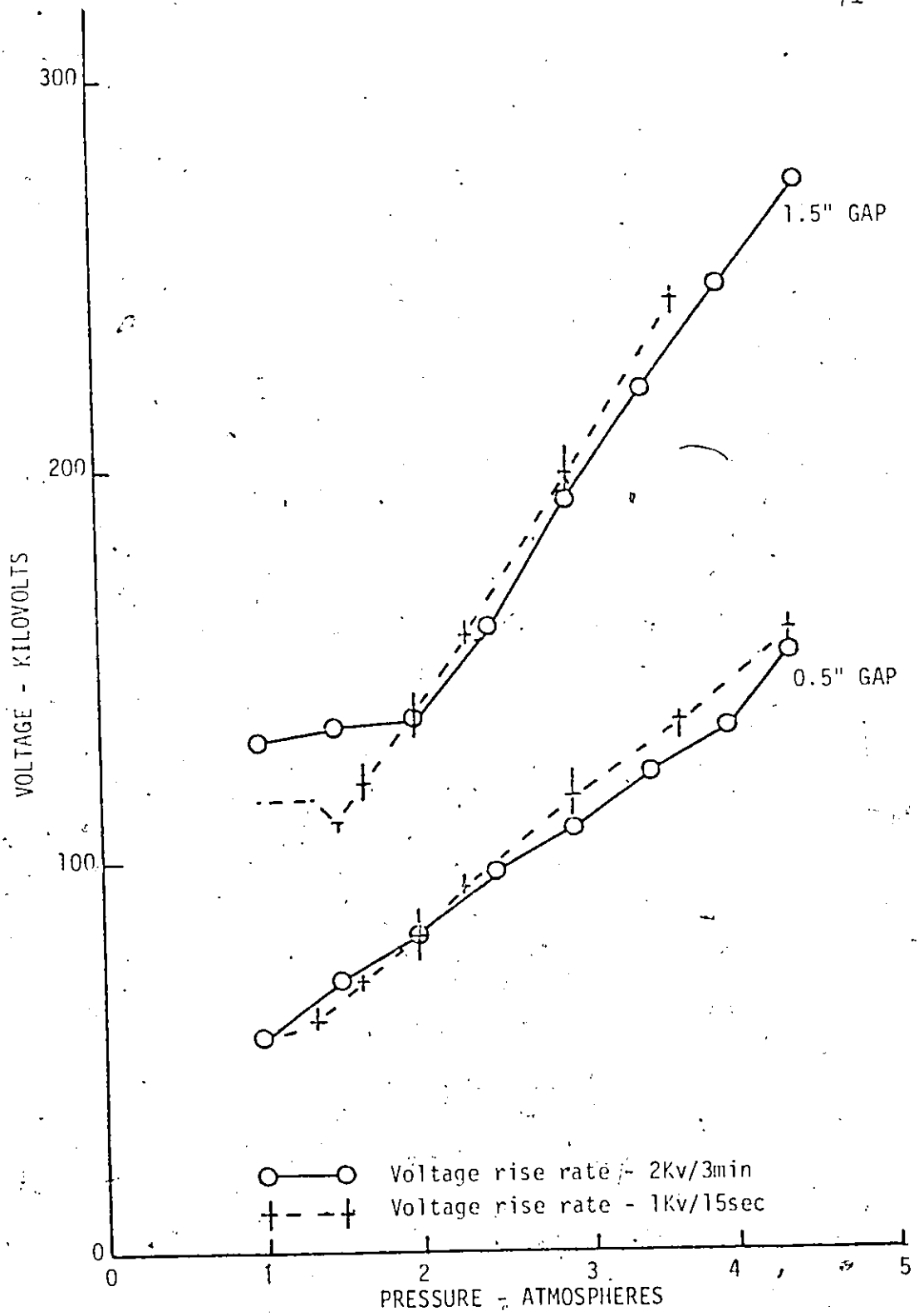

FIGURE 4.11. COMPARISON OF TEST RESULTS OBTAINED IN TWO DIFFERENT TEST SERIES OF A 1/4 INCH DIAMETER ROD-PLANE GAP.

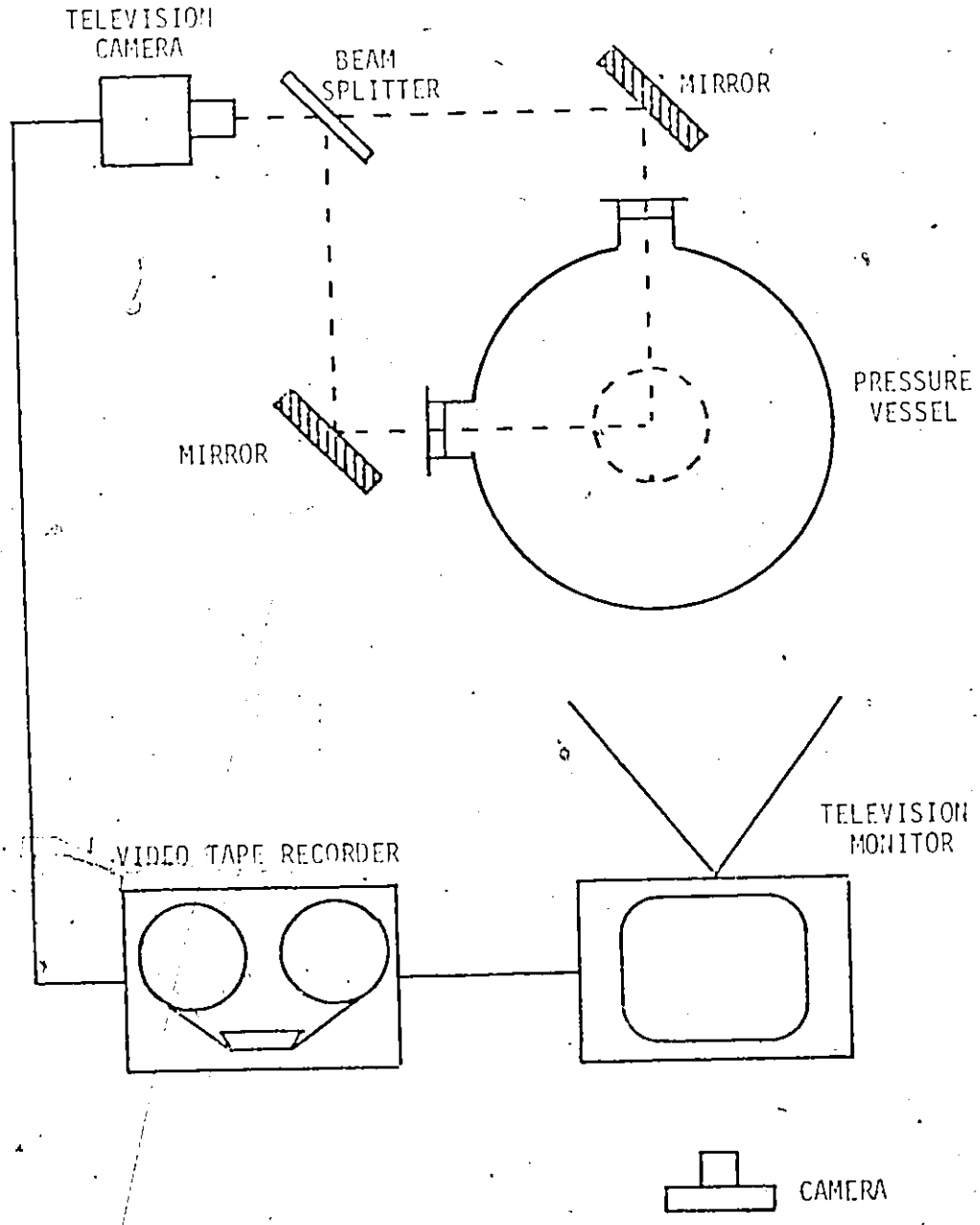

FIGURE 4.12. EXPERIMENTAL SETUP FOR THE ANALYSIS OF SPARK TRAJECTORIES.

therefore, under no circumstance could any spark curvature go undetected. The mirror angles were such that the two images of the test gap, as viewed by the camera, appeared as a single image and the beam splitter was adjusted to equalize the reflection and refraction losses of the two paths. The video tape recorder provided a means of storing the image viewed during the sparking event. It also provided a means of distinguishing the original spark from restrikes, which often occurred, and allowed the spark trajectory to be photographed as a still image on the monitor with the recorder in the stop-frame mode.

Figure 4.13 shows the results of a spark trajectory study conducted on a 1/16 inch diameter rod-plane electrode system with a gap length of 1.5 inches. The results are indicative of the observed behavior of other electrode arrangements; that is, the spark exhibited noticeable curvature only when the gas pressure was near or greater than P_{vmax} and when a steady corona discharge was present in the gap.

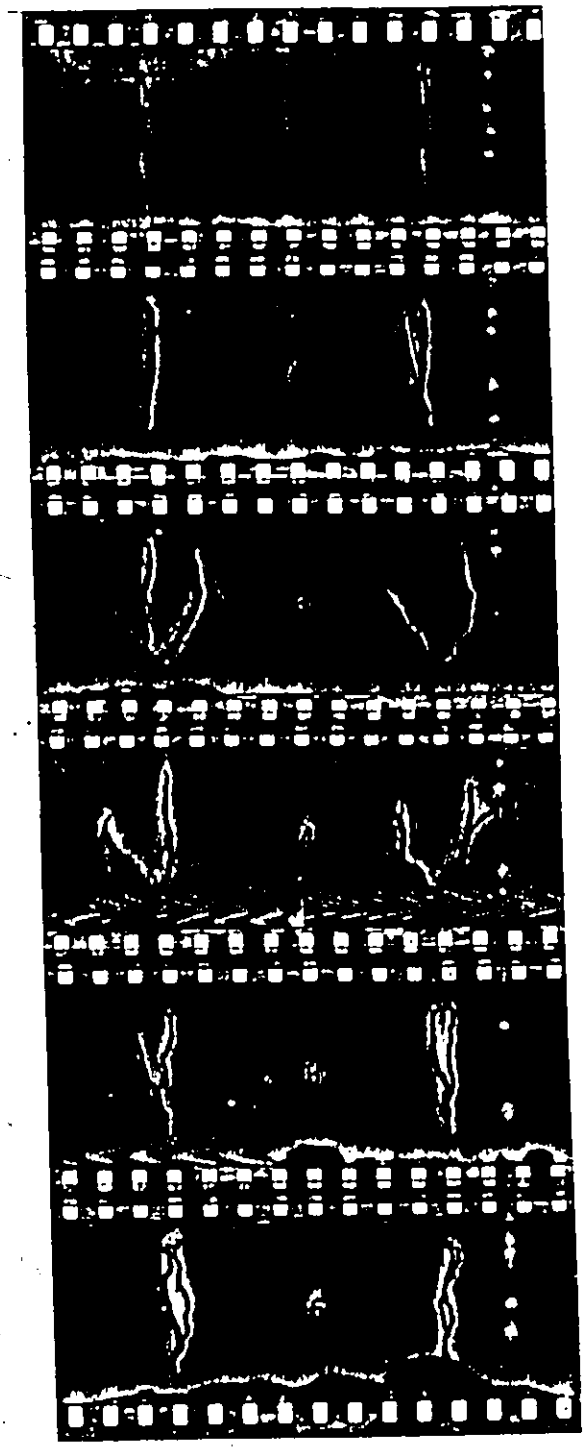

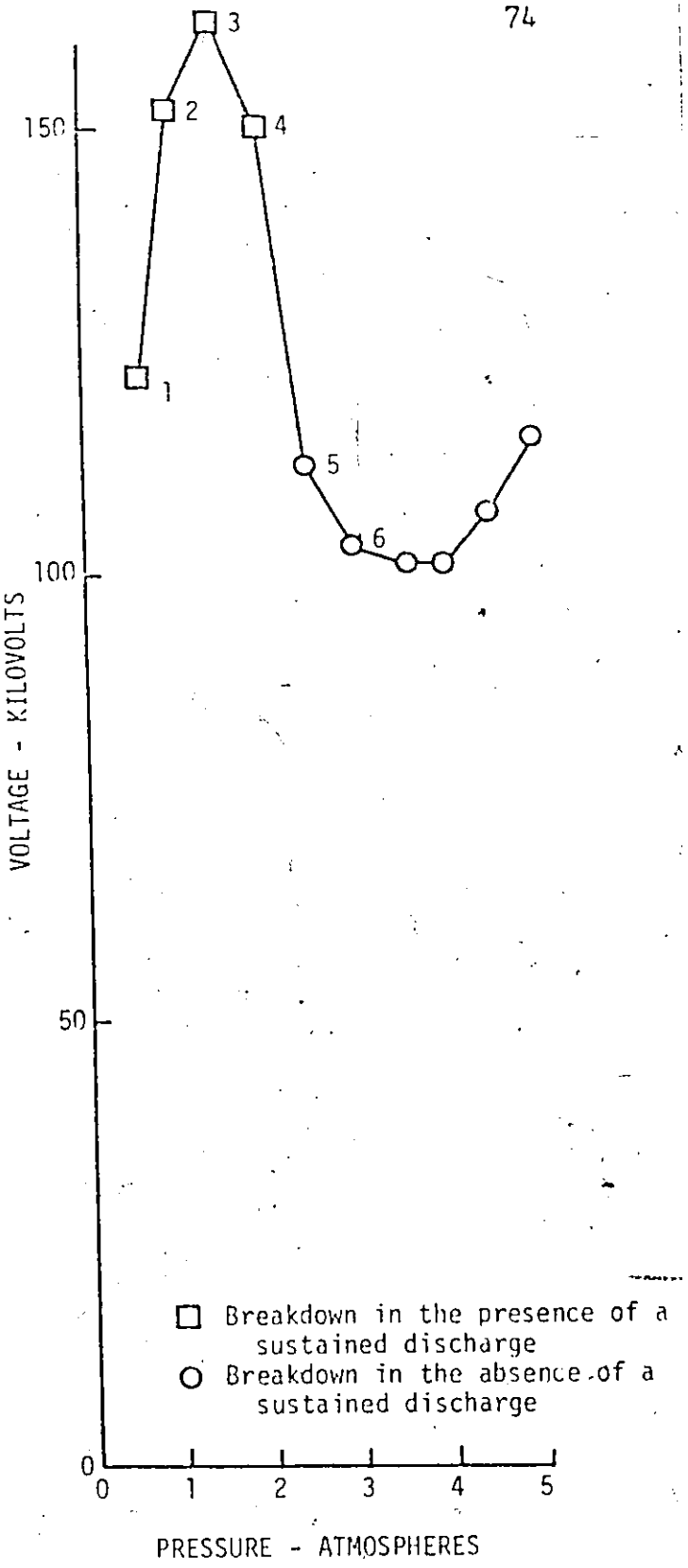

FIGURE 4.13. PHOTOGRAPHS OF SPARK TRAJECTORIES IN A 1/16 INCH DIAMETER ROD-PLANE GAP OF 1.5 INCH LENGTH. THE TWO FILAMENTS ARE THE TRAJECTORIES OF A SINGLE SPARK AS OBSERVED FROM TWO ORTHOGONAL LINES OF SIGHT.

CHAPTER V

DISCUSSION OF TEST RESULTS

One of the prime objectives of this work is to further the understanding of the dominant processes which characterize the behavior of SF_6 insulation subjected to non-uniform electric fields. There are a large variety of non-elastic collision reactions which can in part determine the performance of the gas under high electrical stress even under highly controlled experimental conditions, low gas pressures, and uniform electric fields. The presence of a non-uniform electric field compounds the analytic difficulties as the energy distributions of electrons and ions change from point to point in the gas and the accumulation of ions in the low field regions of the gas makes it difficult, if not impossible, to determine the true electrical stress at any point in the gas. It is an exceedingly difficult task to formulate a comprehensive explanation of the observed discharge phenomena in a non-uniform field in terms of the significant reactions which take place in highly stressed, high pressure SF_6 gas. Little information is available in the literature on many of these reactions and those which have received intensive investigation have been studied under uniform field, low pressure conditions.

The above mentioned difficulties rule out a comprehensive quantitative analysis of the observed discharge phenomena in SF_6. This chapter is devoted to a qualitative explanation of

the characteristics of corona discharges in SF_6. The theories presented are based on the experimental results of the present study as well as reported experimental and analytic investigations of anode coronas in SF_6 and other gases. Much of the following discussion is in reference to studies of anode coronas in air and consequently a summary of the pertinent characteristics of these discharges is first presented.

5.1 Corona Current Studies

5.1.1 Anode Corona in Air

From the time that Townsend first initiated an intensive investigation of electrical discharges in gases many studies have been made on an important form of electrical discharge, the corona discharge. Loeb (20) has summarized and analized the majority of the important contributions to this field up to 1965. Most of the work to this date has been devoted to the analysis of the various forms of corona in air because of its importance as a high voltage insulation. The strongly electronegative gases, whose use as a high voltage insulation has become widespread only in recent years, have received little attention. This is especially true with regard to a fundamental analysis of corona discharges within these gases.

Some authors suggest that there is little difference between corona discharges in air and other electronegative gases such as SF_6. The results of the present study indicate that this appears not to be the case and in this chapter the essential differences will be examined. First however,

the various forms of static field anode corona in air will be summarized (42, 43, 44). The form in which a corona discharge appears is a function of many parameters and this summary will only apply to discharge phenomena in a sphere or rod-plane gap of high field non-uniformity insulated with air at atmospheric pressure.

As the gap voltage is increased from zero volts the discharge phenomena at the anode surface goes through three modes of activity; onset pulses, glow discharge (Hermstein's glow), and pre-breakdown streamers, in that order.

The onset pulses are of one or both of two types, streamer pulses and burst pulses. A streamer pulse is essentially a filamentary growth of ionized gas normal to the electrode surface and a burst pulse can be described as a corrupt streamer (42). Burst pulse ionization tends to spread over the anode surface. The current pulses arising from a streamer discharge appear as single pulses with rise and fall times in the order of 20 and 100 nsec respectively. Burst pulse currents generally appear as a sequence of pulses with smaller amplitudes and slower risetimes than streamer pulses. A sequence of burst pulses can exist for time durations in the order of 100 μsec. A streamer pulse may promote the appearance of a subsequent burst pulse however a burst pulse will temporarily inhibit the formation of streamer pulses.

Loeb (20) has proposed that it is the length of the mean photoionizing free path relative to the ionizing length

(the minimum length out from the anode surface at which ionization by electron collision ceases) which determines whether a streamer or burst pulse will occur. If the mean free path is much larger than the ionizing length the ionization will manifest itself as a burst pulse. If the mean free path is nearly equal to or shorter than the ionizing distance streamer pulses will prevail. Small amounts of additives or impurities greatly effect the photon absorption properties of air and consequently have a significant effect on the onset pulse characteristics of a gap.

The repetition rate of streamer pulses in the onset region is a function of the magnitude of the applied voltage as well as the geometry of the anode. Maximum repetition rates of the order of several kilohertz have been observed (43). At sufficiently high rates the streamer discharges become visible, taking on the appearance of a brush.

With increasing gap voltage the onset pulse phenomenon gives way to a glow discharge. If the anode possesses a relatively large radius of curvature, the transition is gradual. As the voltage is increased, the repetition rate of burst pulses increases, a DC current component appears, and the discharge current takes on the form of a DC current with a small ripple of a frequency in the order of one Mhz. The glow discharge derives its name from its visual appearance which is a closely adhering soft glow over the anode surface.

The glow suppresses the development of streamer type discharges. Streamers reappear only after the applied voltage is increased considerably beyond the onset voltage of the glow. The characteristics of these streamers are similar to those of the onset streamers, however, because they ultimately initiate a complete breakdown of the gap, they are termed "pre-breakdown streamers". In short gaps the streamers create a highly ionized channel and in consequence breakdown occurs when they succeed in crossing the gap and initiate a return stroke. If the gap is long or if a high resistance is inserted in the test circuit, the streamer channels will not be as highly ionized and the corona discharge will extend completely across the gap and yet not initiate breakdown. Such a discharge phenomenon is termed a diffused discharge. Breakdown will occur at a voltage slightly higher than the onset voltage of this phenomenon.

The results of the present investigation of corona discharge activity in SF_6 indicate that there are substantial differences between anode coronas in air and in SF_6. The most apparent difference appears at the onset region of a steady or DC corona current. In air the onset of a DC corona current coincides with the inception of a glow discharge whereas in SF_6 it coincides with the appearance of a very narrow, well defined filament with a bright root. The appearance of this filament is very different from the brush-like discharge observed in air in the onset pulse region.

The brush discharge exhibits a diffuse tip in the low field region, the result of a branching of the streamers which constitute the discharge. The filamentary discharge in SF_6 does not exhibit a diffuse tip and the discharge column is much narrower than that of the brush.

A study by Weissler and Mohr (45) of the visual appearance of anode coronas at static voltages in air-Freon mixtures demonstrates that the addition of even small amounts of Freon, a highly electronegative gas, markedly alters the visual appearance of the corona discharge in air. To some extent, the visual appearance of a corona discharge in air with the addition of 1% of Freon resembles the discharge in SF_6. In both cases the initial appearance of the discharge is that of a very narrow, well defined filament. At voltages somewhat above the onset voltage the visual appearance of each discharge changes and the resemblance ceases.

Loeb (20) has proposed a tenative explanation for the visual manifestations of corona discharges in air with small additions of Freon. The presence of the Freon will have little effect on the electron collision ionization processes because of its small concentration. It will however substantially effect the photoionization processes by significantly reducing the mean photoionizing free path. This will effect the discharge primarily in two ways. The spread of ionization over the anode surface in the form of burst pulses will be prevented and in consequence the glow discharge will fail to

materialize. Secondly, branching of the streamer type ionization growth will also be curtailed. Weissler and Mohr (45) proposed that the channel of positive ions created by the passage of a streamer is rapidly neutralized by electron-positive ion recombination reactions and electron attachment reactions which form negative ions. Because of the latter a neutral but still highly ionized channel remains. Subsequent streamers prefer to follow the existing channel and consequently this, as well as inhibited streamer branching, gives the discharge a highly confined appearance.

5.1.2 Momentary Discharge Phenomenon in SF_6

On the basis of Loeb's explanation for the discharge characteristics of 1% Freon-air mixtures, the following assumption will be made. The filamentary appearance of the corona discharge at the onset of a sustained discharge in SF_6 is evidence that the mean photoionization free paths of the principal ionization photons in SF_6 are very short, at least with regard to discharge activity slightly above or below the onset voltage level of a sustained discharge.

At first glance one might interpret a momentary discharge as a streamer pulse followed by a sequence of burst pulses. Oscillogram #11 of Figure 3.2 illustrates that the initial pulse of a momentary discharge has a rise and fall time somewhat characteristic of a streamer in air. This leaves little doubt that the initial pulse is a streamer. There are several reasons however for suspecting that the

subsequent pulses are not bursts, or perhaps more accurately, do not indicate a burst type spread of ionization over the anode surface. The short photoionizing paths in SF_6 should preclude the growth of discharges over the anode surface and favour a growth normal to the surface. Also, near the onset voltage of momentary discharge activity, the pulses subsequent to the initial streamer pulse undergo a successive increase in magnitudes to a level which is apparently far above the magnitude of the initial streamer pulse. Burst pulses in air exhibit an amplitude which is much smaller than that of streamer pulses in the same gap at the same voltage. Also, succeeding burst pulses generally exhibit a decrease, not an increase in pulse amplitude. Finally, the repetition rate of the pulses of a momentary discharge is virtually the same as the repetition rate of pulses constituting a sustained discharge. The visual appearance of the latter establishes that a sustained discharge is a sequence of streamer pulses. It is therefore likely that a momentary discharge is a sequence of streamer pulses.

The high repetition rate of the pulses which constitute a momentary discharge can probably be attributed to the high electronegativity of SF_6. Mobility measurements of SF_6^- (21, 22), the predominant negative ion in an SF_6 discharge[1], yield a typical value of 0.45 cm^2 $volt^{-1}$ sec^{-1} at

---

[1] Ionization and attachment mechanisms are discussed in more detail in Chapter VI, page 109.

760 mmHg and 0°C. In a field characterized by an E/p of 89 kv cm^{-1} atm^{-1}, a negative ion would drift a mean distance of 0.04 cm in one microsecond. Assuming a similar mobility for positive ions, a pulse repetition rate of approximately one pulse per microsecond certainly does not allow for a substantial ion drift clearing of the positive ion space charge produced by a streamer. This space charge effects a reduction of the voltage gradient at the anode surface and in consequence inhibits subsequent streamer discharges. Many positive ions are eliminated however by recombination reactions with electrons. Also, because of the high electronegativity of SF_6, a large number of negative ions are produced by electrons suffering attachment collisions and these neutralize the positive ion space charge to a large degree, especially in the low field regions. Thus, through several mechanisms, the inhibiting effects of the space charge created by streamer ionization are reduced with sufficient rapidity to allow high pulse repetition rates.

Pulses immediately subsequent to the initial pulse of a momentary discharge are of smaller amplitude than the initial pulse because of incomplete neutralization of the streamer space charge. The momentary discharge inception voltage is somewhat higher than that of single pulse activity because, at the inception voltage of the latter, the voltage gradient is just sufficient to allow the formation of a streamer initiating avalanche. The presence of a space

charge in the gap precludes further streamer development.

The sequence of pulses subsequent to the initial pulse of a momentary discharge displays a temporary growth phase during which the pulses display an almost successive increase in magnitude. It is very probably that this growth results from a successive enhancement of the voltage gradient at the anode surface with the passage of each pulse. Only the formation of a negative ion space charge can account for an enhancement of the gradient at the anode surface. Such a space charge could result from negative ions created by attachment reactions between neutral molecules and electrons produced in the low field regions by streamer ionization. Large numbers of negative ions would be produced in this manner in the highly electronegative SF_6. In view of earlier arguements it is doubtful that photoionization plays a significant role in the creation of a negative ion space charge.

Negative ions formed in the low field regions by streamer activity will drift toward the anode and mutual repulsion as well as attraction to positive ions drifting toward the cathode will tend to spread the advance of the negative ions laterally over the anode surface. Measurements by Eccles et al (23) show that the predominant negative ions in SF_6 suffer field induced detachment reactions at E/p values exceeding 76 kv cm^{-1} atm^{-1}. Since electron avalanches will not occur in SF_6 at E/p values of less than 89 kv cm^{-1} atm^{-1} (10), the voltage gradient at the anode surface must

be such that the majority of the negative ions approaching the anode are neutralized before reaching the surface. This results in a dynamic separation between the negative ion space charge and the anode surface. In the region of separation, the electric field gradient will exceed the space charge free value. The negative ion sheath will also effect a reduction of the voltage gradient between the sheath and the cathode. The growth phase of the momentary discharge activity indicates that the field enhancement is maintained over a distance which is sufficient for streamer development. The reduced voltage gradient between the negative ion sheath and the cathode curtails the propagation of streamers into the gap and in consequence imposes a limit on the maximum current pulse which a streamer can induce. The pulse amplitudes therefore do not increase indefinitely but level off at some maximum value.

The current oscillograms of Figure 3.2 do not suggest an obvious reason for the self-extinction of a momentary discharge. It is quite probable, however, that the discharge is terminated by the movement of the negative ion space charge toward the anode. The resulting reduction in the field enhancement distance will then prevent the occurrence of further ionization. Eccles et al (23) have shown that the probability of field induced negative ion detachment in SF_6 changes rather slowly with a wide variation of E/p. It is thus conceivable that extensive variations in the field

enhancement distance could occur because of statistical fluctuations in the detachment process. The slow variations in the pulse amplitudes observed after the initial rise to a maximum value are probably due to gradual changes in the negative ion space charge population. This population should be self-stabilizing to some degree because an increase in the sheath population will effect a decrease in the distance over which field enhancement occurs and enhance the low field barrier. Therefore, the level of discharge activity will be reduced and as a result the negative ion population will begin to decrease.

An increase in the applied voltage beyond the inception level of momentary discharge activity should in theory increase the distance of separation between the anode surface and the negative ion sheath. The result is an increase in the magnitude of the pulses as well as a decrease in the probability of the extinction of the discharge by the mechanism discussed above. The experimental results of Figure 3.3 suggest that this is indeed what happens.

Oscillogram #10 indicates that an increase in voltage enhances the initial pulse of a momentary discharge to a far greater extend than the subsequent pulses. An increase in the negative ion population resulting from an enhancement of the ionization processes would tend to suppress the increased activity to some extent. There is essentially no space charge in the gap when the first pulse occurs. The increase in the

intensity of the inital streamer results in a more rapid build up of the negative ion sheath to a point where the temporary growth phase is virtually nonexistent (see oscillogram #10, Figure 3.2, p.39)

5.1.3 Sustained Discharge Phenomenon in SF_6

The corona current waveforms which result from the presence of a sustained corona discharge in SF_6 bear a considerable resemblance to the waveforms associated with a momentary discharge. Both appear as a sequence of pulses, approximately 5 to 10 per microsecond, with peak amplitudes much greater than that of the average current. A sustained discharge, unlike a momentary discharge however, was never observed to suffer a self-extinction. The similarity in waveforms would suggest that a sustained discharge is a momentary discharge which does not suffer self-extinction.

The transition from a momentary to sustained discharge is very abrupt with respect to a change in voltage level. At the inception voltage, a sequence of momentary discharges occurring at a rate typically in the order of 10 per minute with each discharge lasting in the order of 100 μsec, is suddenly transformed to a sustained discharge. The transformation is marked by a very large increase in the average corona current. Reversion to a momentary discharge results only when the gap voltage is significantly decreased. Therefore, at the inception voltage, there is a discontinuous change in the probability of discharge extinction. This,

plus the fact that the average current level of a sustained discharge undergoes much smaller temporal variations, suggest that the two types of discharge phenomena are not entirely similar.

It is quite likely that a transformation from a momentary to sustained discharge occurs when the momentary discharge repetition rate is sufficient to generate foreign products (through the inducement of chemical reactions by high energy electrons and photons) in concentrations sufficient to alter the properties of the gas. Changes in the chemical composition will alter the photon spectrum and absorption properties and, to a lesser degree, effect changes in the ionization and attachment coefficients (20).

Experimentally it was observed that the transition from a momentary to sustained discharge was a process which in most cases took in the order of a second to complete. The transition was marked by a sudden acceleration in the momentary discharge repetition rate and an accompanying rise in the DC current level. This suggests a run-away process in which each discharge contributes to the accumulation of foreign products in the gas. This promotes further discharges and, as the accumulation increases so to does the repetition rate until the discharge becomes sustained.

A sustained discharge, once established, generates sufficient chemical by-products to maintain itself at voltages below the onset level with the result being an

offset voltage lower than the onset value. The reduced onset voltage of a sustained discharge of a 1/16 inch diameter anode, observed to exist for several minutes after the extinction of the same, suggests that a discharge of sufficient intensity will effect changes in the gas composition which last for several minutes.

An inspection of the surface conditions of the sphere and rod electrodes subjected to breakdown and corona discharge tests showed that the presence of a sustained corona discharge resulted in the discolouration of the anode surface. This discolouration was most in evidence on the surface of the 1/16 inch diameter rod and appeared to be some form of insulating layer on the electrode surface. This layer probably resulted from chemical reactions between the constituent radicals of SF_6 generated in the discharge, and the electrode.

The visual changes in the discharge manifestations resulting from an increase in the gap voltage may in part be due to further changes in the gas composition brought about by an increase in the discharge activity with increasing voltage. The spread of the visible discharge with increasing voltage was observed for the most part to be tangential rather than normal to the electrode surface. This indicates that a low field barrier to discharge growth was present at all voltages up to the breakdown.

In view of the highly localized nature of the sustained discharge at onset, it is possible that a local

temperature rise of the gas may act to stabilize the discharge. Kay and Page (25) report SF_6^- and SF_5^- electron affinities of 1.4 ev and 3.6 ev respectively. A high gas temperature (10^3 - 10^4 °K), could increase the negative ion detachment rate in the high field region and thus stabilize the discharge by limiting fluctuations in the field enhancement distance. Also, the SF_6 gas temperature has a significant effect on the relative proportions of SF_5^- and SF_6^- ions produced in a discharge (24). This may be of significance.

Irradiation of the gap with 2537 Å U.V. radiation was observed to significantly reduce the onset voltage of a sustained discharge. This reduction can probably be attributed to the increase in the repetition rate of momentary discharge activity effected by the radiation. It should also be considered, however, that the photon energy of the radiation (4.28 ev) is significantly greater than the electron affinity of the negative ions and thus irradiation of the gap could significantly alter the detachment processes.

5.2 Non-uniform Field Breakdown in SF_6

It appears virtually beyond argument that the presence of a corona discharge in a positive point-plane gap insulated with SF_6 considerably enhances the breakdown strength of the system. The pressure range over which this apparent enhancement occurs is often referred to as the "corona stabilized breakdown region" and the high pressure limit of this range is the pressure at which the breakdown and the corona onset

voltage coincide, i.e., breakdown is not preceded by corona.

A study of the literature indicates that there is some ambiguity in the concept of the corona onset voltage of an SF_6 insulated system. In some investigations it appears that the onset voltage of the single streamer pulses is considered the corona onset voltage while in others it is the onset voltage of a continuous discharge. To exemplify the discrepancy which this ambiguity can introduce, consider the phases of corona development in a 1/16 inch diameter rod-plane gap of 1.5 inch gap length, as illustrated in Figure 4.6. The inception voltage levels of the single pulse and the sustained discharge activity differ by as much as 75% of the single pulse inception level. A further complication is introduced by the significant effect of ultra-violet radiation on the onset voltage of the sustained discharge inception level. The difference between the irradiated and non-irradiated sustained discharge inception levels is as high as 28% of the non-irradiated value.

The widely differing range of voltage levels over which the various prebreakdown discharge activities occur also leads to a considerable discrepancy in the pressure range over which the breakdown of the system is considered to be "corona stabilized". Again in reference to Figure 4.6, the assumption that the corona onset voltage corresponds to either the single pulse, irradiated sustained discharge, or non-irradiated sustained discharge inception levels leads

to a maximum pressure of "corona stabilized breakdown" of 4.0, 3.0, and 2.5 atmospheres respectively, a considerable variation.

One of the objectives of this work was to provide detailed information on the discharge and breakdown behavior of a positive rod-plane gap insulated with SF_6 as a function of the gas pressure. Particular attention was paid to the nature of the prebreakdown discharge in the gap at the voltage at which breakdown occurred. The results of this study may throw some additional insight into the relationships between breakdown and prebreakdown phenomena, and hopefully indicate more accurately over what pressure range "corona stabilized breakdown" occurs.

To summarize the experimental results of the study, the data obtained for a 1/16 inch diameter rod-plane gap of 1.5 inch gap spacing will be examined as the high non-uniformity of this configuration yielded results which best exemplify the non-uniform field behavior of the gas. To assist in the discussion of the variations in the discharge and breakdown behavior as a function of gas pressure, the applied voltage-pressure graph on which the results are plotted is divided into four regions, as shown in Figure 5.1.

Region I is characterized by a breakdown strength which is much higher than the onset levels of the various types of corona activity observed and also a breakdown strength which increases with an increase in gas pressure.

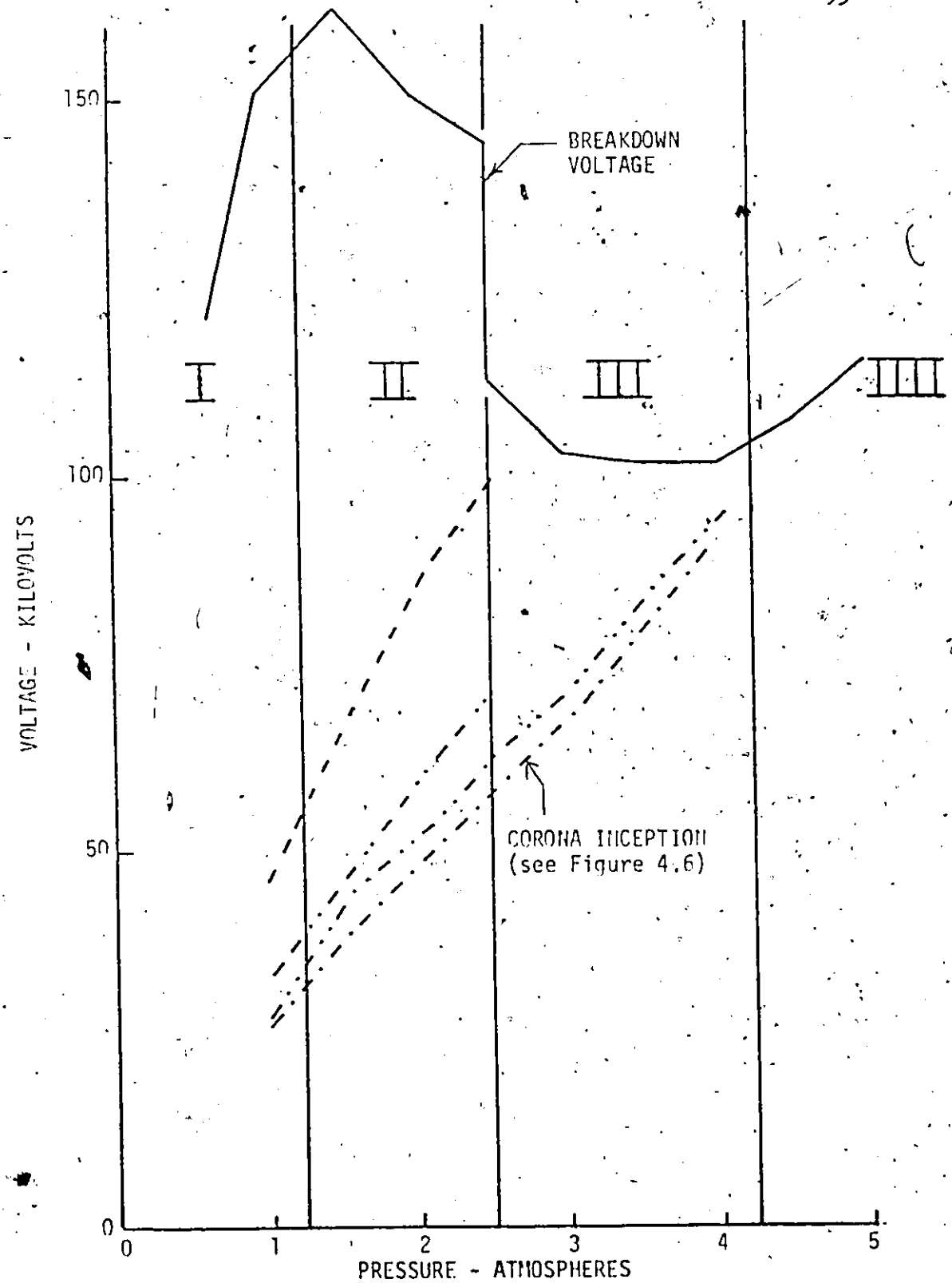

FIGURE 5.1. BREAKDOWN AND CORONA DISCHARGE INCEPTION VOLTAGES OF A 1/16 INCH DIAMETER ROD-PLANE GAP OF 1.5 INCHES GAP LENGTH.

The spark trajectory studies indicate that the breakdown sparks in this region are relatively straight suggesting that breakdown probably occurs when streamers, confined by the space charge, gain sufficient intensity to penetrate the space charge, reach the cathode, and initiate a spark.

Region II is characterized by a rapid decrease in the slope of the breakdown voltage-gas pressure curve to the extent that the breakdown voltage is decreasing with increasing gas pressure at the upper pressure limit of this region. Breakdown sparks in this region exhibit a pronounced curvature and this, in conjunction with the fact that a continuous discharge is present in the gap at the time of breakdown, suggests that the spark is initiated by streamers which are able to propagate around the space charge formed by the discharge. This would account for the decrease of breakdown voltage with the increase in gas pressure in this region.

As the gas pressure increases, the ability of a streamer to propagate is enhanced. The photon absorption coefficient of the gas increases with increasing gas pressure and thus a greater percentage of the photons produced by the streamer are absorbed sufficiently close to the streamer tip to initiate secondary avalanches. This effects an increase in the space charge accumulation at the streamer tip which enhances the local field and thus the ability of the streamer to propagate. The space charge is localized

to a higher degree at higher gas pressures as a result of reduced diffusion of electrons in the streamer. This increases the electron-ion collision rate and in consequence increases the rate of photon generation and hence avalanche production at the streamer tip. Since the propagation properties are enhanced by an increase in gas pressure so too is the facility of the streamers to circumvent the space charge field at the anode tip. Thus the breakdown voltage of the gap decreases with increasing pressure.

Region III differs from regions I and II in that a sustained discharge is not present in the gap when a breakdown occurs. Momentary discharge activity was observed in the gap at breakdown in this pressure range and in some cases the repetition rate of the discharges was sufficient to cause a noticable deflection of the microammeter in series with the gap. Breakdown in the presence of high momentary discharge currents were observed in the majority of the rod-plane configurations examined under both irradiated and non-irradiated conditions. However, such activity was much more prevalent in irradiated gaps. For example, in the gap referred to in this discussion, at a gas pressure of 3 atmospheres the microammeter indicated a considerable corona current when the gap was irradiated (see Figure 3.1). However, the microammeter gave no indication of a corona current in the non-irradiated gap at the same pressure at any level of applied voltage up to the breakdown.

The high levels of momentary discharge activity do not appear to have a significant effect on the breakdown voltage of the gap. Experimental results obtained at a gas pressure of 3 atmospheres show a breakdown voltage in the presence of considerable discharge activity (irradiated breakdown voltage) which was somewhat lower than the non-irradiated breakdown voltage. In the latter case the discharge activity was too small to cause a deflection of the microammeter. Similar behavior was observed in the 1/8 inch diameter rod-plane gaps of 0.5 and 1.5 inch length at 2.0 atmospheres pressure.

The trajectory of the breakdown sparks in region III were observed to be relatively straight. This suggests that the breakdown in region III occurs in a gap essentially free of space charge. Very likely, the streamer pulses which initiate the momentary discharges progress increasingly far into the gap with increasing level of applied voltage until, at the breakdown voltage, one of the streamers progresses sufficiently far into the gap to initiate breakdown. As this streamer is the initial pulse of a momentary discharge it is not inhibited by a space charge and thus the spark is straight.

The transition from region II to region III is apparently very abrupt. At a gas pressure of 2.5 atmospheres, a breakdown characteristic of those observed in region II was recorded at 145 kv in the 1/16 inch diameter rod-plane gap. The breakdown was in the presence of a sustained discharge

and the spark channel displayed a pronounced curvature. At the same gas pressure, a breakdown having the characteristics of those of region III was also observed. The breakdown voltage in this case was 112 kv, breakdown occurred in the presence of momentary discharge activity, and the spark channel was relatively straight (see Figure 4.13). An abrupt change from region II to region III type breakdowns was also observed for a 1/16 inch diameter rod-plane gap of 1/4 inch gap length. The difference in breakdown levels was not as significant in this case, a fact which can probably be attributed to the lower field non-uniformity of the 1/4 inch gap. There were no measureable changes in any of the controllable parameters of the two systems which might account for the two distinct breakdown levels indicated by the tests.

Works and Dakin (5) apparently encountered the same phenomenon when they reported that in some cases breakdown studies of positive rod-plane gaps appeared to indicate two distinct breakdown levels at a single gas pressure falling in the negative slope region.

In region IV no discharges of any nature were observed prior to a complete breakdown of the gap. This suggests that the first streamer formed in the gap is capable of penetrating sufficiently far into the gap to initiate a breakdown spark.

The results of this investigation suggest that "corona stabilized breakdown" only occurs in the presence of a sustained discharge, i.e., in the case of a 1/16 inch diameter

rod-plane gap with a spacing of 1.5 inches, such a breakdown occurs at or below 2.5 atmospheres. Also, it appears that more descriptive terms than "corona onset voltage" should be adopted in discussions of prebreakdown and breakdown phenomena in SF_6.

CHAPTER VI

THEORETICAL PREDICTION OF DISCHARGE CHARACTERISTICS

Since 1940, when the streamer theory of breakdown was first proposed by Meek (29) and independently by Raether (30), a number of authors have presented methematical formulations to account for the physical phenomena which play a dominant role in the avalanche-streamer transition and streamer propagation. An excellent review of literature describing early work on this topic can be found in reference 31.

Avalanche-streamer transition theories are of particular interest when consideration is given to the possibility of predicting the discharge characteristics of non-uniform field gaps insulated with SF_6. The experimental studies discussed in Chapter 4 indicate that the behavior of the SF_6 insulation subjected to high, non-uniform DC stress is directly related to a streamer type ionization phenomenon.

This chapter is devoted in part to an analysis of the principal streamer onset and breakdown criteria proposed in the literature. This analysis is based on a comparison of experimentally determined streamer onset and breakdown voltages with comparable theoretical values determined using these criteria as a basis. Also, this chapter presents a method of predicting the onset gas pressure of a corona free breakdown in an SF_6 insulated, DC stressed gap. The method

is assessed on the basis of a comparison of experimental and theoretical results.

6.1 Calculation of Electric Field Distribution

With the exception of purely empirical formulations based on experimental data, virtually all of the proposed theoretical and semi-empirical criteria developed for the calculation of discharge onset voltages are based on an accurate knowledge of the electric field distribution in the gap due to the potential difference applied between electrodes. The electric field distributions of the electrode geometries used in the experimental work are not easily determined by analytic methods. This difficulty was overcome in two ways. The sphere-plane electrode system was approximated as an isolated sphere-sphere gap of the same sphere diameter and twice the gap length of the experimental gap. The gradient in the gap and along the symmetry axis is (32)

$$E(x) = \frac{2DV[D^2(f+1)+4(D/2-x)^2(f-1)]}{[D^2(f+1)-4(D/2-x)^2(f-1)]^2} \qquad (6.1)$$

where D = the gap length along the symmetry axis

V = the gap voltage (twice the experimental gap voltage)

x = the distance from the surface of either sphere

$f = \frac{x/R+1+\sqrt{(x/R+1)^2+8}}{4}$

R = the radius of the spheres.

The field distributions of the rod-plane electrode systems were determined numerically using a finite difference technique.

The boundaries within which the rod-plane field distributions were determined corresponded to the surfaces which confined the gas within the pressure vessel, and included the vessel walls, the base plate, the bushing, and the electrodes. Since the system is rotationally symmetric about the center of the electrodes the total volume of the enclosed gas can be represented by any cross-section containing the symmetry axis. Also, as a consequence of this field symmetry, it is necessary to determine the field distribution in one half of the cross-section only.

Several approximations to the electrode geometry were made to simplify the boundary conditions of the numerical solution. Figures 6.1 and 2.2 compare the actual and assumed geometry of two electrode configurations and Figure 6.1 illustrates the total bounded area in which the field distribution was determined. The boundaries imposed by the upper connecting rod, bushing end plate, bushing rod, mounting flange, and upper portion of the cylinder wall were approximated by a Neumann boundary[1] as illustrated in Figure 6.1. The portion of symmetry axis between the two electrodes was

---

[1] At a Neumann boundary the gradient of the function is specified.

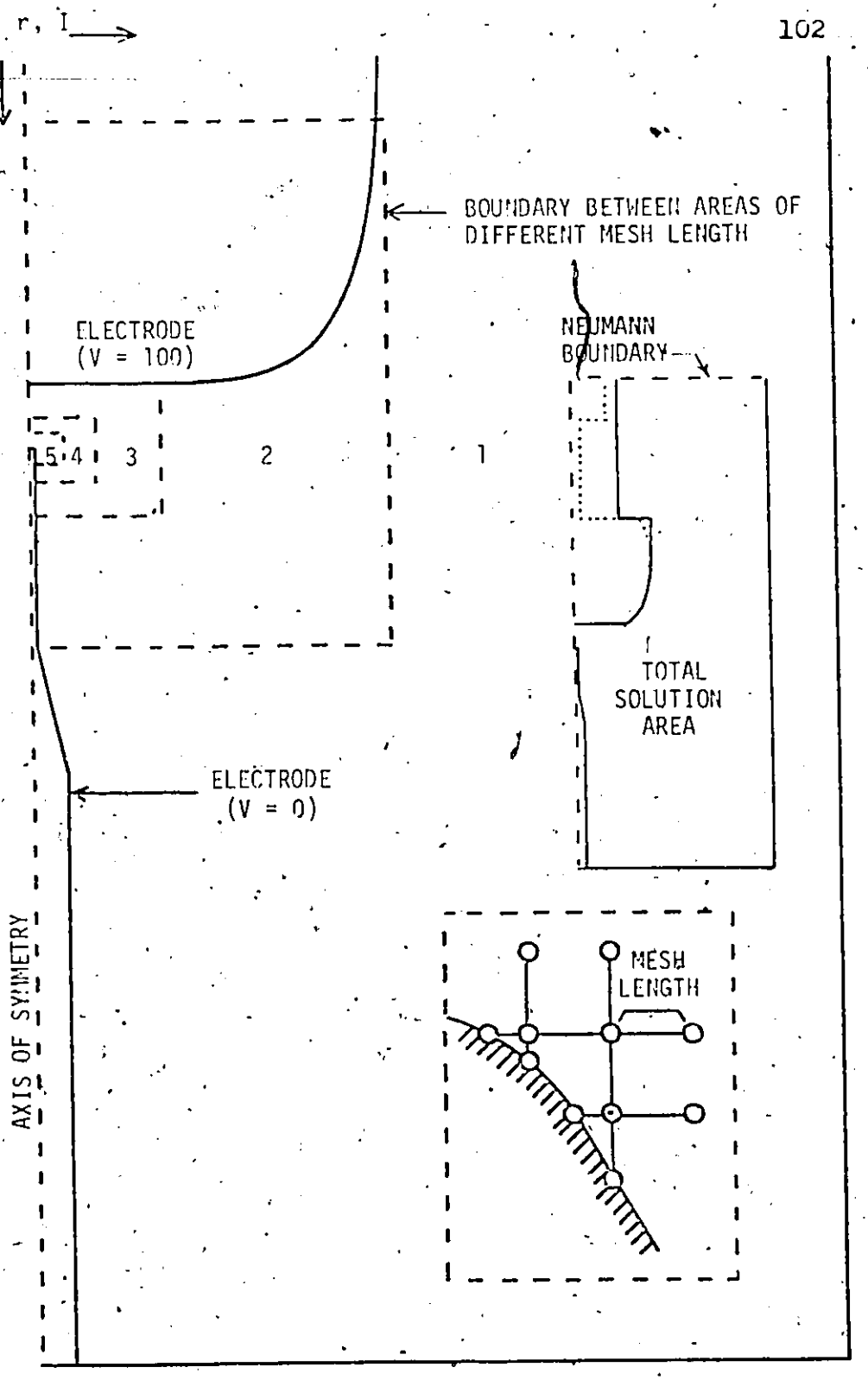

FIGURE 6.1. BOUNDARY CONDITIONS FOR THE NUMERICAL SOLUTION OF THE ELECTRIC FIELD DISTRIBUTION.

also represented as a Neumann boundary. The remaining boundaries of the field were represented as Dirichlet[1] boundaries. The uniform field electrode was assigned a potential of 100.0 and the non-uniform field electrode and vessel walls were assigned a potential of 0.0 in all calculations.

The bounded area was reduced to a square mesh and the potential at each mesh point was calculated numerically using the extrapolated Liebmann method (33). Storey and Billings (34) have developed finite difference equations for the calculation of mesh point potentials of a three dimensional, axially symmetric field. These equations apply to a solution space which is mapped in a plane and then reduced to a finite number of points defined as the intersection points of grid lines running parallel and perpendicular to the axis of symmetry. The calculation of the potential at a mesh point is based on an assumed knowledge of the potentials of the four adjacent mesh points. These need not be equidistant from the mesh point under calculation and thus the mesh can be fitted exactly to the boundaries, as illustrated in Figure 6.1. The equations developed by Storey and Billings are summarized in Appendix A, which also includes the Neumann boundary formulation appearing in the field calculations.

---

1. At a Dirichlet boundary the value of the function is specified.

The finite difference equations developed by Storey and Billings are derived from a truncated Taylor series expansion of the potential at the mesh point. Thus inherent in the equations is a truncation error which is related to separation distance of the mesh points (mesh length) and which increases with increasing separation. From this standpoint a small mesh length is desirable. On the other hand, the total number of mesh potentials which must be determined as part of the overall field calculation is in inverse proportion to the mesh length. Therefore, computation times (and costs) can reach excessive levels if a very small mesh length is adopted. It is therefore the best compromise to choose the coarsest mesh which will give the accuracy desired. Unfortunately, it is virtually impossible to determine beforehand the accuracy of the solution which a given mesh size will yield. It is necessary to rely on experience in choosing a suitable mesh or, if the experience is not available, (as in the present case) a trial and error technique must be adopted.

In view of the difficulties expressed above, the field distribution within the pressure vessel was determined using a number of different mesh lengths. A solution was only adopted for subsequent calculations if a comparison of the results corresponding to different mesh lengths indicated that the field distribution adopted would not significantly differ from that obtained using a finer mesh length.

Aside from accuracy considerations, other factors are important in determining the mesh size. Irregular mesh lengths increase the complexity of the computer programme and have shown in practice to lead to greater truncation errors. It is therefore advisable to choose a mesh size which minimizes the number of irregular mesh lengths at the boundaries. When only a small region of the total field distribution is of interest, the field can be divided into a number of areas each characterized by a different mesh length, with the area of interest possessing the shortest mesh length and the area most remote from this region possessing the longest mesh length. An example of this is illustrated in Figure 6.1 in which case the field was divided into five areas.

With the above considerations in mind, the following general procedure was adopted for determining the mesh size:

1. The field was divided into a number of areas with the mesh length of each determined by the proximity of that area to the tip of the rod electrode (the region of greatest interest).

2. The mesh length of the area which included the tip of the rod electrode was a simple fraction of the rod radius.

3. The coarsest mesh was 1/8 inch.

4. The ratio of mesh lengths of adjacent areas equalled either two or three.

5. Irregular mesh lengths were avoided wherever

possible.

When using areas of different mesh length, as illustrated in Figure 6.1, a problem arises in the calculation of mesh potentials at the boundary of these areas. Figure 6.2 illustrates several mesh points in the vicinity of a boundary. The potentials at P_4, P_6, and P_8 can be easily determined using the irregular mesh length equation (i.e., P_6 is determined from potentials at P_2, P_5, P_7, P_{11}). The use of this equation however proved to introduce serious errors. This problem is easily avoided by the use of the regular mesh equation; for example, P_6 can be determined from potentials P_2, P_4, P_8, P_{16}. To calculate the potential at points P_5, P_7, ..., points P_5', P_7', ... are introduced. The potentials of these points are determined by performing a linear interpolation between each set of potentials at opposite corners of the square in which the point is centered and averaging the interpolated values. For example

$$V_{P5'} = \frac{1}{4}(V_{P6}-V_{P1}) + \frac{1}{4}(V_{P4}-V_{P2}) + \frac{1}{2}(V_{P1}+V_{P2})$$

The potential at P_5 can now be determined with the regular mesh equation. This technique can be extended to boundaries with a 3:1 transition in mesh lengths as well.

Irregular mesh equations can also be avoided at the boundaries of cylinders centered on the axis of symmetry. These boundaries appear as a straight line in the two

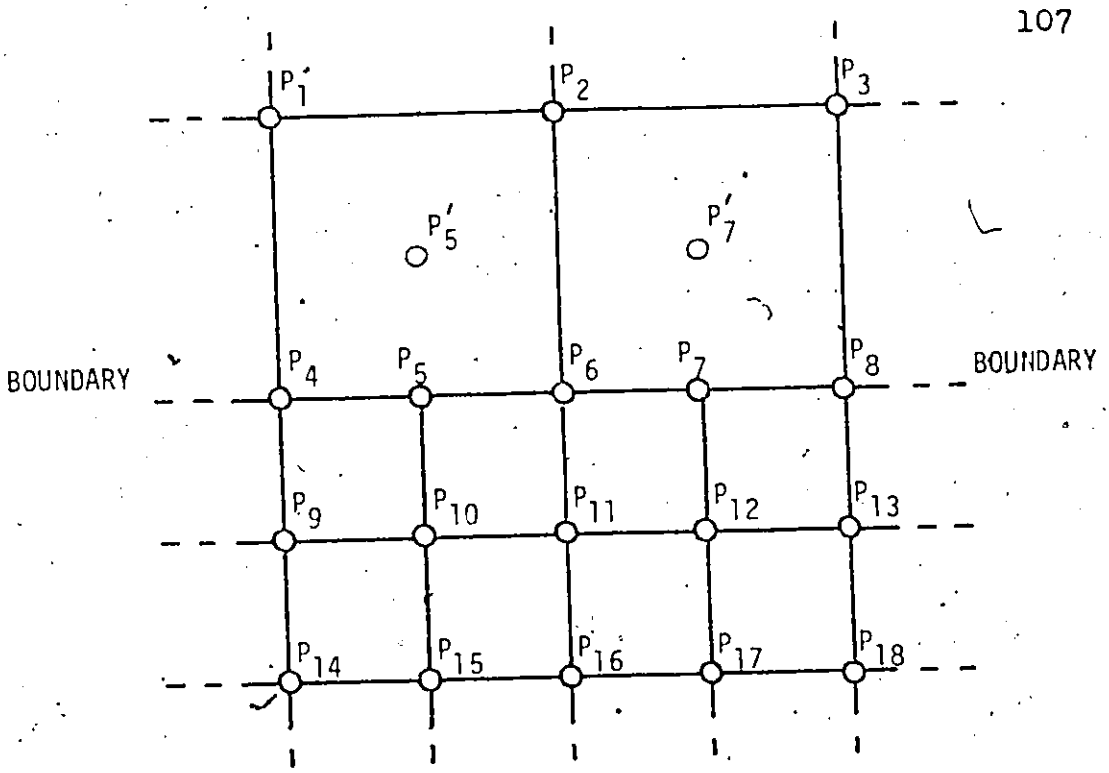

FIGURE 6.2. BOUNDARY BETWEEN TWO AREAS OF DIFFERENT MESH LENGTH.

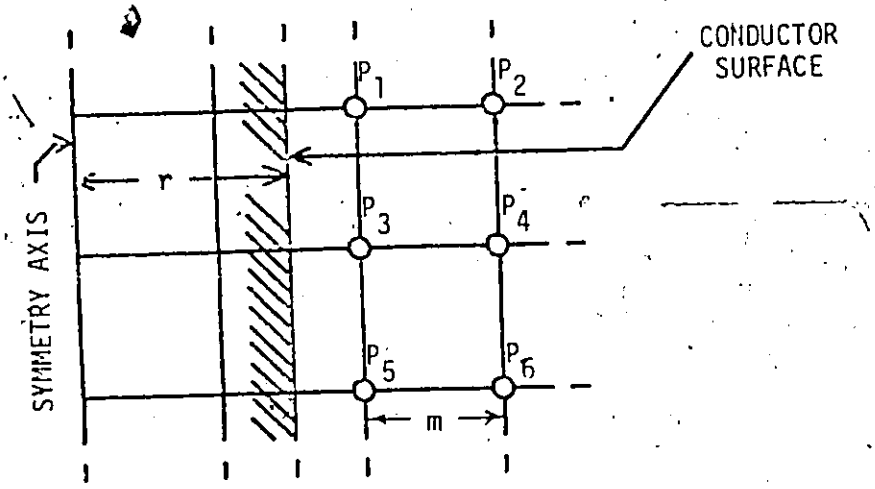

FIGURE 6.3. MESH POINTS ADJACENT TO A DIRICHLET BOUNDARY.

dimensional mapping. Figure 6.3 illustrates the boundary of a cylinder of radius r, centered on the symmetry axis. Points P_1, P_3 and P_5 can be calculated using the irregular mesh formulation, however, this can be avoided if the assumption is made that the equipotentials run parallel to the conductor surface at least to a distance 3m-r from the surface, where m is the mesh length. If other boundaries are remote (with respect to 3m-r) this assumption introduces little error. The potentials at points P_1, P_3, and P_5 can be calculated from the analytic solution for the field distribution between concentric cylinders. For example

$$V_{P3} = \frac{(\log_e 2m - \log_e r)}{(\log_e 3m - \log_e r)} \cdot V_{P4}$$

Apart from the cases just cited, an irregular mesh was used whenever necessary to provide an exact mesh fit to the electrode surfaces.

In the calculations pertaining to the discharge phenomena in the gas, it was assumed that the ionization activity occurred along the axis of symmetry, near the surface of the rod or sphere electrode. It was necessary to develope a mathematical expression for the electric field gradient along the axis and this was accomplished by fitting a polynomial to the numerically determined potentials of mesh points lying on the axis of symmetry and in the vicinity

of the rod tip. The subroutine LSCF[1] was adopted for this purpose.

This subroutine determines the coefficients of the polynomial of order prescribed by the user (10th order is the maximum allowed) which gives the minimum mean squared error fit to a set of data points.

6.2 Mathematical Modelling of Ionization and Attachment Processes in SF_6

The fundamental processes which characterize the behavior of SF_6 gas subjected to high electric stress are both numerous and complex. They can however be lumped into broad classifications, i.e., ionization reactions, attachment reactions, electron and ion displacement processes such as drift and diffusion, etc.

Dibeler and Mohler (35) have studied dissociative reactions in SF_6 and list a considerable number of possible electron collision reactions yielding positive ions. The reaction requiring the lowest electron energy upon impact (15.9 ev) is

$$SF_6 + e \rightarrow (SF_6^+)^* + 2e \rightarrow SF_5^+ + F + 2e$$

Mass spectrometry studies (36, 37, 38) indicate that SF_6^- and SF_5^- are the predominant negative ions resulting from

---

[1] This subroutine was developed by Dr. Walton for the University of Windsor Computer Center.

electron collisions in SF_6, exceeding other possible ions such as F^- and F_2^- by at least a hundredfold. The formation of the vast majority of SF_6^- ions is initiated by the reaction (36, 38)

$$SF_6 + e \rightarrow (SF_6^{-*})^1 \qquad \text{(i)}$$

where $(SF_6^{-*})^1$ is a metastable with a lifetime of the order of 10 μsec. Reaction (i) is a resonance capture process with a maximum cross-section of 10^{-15} cm^2 at an electron energy of about 0.05 ev. The variation of the cross-section of this reaction with electron energy is very sharp, thus the cross-section drops to an insignificant value for electron energies differing by more than a small fraction of an electron volt from 0.05 ev. There are several possible reactions subsequent to (i).

$$(SF_6^{-*})^1 \rightarrow SF_6 + e \qquad \text{(ii)}$$

$$(SF_6^{-*})^1_v + (SF_6)_o \rightarrow (SF_6^-)_o + (SF_6)_v \qquad \text{(iii)}$$

$$(SF_6^{-*})^1_v + (SF_6)_o \rightarrow (SF_6)_o + (SF_6^-)_v \qquad \text{(iv)}$$

Reaction (ii) is termed "autodetachment". Reactions (iii) and (iv) involve a collision with a neutral SF_6 molecule and the resulting negative ion is termed a "collision stabilized ion". Subscripts o and v refer to zero order and excited vibrational states respectively. Reaction (iv)

is the more probable of reactions (iii) and (iv).

The formation of the majority of SF_5^- ions follows a somewhat similar process. Initially a metastable is formed by the reaction

$$SF_6 + e \rightarrow (SF_6^{-*})^2 \qquad (v)$$

The lifetime of $(SF_6^{-*})^2$ is exceedingly short and as such, the following subsequent reaction almost invariably occurs

$$(SF_6^{-*})^2 \rightarrow SF_5^- + F \qquad (vi)$$

The formation of SF_5^- is a resonance capture process and has a significant cross-section (10^{-17} cm^2) only at electron energies which vary little from 0.05 ev.

There are a number of possible inelastic collision reactions which do not increase the ion population but play a significant role in the overall determination of the discharge properties of the gas. Also significant are dissociation reactions which produce both a positive and negative ion, i.e.

$$SF_6 + e \rightarrow SF_5^+ + F^- + e$$

A mathematical model of gas discharge phenomena based on individual reaction types and their probabilities would be exceedingly complex and perhaps impossible to formulate. It is,however,possible to consider the overall effect of

these individual reactions and this is commonly achieved with the introduction of ionization and attachment coefficients which are related to the probability of an electron undergoing an ionization or attachment reaction as it moves in the gas. Mathematical formulations of electrical discharge processes based on these coefficients are in general relatively simple and in many cases they accurately predict the performance of a gas insulated system.

Ionization and attachment coefficients of SF_6 have been measured by Bhalla and Craggs (11) and more recently by Boyd and Crichton (39). Agreement between these independent determinations is very good. The measurements of Boyd and Crichton are presented graphically in Figure 6.4. These results were found to be independent of the gas pressure within the range 5.2 to 402 torr. Experimental difficulties precluded the possibility of measuring the coefficients at higher gas pressures.

As Figure 6.4 suggests, the quantities α/p, η/p, and $(\alpha-\eta)/p$ can be represented accurately by a single mathematical relationship in the range of E/p values illustrated. These relationships are

$$\alpha/p = 29.0\ (E/p) - 1260$$
$$\eta/p = -4.0\ (E/p) + 1140$$
$$(\alpha-\eta)/p = 27.0\ (E/p) - 2400 \qquad (6.2)$$

where α/p, η/p, and $(\alpha-\eta)/p$ are of units $cm^{-1}\ atm^{-1}$ and E/p is of units kv $cm^{-1}\ atm^{-1}$.

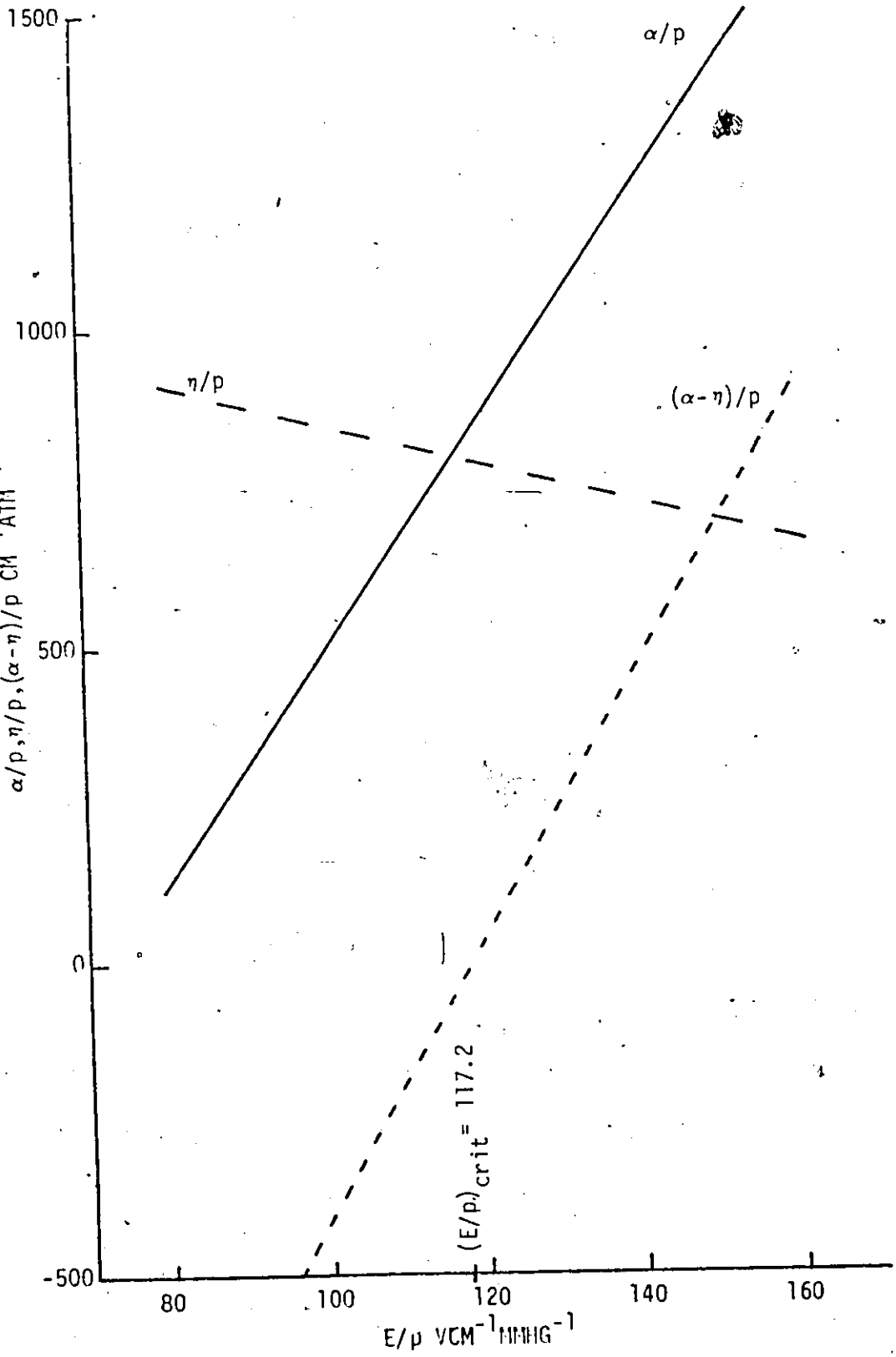

FIGURE 6.4. IONIZATION AND ATTACHMENT COEFFICIENTS OF SF_6.

6.3 Streamer Onset Voltage Calculations

Streamer onset voltages of the experimental systems were calculated using as a basis a number of the avalanche-streamer transition criteria proposed in the literature.

6.3.1 Critical Avalanche Field Criterion

Loeb and Meek (31) and Raether have proposed that an avalanche-streamer transition occurs when the radial field at an avalanche tip, resulting from positive ions created within an avalanche, is within an order of magnitude of the external field. In the case of electronegative gases, the radial field under consideration is that resulting from both positive and negative ions created within the avalanche. The radial field can be calculated as follows.

Assuming the ions to be confined to a sphere of radius r at the head of the avalanche, the radial field E_r produced by the ions at a radius r is given by

$$E_r = \frac{4}{3}\pi r N e$$

where N is the net positive ion charge density and e is the electronic charge. The positive ion charge density N_+ produced in a distance dx in an avalanche which has traversed a distance x, is given by

$$N_+ = \frac{\alpha}{\pi r^2} \exp\left[\int_0^x (\alpha-\eta)dx\right]$$

Similarly, the negative ion charge density N_- is given by

$$N_- = \frac{\eta}{\pi r^2} \exp\left[\int_0^x (\alpha-\eta)dx\right]$$

Consequently

$$N = N_+ - N_- = \frac{(\alpha-\eta)}{\pi r^2} \exp\left[\int_0^x (\alpha-\eta)dx\right]$$

Following the procedure of Loeb and Meek (31), this analysis can be extended and the following expression for E_r obtained:

$$E_r = \frac{5.27\cdot 10^{-7}(\alpha-\eta)\exp\left[\int_0^x (\alpha-\eta)dx\right]}{(x/p)^{1/2}} \text{ volts cm}^{-1} \qquad (6.3)$$

where p is the gas pressure in mmHg. An avalanche-streamer transition occurs when

$$E_r = KE \qquad (6.4)$$

where E is the external field gradient and K=1. The constant 5.27×10^{-7} was arrived at by Loeb and Meek assuming the avalanches to be in air. There is insufficient information in the literature to suggest an appropriate constant for SF_6, however the difference should be insignificant.

Streamer onset voltages were calculated using equations (6.3) and (6.4). The numerical techniques adopted for the computations are basically the same as those discussed in Section 6.3.4.

6.3.2 Critical Avalanche Electron Population Criterion

Raether (40) has proposed that an electron avalanche becomes unstable when the electron population N_{el} in the avalanche reaches 10^8 to 10^9. Since

$$N_{el} = \exp\left[\int_0^x (\alpha - \eta)dx\right]$$

for an avalanche initiated by a single electron at x = 0 in an electronegative gas, this instability criterion can be expressed as $\int_0^x (\alpha-\eta)dx \simeq 20$. The instability manifests itself as an avalanche-streamer transition and thus the above criterion can be used as a basis for streamer onset voltage calculations. As discussed in Chapter I, Nitta and Shibuya (15) developed a mathematical formulation which directly determines the streamer onset voltage of an SF_6 insulated system (equation (1.7)) on the basis that an avalanche streamer transition occurs when N_{el} reaches 10^8.

Streamer onset voltages of the experimental systems were calculated using equation (1.7). The maximum electrical stress in the gap (surface gradient of the rod or sphere electrode at the axis of symmetry) was determined by two methods.

1. The differential of the polynomial approximation to the potential distribution along the axis of symmetry was evaluated at the point corresponding to the electrode surface.

2. The equipotential surface passing through the mesh point one mesh length from the anode surface and on the axis of symmetry was assumed to be that of a sphere concentric with the spherical surface of the anode and of a potential equal to that of the mesh point. The surface gradient of the anode was therefore determined from the analytic expression of the field distribution between concentric spheres.

A comparison of numerical values yielded by these two methods is presented in Section 6.4.

6.3.3 Critical Electric Stress Criterion

As indicated in Chapter I, several workers have proposed calculating the corona onset or breakdown voltage of an SF_6 insulated system on the assumption that breakdown or corona onset occurs when

$$\frac{E_{max}}{p} = 89 \text{ kv cm}^{-1} \text{ atm}^{-1} \qquad (6.5)$$

where E_{max} is the maximum electric stress in the gas and p is the gas pressure. Corona onset and breakdown voltages of several of the test systems were calculated using this hypothesis (referred to in subsequent discussions as the critical (E/p) hypothesis) as a basis.

6.3.4 Critical Positive Ion Density Criterion

Pedersen (12) assumes that an avalanche-streamer transition occurs when the positive ion density in the avalanche reaches a critical value and on this basis has

formulated the semi-empirical streamer onset condition

$$\int_{L_1}^{L_2} (\alpha - \eta) dx = K \qquad (6.6)$$

where α and η are the ionization and attachment coefficients of SF_6 and K is a constant. The integration is performed along the line of highest field strength and the limits L_1 and L_2 correspond respectively to the location on this line where $\alpha - \eta = 0$, and the point of intersection of the highly stressed electrode and the line of integration. Pedersen considers 18 as an appropriate choice of a K value.

The theoretical streamer onset voltages of the sphere and rod-plane test systems were determined for the various combinations of gap length, rod diameter, and gas pressure with the use of equation (6.6). The integration was performed along the axis of symmetry with L_2 corresponding to the intersection point of the sphere or rod surface and the axis. The theoretical streamer onset voltage of the rod-plane systems were determined in the following manner.

The voltage distribution along the axis of symmetry is first determined using the finite element technique and polynomial curve fit, as described earlier, assuming a voltage of 100 applied across the gap. A voltage of V_g kv applied across the gap results in the voltage distribution

along the axis of symmetry

$$V(x) = \frac{V_g}{100}(a_2x + a_3x^2 + a_4x^3 + \cdots) \text{ kv} \qquad (6.7)$$

where V(x) is the voltage at a point on the axis of symmetry x cm from the rod electrode tip. The coefficients a_2, a_3, ... are determined from the curve fit to the mesh point potentials. The potential of the rod electrode is assumed to be 0 kv.

Differentiation of equation (6.7) yields the potential gradient distribution along the symmetry axis

$$E(x) = \frac{V_g}{100}(a_2 + 2a_3x + 3a_4x^2 + \cdots) \qquad (6.8)$$

The value of $\alpha - \eta$ at each point on the symmetry axis can be determined by combining equation (6.2) and (6.8) to yield

$$\alpha(x) - \eta(x) = 27\,\frac{V_g}{100}\,(a_2 + 2a_3x + 3a_4x^2 + \cdots) - 2400p \qquad (6.9)$$

Substitution of equation (6.9) into equation (6.6) reduces the integral equation to the polynomial expression

$$K = 27\,\frac{V_g}{100}\,(a_2L + a_3L^2 + \cdots) - 2400pL \qquad (6.10)$$

or

$$V_g = \frac{K + 2400pL}{(a_2L + a_3L^2 + \cdots)} \cdot \frac{100}{27} = V_{gs} \qquad (6.11)$$

where L is the distance separating the rod tip and the point in the gap where $\alpha - \eta = 0$. The voltage V_g which satisfies equation (6.11) is the streamer onset voltage V_{gs} according to the adopted criterion expressed as equation (6.5). Since

$\alpha - \eta = 0$ at $x = L$, L can be determined from equation (6.9)

$$27 \frac{V_g}{100} (a_2 + 2a_3 L + \cdots) - 2400p = 0 \qquad (6.12).$$

Solution of equation (6.11) requires a knowledge of L, however L is a function of the gap voltage as equation (6.12) indicates.

The streamer inception voltage V_{gs} can be determined numerically from equations (6.11) and (6.12) by first estimating V_{gs}. This estimate is substituted into equation (6.12) and L is calculated using Newton's method for determining polynomial roots. This value of L is substituted into equation (6.11) and V_{gs} is determined. This new value of V_{gs} is used to recalculate L and subsequently the recalculated L is used to determine a new value of V_{gs}. This iteration procedure can be terminated when the calculated values become stationary within the accuracy limits desired.

If the estimate of V_{gs} is poor, the calculations may converge to a solution with a meaningless physical interpretation. However, it was found that an accurate estimate was not required to obtain the correct convergence; an initial guess within 50% of the proper solution usually resulted in the correct convergence. Appendix B presents a method of determining an accurate estimate from the polynomial coefficients.

As a result of simplifying assumptions, an analytic expression (equation (6.1)) is available for the axial field distribution in the sphere-plane test gaps. The form of this expression, however, does not lend itself to the

solution of the integral equation (6.6) and therefore the solution was approximated as a polynomial and streamer onset voltages for the sphere-plane gaps were obtained using equations (6.11) and (6.12).

6.4 Comparison of Experimental and Theoretical Results

Before comparing the experimental breakdown and discharge onset voltages with the theoretical values determined by the various methods outlined, consideration will be given to the possible sources of error inherent to the experimental apparatus and calculation techniques.

6.4.1 Experimental Error Limits

Errors in the experimental measurements may be introduced by the following factors.

1. All electrode dimension and gap lengths were measured to an accuracy of ±.001 inches. Other dimensions (vessel diameter, bushing dimensions, etc.) were measured to an accuracy of better than ±1%. Therefore, dimensional inaccuracies should introduce insignificant errors with the exception of the 1/16 inch diameter rod-plane gaps. The actual rod diameter could differ from the assumed value by as much as ±1.6%. A comparison of discharge inception voltages for 1/4, 1/8, and 1/16 inch diameter rod-plane gaps of the same length and otherwise similar conditions suggests that the tolerance limitations could introduce an error of ±1% in the extreme case.

2. As indicated in Chapter II, the pressure vessel

was observed to expand with increasing internal gas pressure, effecting an increase in the gap length. A comparison of experimental discharge onset data at various gap lengths suggests that these variations should have an insignificant effect on calculations made under the assumption of constant gap length, with the exception of the 2 inch diameter sphere-plane gaps. In this case the effect was observed to be significant, however, it was easily accounted for in the calculations.

3. A maximum difference of ± 1% could exist between the measured and actual vessel gas pressure. An error of this magnitude would introduce a discrepancy between the experimental and calculated discharge onset voltages of as much as ± 1%. However, in the more non-uniform fields, experimental data indicates that it has a somewhat smaller effect, i.e., in the case of a 1/8 inch diameter rod-plane gap of 1.5 inch length the error in the extreme case is approximately ± 0.8%.

4. A maximum difference of ± 2% could exist between the measured and actual voltage applied across the gap.

5. The experimental work was performed with the ambient temperature of the laboratory at 298 °K ± 1%. Temperature corrections were not applied to the data because a study of the literature leaves doubt as to how such a correction should be made. As an example, reference 41 quotes data obtained under different test conditions than that of

this work, and indicates that the breakdown voltage of SF_6 decreases substantially more with increasing gas temperature than does the breakdown voltage of air under the same conditions.

6.4.2 Sources of Error in Calculations

Apart from the experimental inaccuracies described above, there are a number of mathematical sources of error inherent in the calculation techniques employed which give rise to discrepancies between experimental results and theoretical predictions. These are

1. Errors introduced by the selection of boundary conditions to characterize the numerical solution space for rod-plane gaps.

2. Errors introduced by the finite difference approximation to Laplace's equation.

3. Errors introduced by the polynomial approximation to the potential distribution along the symmetry axis.

4. Errors due to the approximations introduced to simplify the sphere-plane gap geometry.

Each of these sources of error will be discussed in turn.

The actual space confining all equipotentials of the rod-plane gaps is unbounded. A finite solution space is obtained by approximating the bushing, the connecting rod, and the upper section of the Rogowski profile electrode by the Neumann and Dirichlet boundaries illustrated in Figure 6.1. Calculations were made using several other approximations to

this region which introduced much more uniform or much more non-uniform field conditions than actually present. Such wide variations of field conditions in this region were observed to have little effect of the field distribution in the vicinity of the rod electrode (less than a 1% difference between the two extreme cases). Therefore, the approximation adopted introduces at most a ± 0.5% error.

The accuracy of the numerically determined field distribution is a function of the mesh length of the finite element approximation to the solution space. In order to ascertain that the mesh length adopted for the calculations would introduce little error, the solution to the field distribution was obtained using several different mesh lengths. Variation of mesh length was obtained by adding or eliminating one or more of the highest numbered regions illustrated in Figure 6.1. A change in mesh length also resulted in the addition or elimination of a boundary between regions of two different mesh lengths. Tables 6.1 and 6.2 illustrate calculations of minimum streamer onset voltages obtained for a number of different mesh lengths and two different field configurations. An inspection of the data indicates that a mesh length of less than one third of the rod radius introduces an insignificant error to the calculations. The data likewise indicates that the division of the field into regions of different mesh length does not introduce a noticable error.

TABLE 6.1. EFFECT OF MESH LENGTH ON CALCULATED STREAMER ONSET VOLTAGES FOR A 1/16 INCH DIAMETER ROD-PLANE GAP OF 0.5 INCH LENGTH DETERMINED USING EQUATION (6.6) WITH K = 20, AND A 10TH ORDER, 20 MESH POINT POLYNOMIAL. (M.L. - MESH LENGTH, R - ROD RADIUS)

GAS PRESSURE (ATM)	EXPERIMENTAL MINIMUM DISCHARGE VOLTAGE (KV)	CALCULATED STREAMER ONSET VOLTAGE (KV)		% DIFFERENCE FROM EXPERIMENTAL	
		M.L. R/3	M.L. R/6	M.L. R/3	M.L. R/6
1.0	17.0	18.0	17.8	+ 5.9	+ 4.7
1.5	27.0	24.7	24.4	- 8.5	- 9.6
2.0	32.0	31.2	30.7	- 2.5	- 4.1
2.5	42.0	37.6	36.9	- 10.5	- 12.1
3.0	45.0	43.8	43.0	- 2.7	- 4.4
3.5	52.0	50.0	49.1	- 3.8	- 5.6
4.0	60.0	56.2	55.0	- 6.3	- 8.3
4.5	71.0	62.2	61.0	- 12.4	- 14.1

TABLE 6.2. EFFECT OF MESH LENGTH ON CALCULATED STREAMER ONSET VOLTAGES FOR A 1/4 INCH DIAMETER ROD-PLANE GAP OF 1.5 INCH LENGTH DETERMINED USING EQUATION (6.6) WITH K = 20, AND A 10TH ORDER, 20 MESH POINT POLYNOMIAL. (M.L. - MESH LENGTH, R - ROD RADIUS)

GAS PRESSURE (ATM)	EXPERIMENTAL MINIMUM DISCHARGE VOLTAGE (KV)	CALCULATED STREAMER ONSET VOLTAGE VOLTAGE (KV)			% DIFFERENCE FROM EXPERIMENTAL		
		M.L. R/6	M.L. R/12	M.L. R/24	M.L. R/6	M.L. R/12	M.L. R/24
1.0	68.0	69.0	68.8	68.5	+ 1.5	+ 1.2	+ 0.7
1.5	100.	98.4	97.9	97.7	- 1.6	- 2.1	- 2.3
2.0	135.	127.	127.	126.	- 5.9	- 5.9	- 6.7
2.5	160.	156.	155.	154.	- 2.5	- 3.1	- 3.8
3.0	192.	184.	183.	182.	- 4.2	- 4.7	- 5.2
3.5	216.	212.	211.	210.	- 1.9	- 2.3	- 2.8
4.0	242.	240.	238.	238.	- 0.8	- 1.7	- 1.7
4.5	271.	267.	266.	265.	- 1.5	- 1.9	- 2.2

The polynomial approximation to the potential variation along the axis of symmetry may introduce significant errors. As it is not necessary to describe the potential variation along the total length of the axis, the question arises as to the number of mesh potentials to which the polynomial should be fit to as well as to the order of polynomial which should be used. Streamer onset voltages and maximum surface gradients were calculated using several different point fits and polynomial orders. The results of some of these calculations are listed in Tables 6.3 and 6.4. In calculating streamer onset voltages using a 20 point fit it was found that any polynomial fit of greater than a fourth order yielded the same value within $\pm$ 0.2%. The data of Table 6.3 indicates that a considerable disparity exists between streamer inception voltages calculated using a 5 point fit and those calculated using a 10 or 20 point fit. Surface gradient calculations indicate that significant disparities are effected by variations in both fit and polynomial order. A comparison of surface gradient calculations obtained using the polynomial and the concentric spheres approximation suggests that the 10th order polynomial fit to 20 points yields the best approximation to the true potential distribution along the symmetry axis.

The approximating of the experimental sphere-plane gap as an isolated sphere-sphere gap introduces errors due to the presence of the connecting shaft, the cylinder walls,

TABLE 6.3. EFFECT OF THE NUMBER OF MESH POINTS USED FOR THE POLYNOMIAL APPROXIMATION ON CALCULATIONS OF STREAMER ONSET VOLTAGES FOR A 1/4 INCH DIAMETER ROD-PLANE GAP OF 1.5 INCH LENGTH DETERMINED USING EQUATION (6.6) WITH K = 20, A 10TH ORDER POLYNOMIAL, AND A 1/96 INCH MESH LENGTH.

GAS PRESSURE (ATM)	EXPERIMENTAL MINIMUM DISCHARGE VOLTAGE (KV)	CALCULATED STREAMER ONSET VOLTAGE VOLTAGE (KV)			% DIFFERENCE FROM EXPERIMENTAL		
		5 POINTS	10 POINTS	20 POINTS	5 POINTS	10 POINTS	20 POINTS
1.0	68.0	72.4	68.7	68.8	+ 6.5	+ 1.0	+ 1.2
1.5	100.	106.	97.9	97.9	+ 6.0	- 2.1	- 2.1
2.0	135.	140.	127.	127.	+ 3.7	- 5.9	- 5.9
2.5	160.	174.	155.	155.	+ 8.8	- 3.1	- 3.1
3.0	192.	207.	183.	183.	+ 7.8	- 4.7	- 4.7
3.5	216.	241.	211.	211.	+11.6	- 2.3	- 2.3
4.0	242.	275.	238.	238.	+13.6	- 1.7	- 1.7
4.5	271.	309.	266.	266.	+14.0	- 1.9	- 1.9

and the base. The departure of the Rogowski electrode from an ideal plane electrode also introduces errors. The effect of cylindrical enclosers, shaft diameters, etc. on the breakdown voltage of sphere-sphere gaps was examined by Kuffel and Husbands (18) and the results of their study suggest that the approximation should not introduce an error greater than ± 1%.

TABLE 6.4. THE EFFECT OF THE POLYNOMIAL ORDER AND THE NUMBER OF MESH POINTS TO WHICH THE POLYNOMIAL IS FIT ON CALCULATIONS OF THE MAXIMUM VOLTAGE GRADIENT OF A 1/4 INCH ROD-PLANE GAP.

Mesh Length	10th Order Polynomial 20 pts	10th Order Polynomial 10 pts	10th Order Polynomial 5 pts	5th Order Polynomial 20 pts	Concentric Spheres
1/48	172.7	-	-	161.2	173.6
1/96	174.2	175.7	201.5	171.7	174.4
1/192	175.6	-	-	174.1	175.6

6.4.3 Discussion of Results

Tables 6.5 through 6.15 compare the streamer onset voltages calculated using the techniques discussed in Section 6.3 with the lowest experimental voltages at which any form of discharge activity was observed in the SF_6 insulated electrode gaps. Figure 6.5 gives a graphical comparison of theoretical and experimental results for a 1/16 inch rod-plane

TABLE 6.5. EFFECT OF THE K VALUE ON CALCULATED STREAMER ONSET VOLTAGES FOR A 1/4 INCH DIAMETER ROD-PLANE GAP OF 1.5 INCH LENGTH DETERMINED USING EQUATION (6.6), A 10TH ORDER, 20 MESH POINT POLYNOMIAL, AND A MESH LENGTH OF 1/192 INCHES.

GAS PRESSURE (ATM)	EXPERIMENTAL MINIMUM DISCHARGE VOLTAGE (KV)	CALCULATED STREAMER ONSET VOLTAGE VOLTAGE (KV)			% DIFFERENCE FROM EXPERIMENTAL		
		K = 18	K = 20	K = 22	K = 18	K = 20	K = 22
1.0	68.0	67.6	68.5	69.4	- 0.6	+ 0.7	+ 2.1
1.5	100.	96.5	97.7	98.8	- 3.5	- 2.3	- 1.2
2.0	135.	125.	126.	127.	- 7.4	- 6.7	- 5.9
2.5	160.	153.	154.	156.	- 4.4	- 3.8	- 2.5
3.0	192.	181.	182.	184.	- 5.7	- 5.2	- 4.2
3.5	216.	208.	210.	212.	- 3.7	- 2.8	- 1.9
4.0	242.	236.	238.	239.	- 2.5	- 1.7	- 1.2
4.5	271.	263.	265.	267.	- 3.0	- 2.2	- 1.5

TABLE 6.6. COMPARISON OF EXPERIMENTAL BREAKDOWN VOLTAGES OF A 2 INCH DIAMETER ROD-PLANE GAP OF 0.5 INCH LENGTH WITH CALCULATED STREAMER ONSET VOLTAGES DETERMINED USING EQUATION (1.7) AND EQUATION (6.6) WITH K = 20 AND A 10TH ORDER, 20 MESH POINT POLYNOMIAL.

GAS PRESSURE (ATM)	EXPERIMENTAL MINIMUM BREAKDOWN VOLTAGE (KV)	CALCULATED STREAMER ONSET VOLTAGE VOLTAGE (KV)		% DIFFERENCE FROM EXPERIMENTAL	
		EQN. (1.7)	EQN. (6.6)	EQN. (1.7)	EQN. (6.6)
1.00	90.0	92.0	92.0	+ 2.2	+ 2.2
1.65	149.	148.	148.	- 0.7	- 0.7
2.35	209.	208.	208.	- 0.5	- 0.5
3.00	271.	266.	266.	- 2.0	- 2.0

TABLE 6.7. COMPARISON OF EXPERIMENTAL BREAKDOWN VOLTAGES OF A 2 INCH DIAMETER ROD-PLANE GAP OF 0.25 INCH LENGTH WITH CALCULATED STREAMER ONSET VOLTAGES DETERMINED USING EQUATION (1.7) AND EQUATION (6.6) WITH K = 20 AND A 10TH ORDER, 20 MESH POINT POLYNOMIAL.

GAS PRESSURE (ATM)	EXPERIMENTAL MINIMUM BREAKDOWN VOLTAGE (KV)	CALCULATED STREAMER ONSET VOLTAGE VOLTAGE (KV)		% DIFFERENCE FROM EXPERIMENTAL	
		EQN. (1.7)	EQN. (6.6)	EQN. (1.7)	EQN. (6.6)
1.00	56.0	53.0	53.0	- 5.4	- 5.4
1.67	92.0	87.2	87.3	- 5.2	- 5.1
2.35	127.	121.	121.	- 4.7	- 4.7
3.00	157.	154.	155.	- 1.9	- 1.3
3.70	197.	188.	188.	- 4.6	- 4.6
4.40	228.	222.	222.	- 2.6	- 2.6

TABLE 6.8. COMPARISON OF MINIMUM EXPERIMENTAL DISCHARGE VOLTAGES OF A 1/4 INCH DIAMETER ROD-PLANE GAP OF 1.5 INCH LENGTH WITH CALCULATED STREAMER ONSET VOLTAGES DETERMINED USING EQUATION (1.7) AND EQUATION (6.6) WITH K = 20 AND A 10TH ORDER, 20 MESH POINT POLYNOMIAL.

GAS PRESSURE (ATM)	EXPERIMENTAL MINIMUM DISCHARGE VOLTAGE (KV)	CALCULATED STREAMER ONSET VOLTAGE			
		VOLTAGE (KV)		% DIFFERENCE FROM EXPERIMENTAL	
		EQN. (1.7)	EQN. (6.6)	EQN. (1.7)	EQN. (6.6)
1.0	68.0	67.1	68.5	- 1.3	+ 0.7
1.5	100.	96.2	97.7	- 3.8	- 2.3
2.0	135.	124.	126.	- 8.1	- 6.7
2.5	160.	152.	154.	- 5.0	- 3.8
3.0	192.	180.	182.	- 6.3	- 5.2
3.5	216.	208.	210.	- 3.7	- 2.8
4.0	242.	235.	238.	- 2.9	- 1.7
4.5	271.	263.	265.	- 3.0	- 2.2

TABLE 6.9. COMPARISON OF MINIMUM EXPERIMENTAL DISCHARGE VOLTAGES OF A 1/4 INCH DIAMETER ROD-PLANE GAP OF 0.5 INCH LENGTH WITH CALCULATED STREAMER ONSET VOLTAGES DETERMINED USING EQUATION (1.7) AND EQUATION (6.6) WITH K = 20 AND A 10TH ORDER, 20 MESH POINT POLYNOMIAL.

GAS PRESSURE (ATM)	EXPERIMENTAL MINIMUM DISCHARGE VOLTAGE (KV)	CALCULATED STREAMER ONSET VOLTAGE			
		VOLTAGE (KV)		% DIFFERENCE FROM EXPERIMENTAL	
		EQN. (1.7)	EQN. (6.6)	EQN. (1.7)	EQN. (6.6)
1.0	40.0	38.7	39.7	- 3.3	- 0.8
1.5	60.0	55.5	56.6	- 7.5	- 5.7
2.0	74.0	72.0	73.2	- 2.7	- 1.1
2.5	95.0	88.3	89.5	- 7.1	- 5.8
3.0	107.	104.	106.	- 2.8	- 0.9
3.5	122.	120.	122.	- 1.6	+ 0.0
4.0	132.	136.	138.	+ 3.0	+ 4.5
4.5	152.	152.	154.	0.0	+ 1.3

TABLE 6.10. COMPARISON OF MINIMUM EXPERIMENTAL DISCHARGE VOLTAGES OF A 1/8 INCH DIAMETER ROD-PLANE GAP OF 1.5 INCH LENGTH WITH CALCULATED STREAMER ONSET VOLTAGES DETERMINED USING EQUATION (1.7) AND EQUATION (6.6) WITH K = 20 AND A 10TH ORDER, 20 MESH POINT POLYNOMIAL.

GAS PRESSURE (ATM)	EXPERIMENTAL MINIMUM DISCHARGE VOLTAGE (KV)	CALCULATED STREAMER ONSET VOLTAGE			
		VOLTAGE (KV)		% DIFFERENCE FROM EXPERIMENTAL	
		EQN. (1.7)	EQN. (6.6)	EQN. (1.7)	EQN. (6.6)
1.0	46.0	42.4	44.3	- 7.8	- 3.7
1.5	61.0	60.0	62.1	- 1.7	+ 1.8
2.0	85.0	77.2	79.4	- 9.2	- 6.6
2.5	98.0	94.1	96.4	- 4.0	- 1.6
3.0	115.	111.	113.	- 3.5	- 1.7
3.5	130.	127.	130.	- 2.3	0.0
4.0	154.	144.	146.	- 6.5	- 5.2
4.5	169.	160.	162.	- 5.3	- 4.1

TABLE 6.11. COMPARISON OF MINIMUM EXPERIMENTAL DISCHARGE VOLTAGES OF A 1/8 INCH DIAMETER ROD-PLANE GAP OF 0.5 INCH LENGTH WITH CALCULATED STREAMER ONSET VOLTAGES DETERMINED USING EQUATION (1.7) AND EQUATION (6.6) WITH K = 20 AND A 10TH ORDER, 20 MESH POINT POLYNOMIAL.

GAS PRESSURE (ATM)	EXPERIMENTAL MINIMUM DISCHARGE VOLTAGE (KV)	CALCULATED STREAMER ONSET VOLTAGE			
		VOLTAGE (KV)		% DIFFERENCE FROM EXPERIMENTAL	
		EQN. (1.7)	EQN. (6.6)	EQN. (1.7)	EQN. (6.6)
1.0	27.0	25.5	26.6	- 5.6	- 1.5
1.5	38.0	36.0	37.3	- 5.3	- 1.6
2.0	50.0	46.4	47.6	- 7.2	- 4.8
2.5	60.0	56.5	57.8	- 5.8	- 3.7
3.0	73.0	66.6	67.9	- 8.8	- 7.0
3.5	89.0	76.5	77.9	- 14.1	- 12.5
4.0	96.0	86.3	87.8	- 10.1	- 8.5
4.5	110.	96.1	97.6	- 12.6	- 11.3

TABLE 6.12. COMPARISON OF MINIMUM EXPERIMENTAL DISCHARGE VOLTAGES OF A 1/16 INCH DIAMETER ROD-PLANE GAP OF 1.5 INCH LENGTH WITH CALCULATED STREAMER ONSET VOLTAGES DETERMINED USING EQUATION (1.7) AND EQUATION (6.6) WITH K = 20 AND A 10TH ORDER, 20 MESH POINT POLYNOMIAL.

GAS PRESSURE (ATM)	EXPERIMENTAL MINIMUM DISCHARGE VOLTAGE (KV)	CALCULATED STREAMER ONSET VOLTAGE			
		VOLTAGE (KV)		% DIFFERENCE FROM EXPERIMENTAL	
		EQN. (1.7)	EQN. (6.6)	EQN. (1.7)	EQN. (6.6)
1.0	28.0	27.1	29.2	- 3.2	+ 4.3
1.5	40.0	37.9	40.0	- 5.2	+ 0.0
2.0	49.0	48.2	50.4	- 1.6	+ 2.9
2.5	59.0	58.3	60.6	- 1.2	+ 2.7
3.0	68.0	68.2	70.6	+ 2.9	+ 3.8
3.5	81.0	78.1	80.5	- 3.6	+ 0.6
4.0	93.0	87.8	90.3	- 5.6	- 2.9
4.5	102.	97.4	100.	- 4.5	- 2.0

TABLE 6.13. COMPARISON OF MINIMUM EXPERIMENTAL DISCHARGE VOLTAGES OF A 1/16 INCH DIAMETER ROD-PLANE GAP OF 0.5 INCH LENGTH WITH CALCULATED STREAMER ONSET VOLTAGES DETERMINED USING EQUATION (1.7) AND EQUATION (6.6) WITH K = 20 AND A 10TH ORDER, 20 MESH POINT POLYNOMIAL.

GAS PRESSURE (ATM)	EXPERIMENTAL MINIMUM DISCHARGE VOLTAGE (KV)	CALCULATED STREAMER ONSET VOLTAGE			
		VOLTAGE (KV)		% DIFFERENCE FROM EXPERIMENTAL	
		EQN. (1.7)	EQN. (6.6)	EQN. (1.7)	EQN. (6.6)
1.0	17.0	16.5	17.8	- 2.9	+ 4.7
1.5	27.0	23.1	24.4	- 14.4	- 9.6
2.0	32.0	29.4	30.7	- 8.1	- 4.1
2.5	42.0	35.5	36.9	- 15.5	- 12.1
3.0	45.0	41.6	43.0	- 7.5	- 4.4
3.5	52.0	47.6	49.1	- 8.5	- 5.6
4.0	60.0	53.5	55.0	- 10.8	- 8.3
4.5	71.0	59.4	61.0	- 16.3	- 14.1

TABLE 6.14. COMPARISON OF MINIMUM EXPERIMENTAL DISCHARGE VOLTAGES OF A 1/4 INCH DIAMETER ROD-PLANE GAP OF 0.5 INCH LENGTH WITH CALCULATED STREAMER ONSET VOLTAGES DETERMINED USING EQUATION (6.4), EQUATION (6.5), AND EQUATION (6.6) WITH K = 20 AND A 10TH ORDER, 20 MESH POINT POLYNOMIAL.

GAS PRESSURE (ATM)	EXPERIMENTAL MINIMUM DISCHARGE VOLTAGE (KV)	CALCULATED STREAMER ONSET VOLTAGE VOLTAGE (KV)			% DIFFERENCE FROM EXPERIMENTAL		
		EQN.(6.6)	EQN.(6.4)	EQN.(6.5)	EQN.(6.6)	EQN.(6.4)	EQN.(6.5)
1.0	40.0	39.7	39.0	30.1	- 0.8	- 2.5	- 25.0
1.5	60.0	56.6	55.0	44.3	- 5.7	- 8.3	- 26.2
2.0	74.0	73.2	72.0	59.2	- 1.1	- 2.7	- 20.0
2.5	95.0	89.5	88.0	74.0	- 5.8	- 7.4	- 22.1
3.0	107.	106.	104.	89.3	- 0.9	- 2.8	- 16.6
3.5	122.	122.	120.	103.	0.0	- 1.6	- 15.6
4.0	132.	138.	135.	118.	+ 4.5	+ 2.3	- 10.6
4.5	152.	154.	151.	133.	+ 1.3	- 0.6	- 13.2

TABLE 6.15. COMPARISON OF MINIMUM EXPERIMENTAL DISCHARGE VOLTAGES OF A 1/16 INCH DIAMETER ROD-PLANE GAP OF 1.5 INCH LENGTH WITH CALCULATED STREAMER ONSET VOLTAGES DETERMINED USING EQUATION (6.4), EQUATION (6.5), AND EQUATION (6.6) WITH K = 20 AND A 10TH ORDER, 20 MESH POINT POLYNOMIAL.

GAS PRESSURE (ATM)	EXPERIMENTAL MINIMUM DISCHARGE VOLTAGE (KV)	CALCULATED STREAMER ONSET VOLTAGE VOLTAGE (KV)			% DIFFERENCE FROM EXPERIMENTAL		
		EQN.(6.6)	EQN.(6.4)	EQN.(6.5)	EQN.(6.6)	EQN.(6.4)	EQN.(6.5)
1.0	28.0	29.2	27.0	17.1	+ 4.3	- 3.6	- 32.1
1.5	40.0	40.0	38.0	25.3	+ 0.0	- 5.0	- 36.8
2.0	49.0	50.4	48.0	33.2	+ 2.9	- 2.0	- 32.3
2.5	59.0	60.6	58.0	42.0	+ 2.7	- 1.7	- 28.8
3.0	68.0	70.6	68.0	50.0	+ 3.8	0.0	- 26.4
3.5	81.0	80.5	78.0	59.4	- 0.6	- 3.7	- 26.7
4.0	93.0	90.3	87.0	67.0	- 2.9	- 6.5	- 28.0
4.5	102.	100.	97.0	75.3	- 2.0	- 4.9	- 26.2

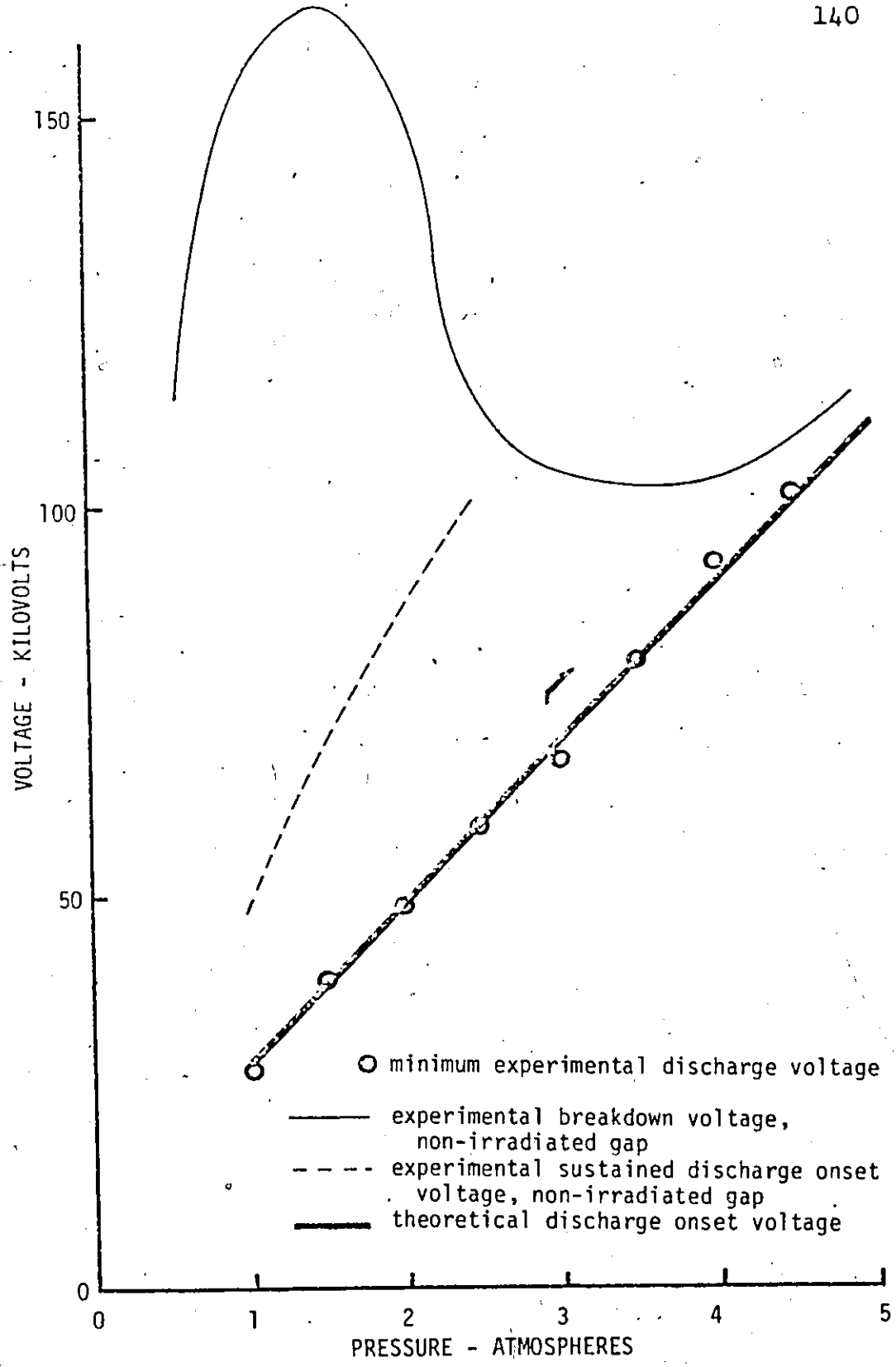

FIGURE 6.5. COMPARISON OF EXPERIMENTAL DISCHARGE ONSET VOLTAGES OF A 1/16 INCH DIAMETER ROD-PLANE GAP OF 1.5 INCHES LENGTH WITH CALCULATED STREAMER ONSET VOLTAGES DETERMINED USING EQUATION (6.6) WITH K = 20 AND A 10TH ORDER, 20 MESH POINT POLYNOMIAL.

gap of 1.5 inch gap length.

The results illustrated in Figure 6.5, as well as all other results, demonstrate that the calculated values of streamer onset voltages correspond to the minimum voltage at which any form of discharge was observed. The results also indicate that, for the most part, the theoretical values are somewhat lower than the experimental discharge onset values. This is to be expected as, at the theoretical onset voltage, only a free electron at a single optimum point in the gap can initiate a streamer producing avalanche. The experimental streamer onset voltage will, in theory, exceed the theoretical value unless the chance occurrence of a free electron at the optimum point coincides, in time, with the application of the streamer onset voltage to the gap.

In a very few cases, discharge activity was observed at voltages slightly below the theoretical minimum. There are several possible explanations for this.

1. The differences between experimental and theoretical values are within the error limits of the measured and calculated values.

2. The calculations are based on statistically averaged ionization and attachment properties of the gas. The instantaneous properties do vary somewhat and this could result in the occurrence of discharges at voltages lower than the theoretical minimum.

3. The theoretical calculations do not account for

the presence of foreign objects in the gas. Some contamination of the gas is unavoidable and partical initiated breakdown could occur.

Pedersen's proposal of 18 (12) as a suitable value for K in equation (6.6) is based on available uniform field breakdown data. The experimental results of the present study afforded the opportunity of examining the significance of the choice of K value on the streamer onset values calculated under a variety of field conditions.

Table 6.5 illustrates changes in calculated onset voltages resulting from variations in the K value. These results and others demonstrate that the K value bore its greatest significance on calculations associated with the most non-uniform field conditions. The calculated streamer onset voltage for a 1/16 inch rod-plane gap of 1.5 inch length increased by 1.3% as a result of a K value increase from 18 to 20. This same change in K had an insignificant effect ($\pm$0.2%) on the calculations of onset voltages for the 2 inch diameter sphere-plane gaps.

The experimental results of this work cannot be used as a basis for an accurate empirical determination of K because of the error limits associated with the data. However, the calculations indicate, that for most technologically oriented work, the effect of the K value on calculations of discharge onset voltages is insignificant.

For the present study, a K value of 20 was used for the majority of the calculations based on equation (6.6) as this value yielded the closest overall agreement between theoretical and experimental results.

Tables 6.5 through 6.15 indicate that three of the four calculation techniques used for determining discharge onset voltages yield results which differ little from each other. However, the results obtained using the critical (E/p) hypothesis (equation (6.5)) are significantly lower than the others, with the percentage difference varying directly with the degree of field non-uniformity.

Aside from the field distribution approximation inherent to equation (1.7), equations (6.5), (6.6), and (1.7) are of the same form, differing only in the choice of K value. Equation (1.7) is based on the assumption that an avalanche-streamer transition occurs when the avalanche electron population reaches 10^8. This is equivalent to the streamer onset condition

$$\int_0^x (\alpha-\eta)dx = 18.4$$

The critical (E/p) hypothesis is equivalent to the streamer onset condition

$$\int_0^x (\alpha-\eta)dx = 0$$

As discussed above, the integral onset equation (6.6) yields streamer onset voltages which are relatively insensitive to the K value. Thus, apart from differences due to an approximation of the field distribution, equation (6.6) with a K value of 20 and equation (1.7) should yield results which differ little from each other (results from equation (1.7) should be less than 1.1% lower than those of equation (6.6) in the extreme case).

Calculations based on equation (6.5) are significantly lower than those obtained from equation (6.6) with K = 20 becuase of the very large difference in the K values. Also since the sensitivity of calculated onset voltages to variations of K increases with increasing field non-uniformity, the percentage discrepancy between the calculations varies directly with the degree of field non-uniformity.

Calculations based on the critical avalanche field criterion (equations (6.3) and (6.4) differ little from those based on equation (6.6) with K = 20. The difference can be made completely insignificant by changing the constant 5.27×10^{-7} of equation (6.3) to 5.43×10^{-7}. The close agreement between these apparently independent methods is not surprising as the term $\exp\left[\int_0^x (\alpha-\eta)dx\right]$ is very much more sensitive to changes in gap voltage than the other terms of equation (6.3).

The difference between calculated values obtained using equations (1.7) and (6.6) with K = 20 can, in part, be attributed to the error introduced by the approximation, in equation

(1.7), of the field distribution at the tip of a hemispherical rod or sphere as that of an isolated sphere. This error is a function of the relative magnitudes of the symmetry axis length over which $\alpha > \eta$ and the radius of the rod or sphere. This point is illustrated in Table 6.16. The isolated sphere approximation is an accurate representation of the field distribution only at distances within a small fraction of the radius of curvature of the electrode surface. Therefore, the accuracy of any calculation based on equation (1.7) is a function of the distance over which the integration is performed. This is exemplified in Table 6.17. For a given electrode system, the integration length is inversely proportional to the gas pressure. Consequently, the difference in calculated streamer onset voltages, based on the two different approximations to the field distribution, should decrease with increasing gas pressure. Evidence of this type of relationship can be observed in Table 6.17 and is observed for all other field conditions as well.

Table 6.18 indicates that the rod diameter appears to have a significant bearing on the accuracy of isolated sphere approximation, although it must be kept in mind that the comparison of calculations is made with results obtained using another approximation, not the exact solution. Errors inherent in the polynomial approximation, however, are undoubtedly much smaller as Table 6.16 would suggest.

TABLE 6.16. COMPARISON OF POLYNOMIAL AND ISOLATED SPHERE APPROXIMATIONS TO THE POTENTIAL DISTRIBUTIONS IN A 1/16 INCH DIAMETER ROD-PLANE GAP OF LENGTH 1.5 INCHES.

MESH POTENTIAL	POLYNOMIAL	ISOLATED SPHERE	DISTANCE FROM ROD SURFACE (INCHES)
0.00	.000033	0.00	0.00
6.03	6.03	6.03	.0052
10.61	10.61	9.30	.0104
14.24	14.24	11.34	.0156
17.20	17.20	12.75	.0208
19.68	19.68	13.77	.0260

TABLE 6.17. COMPARISON OF STREAMER ONSET VOLTAGE CALCULATIONS USING EQUATION (1.7) AND EQUATION (6.6) WITH K = 18 AND A 10TH ORDER, 20 MESH POINT POLYNOMIAL.

INTEGRATION LENGTH		GAS PRESSURE (ATM)	% DIFFERENCE IN CALCULATIONS
INCHES	% OF ROD RADIUS		
.01003	81.5	1.0	3.68
.00704	57.2	2.0	2.96
.00573	46.6	3.0	2.15
.00495	40.2	4.0	1.70

TABLE 6.18. PERCENTAGE DIFFERENCE IN STREAMER ONSET VOLTAGES CALCULATED USING EQUATION (1.7) AND EQUATION (6.6) WITH A 10TH ORDER, 20 MESH POINT POLYNOMIAL AND K = 18

Electrode Geometry (inches)	Non-uniformity Factor (E_{av}/E_{max})	% Difference in Calculations
1/4 - 1/2	.260	1.21
1/4 - 1 1/2	.140	1.23
1/8 - 1/2	.151	2.47
1/8 - 1 1/2	.0814	2.56
1/16 - 1/2	.0832	4.50
1/16 - 1 1/2	.0380	4.56

A comparison of measured and calculated discharge voltages of the experimental systems of this study demonstrates that the calculation techniques, with the possible exception of the critical (E/p) technique, do accurately predict the minimum discharge performance of compressed SF_6 insulated systems. An evaluation of the relative merits of these methods of calculation should be made in consideration of the fact that all of the techniques require, at the least, the degree of non-uniformity of the electric field distribution in the gas. As a result, a field calculation is required in each case; a calculation which overshadows, in both complexity and computation time, the calculations associated with each individual technique. Therefore, the fact that the computations associated with equations (1.7) and (6.5) are much less

complex than those associate equations (6.4) and (6.6) is really of little consequence.

Equation (1.7) alone offers an analytic relationship between the system discharge onset voltage and the gas pressure, gap length, and electrode radius. This is achieved through the use of a simple approximation to the field distribution, an approximation which is only accurate when the electrode surface at the point of maximum electrical stress can be characterized by two orthogonal radii of curvature.

The numerical technique based on equation (6.6) is not limited to specific types of electrode geometry and therefore offers greater general applicability than equation (1.7). The requirement of an initial guess for the discharge onset voltage of the system under calculation is somewhat inconvenient, however, it is possible to determine a sufficiently accurate initial guess from a knowledge of the polynomial coefficients associated with any applied voltage. The method is outlined in Appendix B.

The calculation technique associated with the critical avalanche field criterion is quite similar to that associated with equation (6.6), and possesses the same advantages and disadvantages. It is impossible to state which of the two methods best predicts the discharge performance of an SF_6 insulated system since the deviations between calculated values of the respective methods are well within the experimental and computational error limits.

6.5 Corona Free Breakdown in Compressed SF_6

In discussing the transitions between various types of corona discharges at a positive point in air, Hermstein (20) proposed that the basic factor governing such transitions was the rate of change of voltage gradient at the anode surface. He substantiated his hypothesis by showing that different corona phenomena were related to different ranges of anode surface gradients, independent of the electrode geometry. A somewhat similar hypothesis was examined in this work.

A number of authors (4, 9) have proposed that breakdown in highly non-uniform gaps insulated with SF_6 can occur in the absence of corona pulses at high gas pressures because an enhancement of streamer propagation properties accompanies an increase in gas pressure. If the pressure is sufficiently high, the first streamer formed in the gas can bridge the gap and initiate a spark.

The ability of a cathode directed streamer to propagate in a gas depends on the rate of growth of the ion space charge at the streamer tip. This charge is created by secondary avalanches approaching the tip. These avalanches are initiated by free electrons produced in a volume surrounding the streamer tip where the electric field gradient E_t due to the external voltage and streamer space charge voltage is streamer directed and where $E_t/p > 89$ kv cm^{-1} atm^{-1}. The number of secondary avalanches reaching the streamer is

therefore proportional to the number of free electrons produced within this volume (denoted as the "ionizing volume" in the subsequent discussion). Electrons produced outside the ionizing volume suffer attachment and the resulting negative ions are swept to the anode and do not contribute to the propagation process.

For a given set of field conditions, the number of electrons produced in the ionizing volume is proportional to the photon absorption coefficient μ of the gas and the rate of photon production within the streamer tip. If Q is the photon absorption cross-section of the gas molecules then

$$\mu = NQ$$

where N is the number of atoms per unit volume. N is directly proportional to the gas pressure p. Assuming for the moment that the photons are created at a point source and the ionizing volume is a sphere of radius r with its center at the point source, the probability P_i of a photon escaping the volume is given by

$$P_i = e^{-\mu r} = Ke^{-pr}$$

where K is a constant. Therefore, a linear increase in the gas pressure is accompanied by an exponential decrease in the probability that a photon will not create a free electron

within the ionizing volume.

The growth of the ion space charge at the streamer tip is a function of the total field gradient in the vicinity of the tip. The gradient is determined by the applied field plus the field due to the streamer space charge. For a streamer to propagate in a direction in which the field intensity is decreasing (cathode directed streamer in a positive point-plane gap), the space charge field must increase at a rate which can compensate for the rate of decrease of the applied field. The rate of increase of the space charge field is proportional to the rate of charge accumulation at the streamer tip, which in turn is proportional to the rate of photo-ionization in the ionizing volume.

From the above discussion, it is evident that the probability of a streamer advancing sufficiently far into an SF_6 insulated electrode gap to initiate breakdown is a function of the maximum rate of change of voltage gradient in the gap and the pressure of the gas. On the basis of this statement the following hypothesis is proposed: A streamer initiated breakdown in SF_6 will occur in the absence of corona of any form, when the gas pressure is such that

$$\left.\frac{dE}{dx}\right|_{x=0} e^{-p} \leq -C \qquad (6.13)$$

where $\left.\frac{dE}{dx}\right|_{x=0}$ = the maximum rate of change of anode surface gradient in kv cm^{-2} at a gap voltage equal to the streamer onset voltage

p = gas pressure in atmospheres

C = constant

In order to test the hypothesis and determine a suitable value for C, $\left.\frac{dE}{dx}\right|_{x=0} e^{-p}$ was calculated for various values of p from the data of Figures 4.4 through 4.9. $\left.\frac{dE}{dx}\right|_{x=0}$ was determined using the appropriate polynomial expression for the field distribution at a gap voltage equal to the streamer onset voltage. The results of these calculations are plotted in Figure 6.6 along with the minimum pressure for each electrode configuration at which no single pulse or momentary sustained discharge activity was observed.

There is a reasonable conformity between the experimental results and the predictions of the hypothesis when C = 200. Single pulses were observed experimentally in 1/4 and 1/8 inch rod-plane gaps of lengths 0.5 and 1.5 inches respectively at pressures somewhat higher than the predicted values, however, these pulses were only observed under irradiated conditions and only one pulse was observed in each case in a time span of approximately 3 minutes.

It is possible to express the corona free breakdown criterion of equation (6.13) in terms of the radius of curvature R of the highly stressed electrode, and the gas pressure p. If it is assumed that the highly stressed electrode is an isolated sphere of radius R and possesses a potential $V = E_{max} R$, then

$$E(x) = \frac{E_{max}}{(1 + \frac{x}{R})^2} \qquad (6.14)$$

where E(x) is the potential gradient at a distance x from

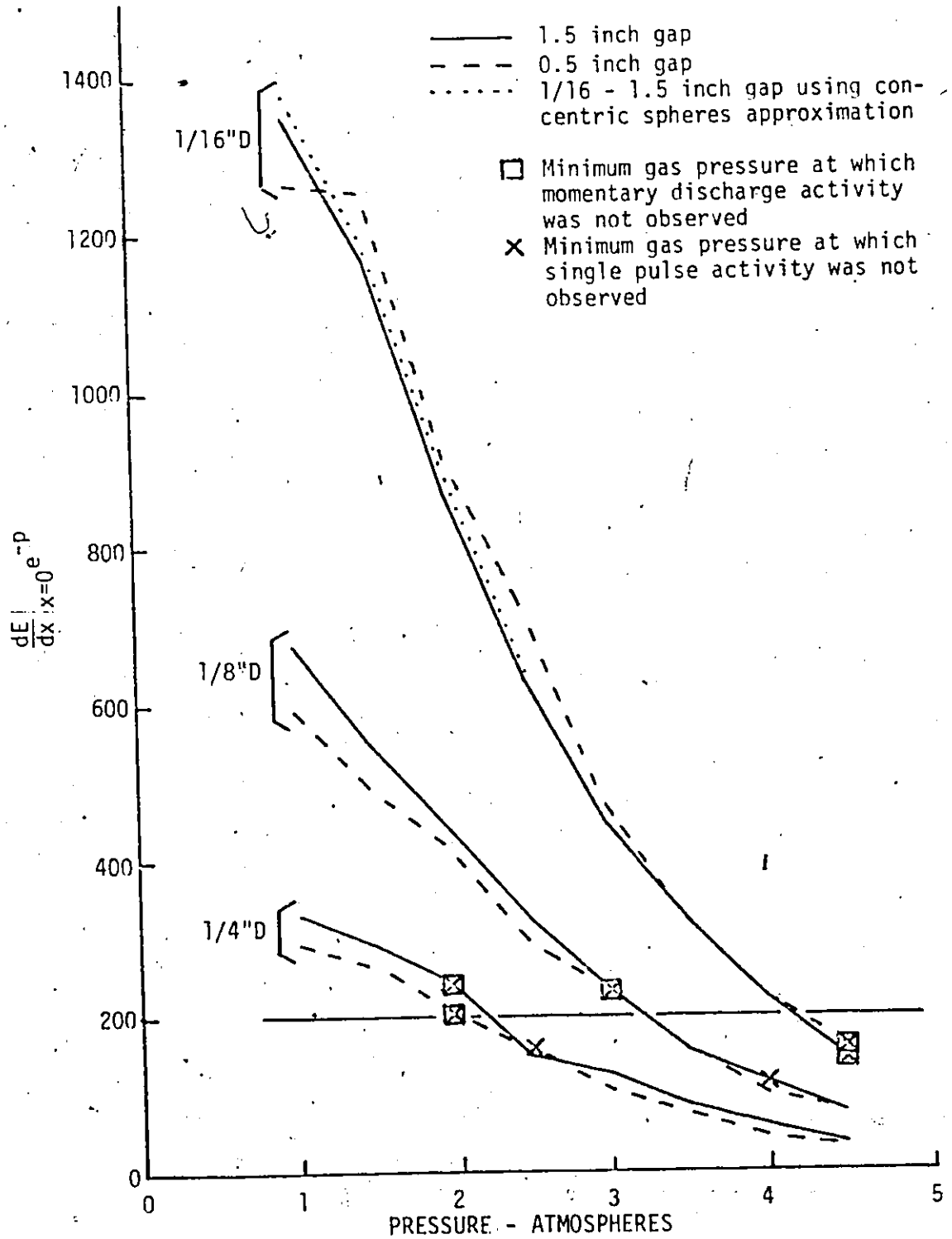

FIGURE 6.6. $\frac{dE}{dx}|_{x=0}e^{-p}$ AT GAP VOLTAGES EQUAL TO THE MINIMUM VOLTAGES AT WHICH DISCHARGE ACTIVITY WAS EXPERIMENTALLY OBSERVED.

the sphere surface and E_{max} is equal to the maximum potential gradient of the actual electrode system. E_{max} can be determined from equation (1.7) which is also based on the above approximations.

From equation (1.7), the streamer onset voltage

$$V_s = \left(\frac{E}{p}\right)_{crit} \cdot \frac{V_s}{L} \cdot \frac{1}{E_{max}} \cdot L \cdot p \left(1 + \frac{k}{\sqrt{pR}}\right) \qquad (6.15)$$

where $V_s/(E_{max} \cdot L)$ is the field non-uniformity factor (u in equation (1.7)). From equation (6.15)

$$E_{max} = \left(\frac{E}{p}\right)_{crit} \cdot p \left(1 + \frac{k}{\sqrt{pR}}\right) \qquad (6.16)$$

and

$$\left.\frac{dE}{dx}\right|_{x=0} = \left(\frac{E}{p}\right)_{crit} \cdot (-2) \cdot \frac{1}{R} \cdot p \left(1 + \frac{k}{\sqrt{pR}}\right) \qquad (6.17)$$

From equation (6.13)

$$\left(\frac{E}{p}\right)_{crit} \cdot (-2) \cdot \frac{1}{R} \cdot p \left(1 + \frac{k}{\sqrt{pR}}\right) e^{-p} = -200 \qquad (6.18)$$

Equation (6.18) represents the corona free breakdown criterion. Inspection of this equation indicates that the occurrence of a corona free breakdown depends only on the parameters p and R.

The locus of p, R combinations which satisfy equation (6.18) is plotted in Figure 6.7. Due to the transcendental nature of the equation, each point of the curve was determined numerically using Newton's method.

The corona free breakdown hypothesis, equation (6.13) can be interpreted with reference to Figure 6.7 as follows. Prebreakdown current phenomena can be observed in all SF_6

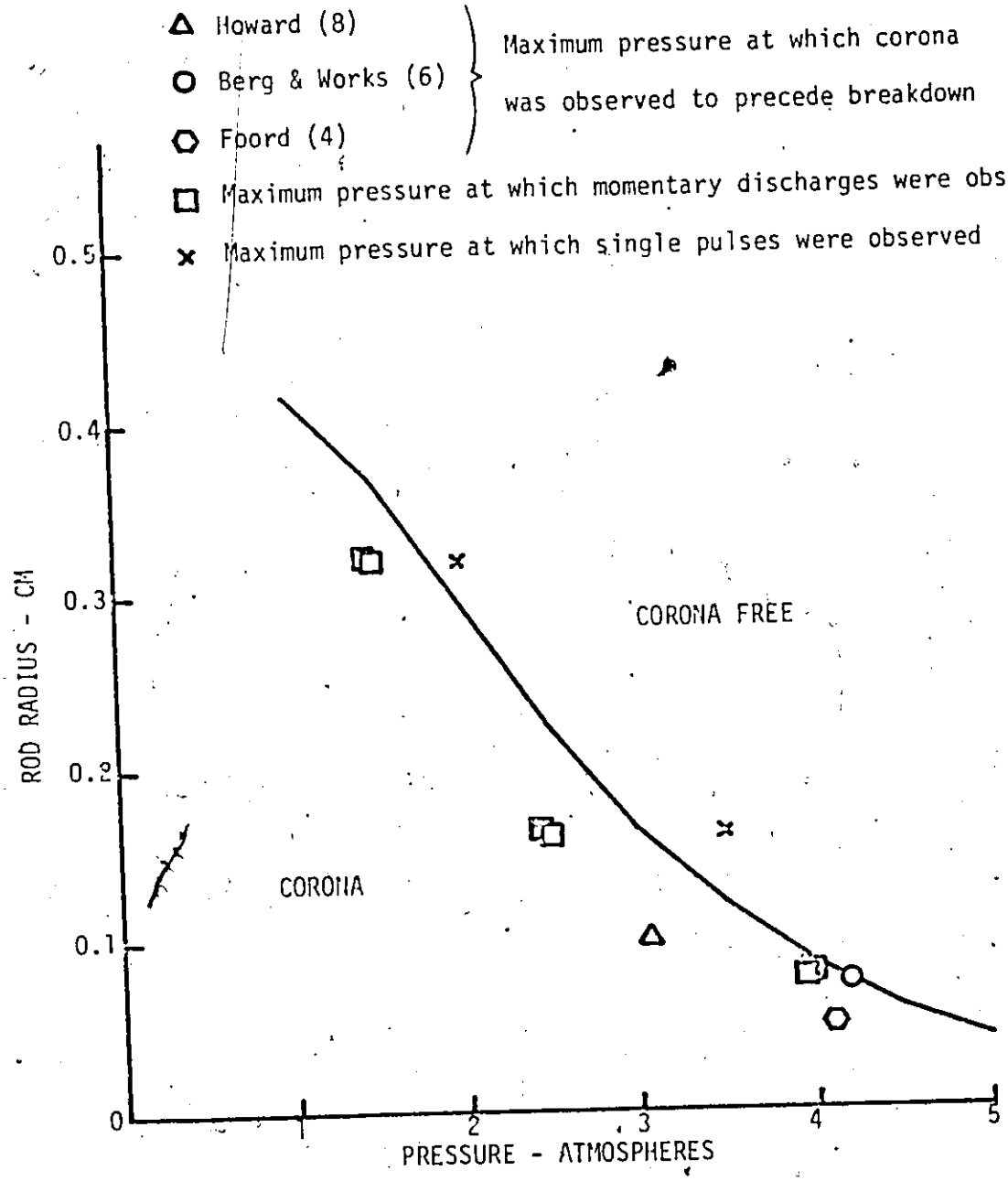

FIGURE 6.7. THEORETICAL CALCULATIONS AND EXPERIMENTAL MEASUREMENTS OF THE ONSET PRESSURE OF CORONA FREE BREAKDOWN IN SF_6.

insulated systems possessing a p, R combination lying to the left of the curve of Figure 6.7. Corona free breakdown occurs in systems with a p, R combination lying to the right of the curve.

Figure 6.7 illustrates the p, R combinations for the maximum pressures at which prebreakdown discharges were observed experimentally in six different rod-plane geometries. The two points in the "no corona" region represent single pulses of a very small magnitude which where observed only under irradiated conditions and then only occasionally.

Results of other studies of corona inception voltages in SF_6 insulated non-uniform field gaps are also plotted in Figure 6.7. In these cases the authors do not specify the nature of the corona discharge. A comparison of published breakdown voltage results and corona onset measurements suggests that Foord (3) and Howard (8) used the term "corona onset voltage" in reference to the onset voltage of a steady discharge. Works and Dakin (5) on the other hand apparently include the single pulse phenomenon as a corona discharge.

Figure 6.7 demonstrates that calculations based on equation (6.13) yield a reasonably accurate prediction of the corona free breakdown onset pressure.

CHAPTER VII

CONCLUSIONS

The following conclusions are drawn from the experimental and analytic studies described in the dissertation.

1. DC breakdown and corona studies of SF_6 gas in non-irradiated test gaps enclosed by a metal vessel are influenced significantly by voltage rates of rise above the order of 1 kv per minute.

2. Static field anode corona in SF_6 differs significantly from its counterpart in air. At low gas pressures a corona discharge in SF_6 at a hemispherical anode goes through three principal stages of development with increasing gap voltage. These are denoted in the dissertation as single pulse, momentary discharge, and sustained discharge. At higher gas pressures or in more uniform gaps a complete breakdown may preclude the development of any of these stages. Ultra-violet radiation alters considerably the inception voltage of a sustained discharge yet has an insignificant effect on the inception levels of single pulse or momentary discharge activity.

3. An analysis of prebreakdown currents and visual manifestations resulting from the various forms of corona activity in SF_6 suggests that the mean photoionizing free paths of the principal photons in an SF_6 discharge are much shorter than those in air. Corona current oscillograms demonstrate that the anode surface gradient is increased by a

sequence of discharge pulses. This indicates the presence of a negative ion space charge which significantly influences the discharge behavior.

4. Sustained discharge activity establishes a low field barrier to breakdown streamers, the result being a breakdown voltage which is much above the corona onset level. If the SF_6 gas pressure is increased sufficiently, a breakdown will occur before a sustained discharge and accompanying low field barrier materialize. The sudden disappearance of sustained discharge activity manifests itself as a discontinuous decrease of the breakdown voltage. This occurs in the negative slope region of the breakdown voltage-pressure characteristics and the pressure at which this discontinuity occurs marks the upper pressure limit of corona stabilized breakdown.

5. A comparison of theoretical streamer onset voltage calculations with experimental results over a wide variety of field non-uniformity, rod radii, and gas pressures indicates that the semi-empirical onset criterion, equation (6.6), when implemented with the use of numerical techniques, yielded the most accurate prediction of the minimum DC voltage at which a streamer related discharge will occur at the anode. Calculations based on the critical (E/p) hypothesis yielded overly conservative streamer onset voltages for the more non-uniform gaps examined.

6. A semi-empirical criterion based on widely accepted theories of the streamer discharge mechanism was developed to predict the minimum gas pressure at which a DC breakdown will preclude the formation of any form of anode prebreakdown discharge. Experimental results indicate that calculations based on this criterion are accurate to within ±0.5 atm over the range of field conditions examined.

7.1 Suggestions for Future Work

The interpretation of the prebreakdown current oscillograms are somewhat limited by the necessary use of a relatively low bandwidth recording system. Further corona current studies should be carried out at higher bandwidths. Also, the corona current studies should be complemented with image intensifier or photomultiplier studies as these can yield spatial as well as temporal information of ionization activity.

There is little information in the literature on static field cathode coronas or AC coronas in SF_6. These phenomena probably differ considerably with coronas in air and the technical importance of SF_6 warrants an investigation in these areas. In this regard corona phenomena in SF_6-air mixtures should also be investigated.

The methods of calculating discharge onset voltages and corona free onset pressure, developed and assessed in Chapter VI, should be examined in reference to more varied electrode geometries and voltage waveforms. The possibility of extending these techniques to SF_6-air mixtures should also be examined.

BIBLIOGRAPHY

1. Goldman, I. and Wul, B., "Breakdown of Compressed Gas in Inhomogeneous Electric Fields," J. Tech Phys. U.S.S.R., vol. 2, p. 545, 1934.

2. Pollock, H. C. and Cooper, F. S., "Effect of Pressure on the Positive Point to Plane Discharge in N_2, O_2, CO_2, SO_2, SF_6, CCl_2F_2, A, He, and H_2," Physical Review, vol. 56, p. 170, 1939.

3. Foord, T. R., "Positive Point to Plane Breakdown in Compressed Gases," Nature, vol. 166, p. 688, 1950.

4. Foord, T. R., "Some Experiments on Positive Point-to-Plane Corona and Spark Breakdown of Compressed Gases," Proceedings IEE, vol. 100, part II (Power Engineering), No. 78, p. 585, 1953.

5. Works, C. N. and Dakin T. W., "Dielectric Breakdown of Sulfur Hexafluoride in Non-uniform Fields," AIEE Transactions, vol. 72, part I, p. 682, 1953.

6. Berg, D. and Works, C. N., "Effect of Space Charge on Electric Breakdown in Sulfur Hexafluoride in Non-uniform Fields," AIEE Transactions, vol. 77, part III, p. 820, 1958.

7. Camilli, G.; Plump, R. E.; and Liao, T. W., Discussion of reference 5, AIEE Transactions, vol. 72, part I, p. 687, 1953.

8. Howard, P. R. "Insulation Properties of Compressed Electronegative Gases," Proceedings IEE, vol. 104, part A, p. 123, 1957.

9. Howard, P. R. "Processes Contributing to the Breakdown of Electronegative Gases in Uniform and Non-uniform Electric Fields," Proceedings IEE, vol. 104, part A, p. 139, 1957.

10. Geballe R. and Reeves M., "A Condition On Uniform Field Breakdown in Electron Attaching Gases," Physical Review, vol. 92, No. 4, p 867, 1953.

11. Bhalla, M. S. and Craggs, J. D., "Measurement of Ionization and Attachment Coefficients in Sulfur Hexafluoride in Uniform Fields," Proc. Phys. Soc., vol. 80, p. 151, 1962.

12. Pedersen, A. "Criteria for Spark Breakdown in Sulfur Hexafluoride," IEEE PAS - 89, No. 8, p. 2043, 1970.

13. Hopwood, W., "The Positive Streamer Mechanism of Spark Breakdown," Proc. Phys. Soc., vol. 62B, p. 657, 1949.

14. Kawaguchi, Y.; Sakata, K.; and Menju, S., "Dielectric Breakdown of Sulfur Hexafluoride in Nearly Uniform Fields," IEEE PAS - 90, No. 3, p. 1072, 1971.

15. Nitta, T. and Shibuya, Y., "Electrical Breakdown of Long Gaps in Sulfur Hexafluoride," IEEE PAS - 90, p. 1065, 1971.

16. Takuma, T. and Watanabe, T., "Theoretical Analysis of Discharge Characteristics in High Pressure SF_6 Gas," Elec. Eng. in Japan, vol. 90, No. 4, p. 26, 1970.

17. Takuma, T. and Wtanabe T., "Discharge Characteristics of Long Gaps in High Pressure SF_6 Gas," Elec. Eng. in Japan, vol. 90, No. 3, p. 166, 1970.

18. Kuffel, E. and Abdullah, M., "High Voltage Engineering," Pergamon Press, 1970.

19. Kuffel, E. and Radwan, R. O., "Time Lags and the Breakdown and Corona Characteristics of SF_6," Proceedings IEE, vol. 113, No. 11, p. 1863, 1966.

20. Loeb, L. B., "Electrical Coronas, Their Basic Physical Mechanism," University of California Press, 1965.

21. McDaniel, E. W. and McDowell, M. H. C., "Low Field Mobilities of Negative Ions in Oxygen, Sulfur Hexafluoride, Sulfur Dioxide, and Hydrogen Cloride," Physical Review, vol. 114, No. 4, p. 1028, 1959.

22. McAfee, K. B., "Pulse Technique for Measurement of the Probability of Formation and Mobility of Negative Ions," The Journal of Chemical Physics, vol. 23, No. 8, p. 1435, 1955.

23. Eccles, M.; Prasad, A. N.; and Craggs, J. D., "Electronic Detachment in Sulfur Hexafluoride" Electronic Letters, vol. 3, No. 9, p. 410, 1967.

24. Fehsenfield, F. C., "Electron Attachment to SF_6" The Journal of Chemical Physics, vol. 53, No. 5, p. 2000, 1970.

25. Kay, J. and Page, F. M., "Determination of Electron Affinities, part 7, Sulphur Hexafluoride and Disulphur

Decafluoride," Transactions of the Faraday Society, vol. 60, part I, p. 1042, 1964.

26. Swarbrick, P.. "Characteristics of an ARC Discharge in Sulphur Hexafluoride," Proceedings IEE, vol. 114, No. 5, p. 657, 1967.

27. Buchet, G. and Goldman, M., "Stability of Positive Continuous Corona Discharges in Electronegative and Non-electronegative Gas Mixtures," 9th International Conference On Phenomena in Ionized Gases, Bucharest, Romania, p. 291, 1969.

28. Buchet, G. and Goldman, M., "On the Stability of Positive Corona Discharges," 9th International Conference On Phenomena in Ionized Gases, Bucharest, Romania, p. 292, 1969.

29. Meek, J. M., "A Theory of Spark Discharge," Physical Review, vol. 57, p. 722, 1940.

30. Raether, H., "Development of Channel Discharge," Arch. Elektrotech, vol. 34, p. 49, 1940.

31. Meek, J. M. and Craggs, J. D., "Electrical Breakdown of Gases", Oxford University Press, 1953.

32. Peek, F. W., "Dielectric Phenomena in High Voltage Engineering", McGraw - Hill, 1929.

33. Vitkovitch, D., editor, "Field Analysis: Experimental and Computational Methods", Van Nostrand, 1966.

34. Storey, J. T. and Billings, M. J., "General Digital-Computer Programme for the Determination of Three-Dimensional Electrostatic Axially Symmetric Fields," Proceedings IEE, vol. 114, No. 10, p. 1551, 1967.

35. DiBeler, V. H. and Mohler, F. L., "Dissociation of SF_6, CF_4, and SiF_4 by Electron Impact," J. Res. U.S. Nat. Bur. Stan. Washington, vol. 40, p. 25, January, 1948.

36. McDaniel, E. W. and McDowell, M. R. C., "Low Field Mobilities of the Negative Ions in Oxygen, Sulphur Hexafluoride, Sulphur Dioxide, and Hydrogen Chloride," Physical Review, vol. 114, No. 4, p. 1028, 1959.

37. McAfee, K. B., Jr., "Pulse Technique for Measurement of the Probability of Formation and Mobility of Negative Ions," The Journal of Chemical Physics, vol. 23, No. 8, p. 1435, 1955.

38. Fehsenfield, F. C., "Electron Attachment to SF_6," The Journal of Chemical Physics, vol. 53, No. 5, p. 2000, 1970.

39. Boyd, H. A. and Crichton, G. C., "Measurement of Ionization and Attachment Coefficients in SF_6," Proceedings IEE, vo. 118, No. 12, p. 1872, 1971.

40. Raether, H. "Electron Avalanches and Breakdown in Gases", Butterworths, London, 1964.

41. Clark, F. M. "Insulating Materials for Design and Engineering Practice", John Wiley and Sons, Inc., 1962.

42. Nasser, E., "Fundamentals of Gaseous Ionization and Plasma Electronics", Wiley, New York, 1971.

43. Giao, T. R. and Jordan, J. B., "Modes of Corona Discharges in Air", IEEE PAS - 87, p. 1207, 1968.

44. Trichel, G. W., "The Mechanism of the Positive Point to Plane Corona in Air at Atmospheric Pressure", Physical Review, vol. 55, p. 382, 1939.

45. Mohr, E. I. and Weissler, G. L., "Positive Corona in Freon-Air Mixtures", Physical Review, vol. 72, p. 294, 1947.

APPENDIX A

FINITE DIFFERENCE EQUATIONS OF AN AXIALLY SYMMETRIC FIELD

The figure below represents five mesh points lying in a plane upon which is mapped a three dimensional axially symmetric field.

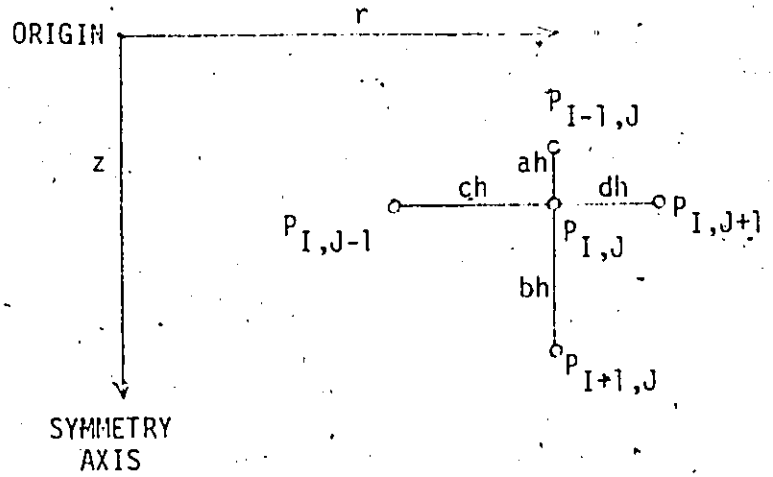

If the field distribution is determined by Laplace's equation ($\nabla^2 P = 0$) then the potential at point I,J can be determined from the equation

$$\frac{\partial^2 P}{\partial r^2} + \frac{1}{r}\frac{\partial P}{\partial r} + \frac{\partial^2 P}{\partial z^2} = 0$$

Reducing the field to a finite number of mesh points allows the derivatives of this equation to be approximated through the expansion of the potential at I,J as truncated Taylor series along the r and z axes. Using this technique Storey and Billings (34) have derived the following finite difference

equation which expresses $P_{I,J}$ as a function of the adjacent mesh points along the r and z axes.

$$P_{I,J} = C_1 P_{I-1,J} + C_2 P_{I+1,J} + C_3 P_{I,J-1} + C_4 P_{I,J+1}$$

where

$$C_1 = \frac{1}{a(a+b)C_5}$$

$$C_2 = \frac{1}{b(a+b)C_5}$$

$$C_3 = \frac{1 - d/2r}{c(c+d)C_5}$$

$$C_4 = \frac{1 + c/2r}{d(c+d)C_5}$$

$$C_5 = \frac{1}{ab} + \frac{1}{cd} + \frac{(c-d)}{2cdr}$$

If $a=b=c=d=1$ the equation simplifies to

$$P_{I,J} = \frac{1}{4}\left(P_{I-1,J} + P_{I+1,J} + (1 - \frac{1}{2r})P_{I,J-1} + (1 + \frac{1}{2r})P_{I,J+1} \right)$$

On the symmetry axis ($r=0$)

$$\frac{\partial^2 P}{\partial r^2} + \frac{1}{2}\frac{\partial^2 P}{\partial z^2} = 0$$

Using the technique outlined above, the potential of a point lying on the symmetry axis ($J=1$) can be determined from the equation

$$P_{I,1} = C_6 P_{I-1,J} + C_7 P_{I+1,J} + C_8 P_{I,2}$$

where

$$C_6 = \frac{1}{a(a+b)C_9}$$

$$C_7 = \frac{1}{b(a+b)C_9}$$

$$C_8 = \frac{2}{d^2 C_9}$$

$$C_9 = \frac{1}{ab} + \frac{2}{d^2}$$

APPENDIX B

COMPUTER PROGRAM TO CALCULATE STREAMER ONSET VOLTAGES

This program can be used to calculate the streamer onset voltage of an SF_6 insulated electrode system. The basis of the program is Pederson's streamer onset condition, equation with a K value of 20. Four inputs are required:

1. The coefficients of a polynomial which fits the potential distribution along the flow line possessing the largest voltage gradient. The highly stressed electrode is assigned a potential of 0 and the total voltage across the insulated gap is 1 kv (coefficient units = kv, cm).

2. The SF_6 pressure in atmospheres absolute.

3. The gap length in centimeters.

4. If required, the program will calculate both the streamer mechanism I (initial streamer crosses the entire gap) and streamer mechanism II onset voltages. Streamer mechanism I is only possible under near uniform field conditions. Both streamer onset voltages are calculated if the variable MODE is assigned a value 0.

An iterative technique is used to solve equations (6.11) and (6.12) and initial values for the streamer onset voltage and avalanche length are required. These values can be obtained from the polynomial coefficients in the following manner.

It is assumed that the polynomial describes the potential distribution along a flow line eminating from an isolated

sphere of radius R. The voltage gradient along this flow line is given by

$$E(x) = \frac{E_{max}}{(1+ x/R)^2} \qquad (i)$$

where E_{max} is the electrode surface gradient. Expanding this expression as a Maclaurin series gives

$$E(x) = E_{max} - \frac{2E_{max}x}{R} + \frac{3E_{max}x^2}{R^2} - \cdots \qquad (ii)$$

The polynomial describing the actual voltage distribution along the flow line possessing the maximum voltage gradient is

$$V(x) = V_g a_2 x + V_g a_3 x^2 + V_g a_4 x^3 + \cdots \qquad (iii)$$

where V_g is the gap voltage and $x = 0$ at the highly stressed electrode surface. The voltage gradient along this flow line is

$$E(x) = V_g a_2 + 2V_g a_3 x + 3V_g a_4 x^2 + \cdots \qquad (iv)$$

Equating the first two coefficients of polynomials (ii) and (iv) we have

$$a_2 = \frac{E_{max}}{V_g} \quad \text{and} \quad a_3 = \frac{E_{max}}{RV_g}$$

Therefore

$$R = -\frac{a_2}{a_3}$$

From equation 1.7 we have

$$V_s = 89 \cdot u \cdot p \cdot L \cdot (1 + \frac{0.175}{\sqrt{pR}})$$

where V_s is the streamer onset voltage under the assumption that the highly stressed electrode is treated as an isolated sphere. The field non-uniformity factor from equation (iv) is

$$u = \frac{E_{av}}{E_{max}} = \frac{V_g/L}{a_2 V_g} = \frac{1}{a_2 L}$$

Therefore

$$V = \frac{89}{a_2} p \ (1 + 0.175\sqrt{-\frac{a_3}{pa_2}})$$

Thus V serves as an approximation to the streamer inception voltage of the system.

Nitta and Shibuya have shown that the isolated sphere approximation yields an integration (avalanche) length

$$s = R\sqrt{\frac{E_{max}}{89 \cdot p}} - R$$

$$= -\frac{a_2}{a_3}\sqrt{\frac{Va_2}{89 \cdot p}} + \frac{a_2}{a_3}$$

s can be used as an approximation to the avalanche length.

Both V and s can be determined simply from the knowledge of the absolute gas pressure in atmospheres and the polynomial coefficients calculated on the basis of a voltage of 1 kv applied across the entire gap.

```
G LEVEL  21                    MAIN                    DATE = 74130          16/59/51

C       THIS PROGRAM CALCULATES THE STREAMER ONSET VOLTAGE OF A SPH
C       INSULATED ELECTRODE SYSTEM.
C       CARD1-ORDER OF POLYNOMIAL DESCRIBING VOLTAGE DISTRIBUTION ALONG
C       FLOW LINE THROUGH MAXIMUM STRESS POINT.(I10)
C       CARD2-SF6 PRESSURE IN ATMOSPHERES ABSOLUTE.(F10.5).
C       CARD3-GAP LENGTH IN CM.(F10.5)
C       CARD4-IF BOTH STREAMER I AND II ONSET VOLTAGES REQUIRED INPUT=1,
C       OTHERWISE INPUT=0.(I1)
C       CARD5 ETC.-POLYNOMIAL COEFFICIENTS FOR A UNIT GAP VOLTAGE.X IN CM.
C       ONE COEFFICIENT PER CARD ARRANGED IN ASSENDING ORDER.(E14.7)
        DIMENSION A(20)
        REAL*8 INT
        INT=20
        READ10,IPOLY,P,G,MODE
   10   FORMAT(I10/F10.5/F10.5/I1)
        IPOLY=IPOLY+1
        DO20I=1,IPOLY
   20   READ30,A(I)
   30   FORMAT(E14.7)
        ICHECK=0
C       DETERMINE STARTING VALUES FOR INTEGRATION LENGTH X AND ONSET
C       VOLTAGE V.
        V=89.*P/A(2)*(1.+0.175*SQRT(-A(3)/P/A(2)))
        X=-A(2)/A(3)*(SQRT(V*A(2)/89./P)-1.)
C       RECALCULATE INTEGRATION LENGTH
        N=0
   40   DO50K=1,100
        XOLD=X
        F=27.*A(2)*V-2400.*P
        FD=0.
        IPOLY1=IPOLY-2
        DO60I=1,IPOLY1
        F=F+27.*A(I+2)*(I+1)*V*X**I
   60   FD=FD+27.*A(I+2)*(I+1)*I*V*X**(I-1)
        X=X-F/FD
        IF(X.GT.G.OR.X.LT.0.)GOTO61
        GOTO62
   61   ICHECK=1
        GOTO70
   62   IF(ABS(X-XOLD)/XOLD.LT.0.0001)GOTO70
```

```
 50   CONTINUE
C     CALCULATE STREAMER ONSET VOLTAGE
 70   DEN=0.
      VOLD=V
      N=N+1
      IPOLY2=IPOLY1-1
      DO80I=1,IPOLY2
 80   DEN=DEN+A(I+1)*X**I
      V=(PIT+2400.*X**2)/DEN/27.
      IF(ABS(V-VOLD)/VOLD.LT.0.0001)GOTO 90
      IF(N.GT.100)GOTO72
      GOTO40
 72   PRINT71
 71   FORMAT(' ','STREAMER II CALCULATION DOES NOT CONVERGE')
 90   X11=X
      IF(MODE.GT.0)GOTO91
C     STREAMER I CALCULATION
      X=0.
      DEN=0.
      DO92I=1,IPOLY2
 92   DEN=DEN+A(I+1)*X**I
      V1=(PIT+2400.*X**2)/DEN/27.
 91   CONTINUE
      PRINT93,G,P
 93   FORMAT('0','GAP LENGTH=',F6.3,'CM',3X,'GAS PRESSURE=',F6.3,'ATM')
      IFBICHECK.EQ.1)GOTO97
      PRINT94,V,X11,N
 94   FORMAT('0','STREAMER II ONSET VOLTAGE=',F10.5,'KV',3X,'INTEGRATION
     1 LENGTH=',E14.7,'CM',3X,'ITERATIONS=',I3)
 97   IF(MODE.GT.0)GOTO95
      PRINT96,V
 96   FORMAT('0','STREAMER I ONSET VOLTAGE=',F10.5)
 95   CONTINUE
      STOP
      END
```

VITA AUCTORIS

1945 Born in Winnipeg, Manitoba on November 25th.

1964 Graduated from High School in Winnipeg, Manitoba.

1968 Graduated from the University of Manitoba with a B.Sc. degree in Electrical Engineering.

1970 Graduated from the University of Manitoba with a M.Sc. degree in Electrical Engineering.

1974 Candidate for Ph.D. degree, Electrical Engineering Department, University of Windsor, Windsor, Ontario.